Uncovering the hidden mechanisms governing the transcriptional regulation of inflammation

Ezio T. Fok

A thesis submitted to the Faculty of Health Sciences at the University of Cape Town in fulfilment of the requirements for the degree of Doctor of Philosophy

Cape Town, 2019

DECLARATION

I, Ezio T. Fok hereby declare that the work on which this thesis is based is my original work (except where acknowledgements indicate otherwise) and that neither the whole work nor any part of it has been, is being, or is to be submitted for another degree in this or any other university.

Signature: Signed by candidate

Date: 12 December 2019

For my parents.

PUBLICATIONS AND PRESENTATIONS

The following publications and presentations are related to the work presented in this thesis:

Publications:

Fok, E.T., Scholefield, J., Fanucchi, S. and Mhlanga, M.M., 2017. The emerging molecular biology toolbox for the study of long noncoding RNA biology. *Epigenomics*, *9*(10), pp.1317-1327.

Fok, E.T., Davignon, L., Fanucchi, S. and Mhlanga, M.M., 2018. The lncRNA connection between cellular metabolism and epigenetics in trained immunity. *Frontiers in immunology*, *9*.

Fanucchi, S., Fok, E.T., Dalla, E., Shibayama, Y., Börner, K., Chang, E.Y., Stoychev, S., Imakaev, M., Grimm, D., Wang, K.C. and Li, G., Sung, W.K., Mhlanga, M.M., 2019. Immune genes are primed for robust transcription by proximal long noncoding RNAs located in nuclear compartments. *Nature genetics*, *51*(1), p.138.

Fok, E.T., Moorlag, S., Negishi, Y., Groh, L.A., Dos Santos, J.C., da Cunha Jolvino, D.P., Migliorini, L. B., Neto, A.S., Severino, P. Joosten, L.A.B., Netea, M.G., Fanucchi, S., Mhlanga, M.M. A chromatin-regulated biphasic circuit between *IL-1β* and *IL-37* coordinates inflammation and trained immunity. (manuscript in preparation)

Presentations:

Biophysics in the Understanding, Diagnosis and Treatment of Infectious Diseases conference, Stellenbosch, South Africa, 16-20 November 2015, TNF-responsive genes are rapidly activated from a poised state via the action

of a long non-coding RNA. Fanucchi, S., Fok, E.T., Dalla, E., Shibayama, Y., Stoychev, S., Imakaev, M., Sung, W.K., Mhlanga, M.M.

Synergy in Immunology, VII Conference of the South African Immunology Society, KwaZulu Natal, South Africa, 18-20 June 2019, Finding the missing "lncs" of the innate immune system. Fanucchi, S., Fok, E.T., Dalla, E., Shibayama, Y., Börner, K., Chang, E.Y., Stoychev, S., Imakaev, M., Grimm, D., Wang, K.C., Sung, W.K., Mhlanga, M.M.

Genome Architecture in Cell Fate and Disease Gordon Research Conference, Hong Kong, Hong Kong, 4-9 August 2019, A chromatin-regulated biphasic circuit between *IL-1β* and *IL-37* coordinates inflammation and trained immunity. Fok, E.T., Moorlag, S., Negishi, Y., Groh, L.A., Dos Santos, J.C., da Cunha Jolvino, D.P., Migliorini, L. B., Neto, A.S., Severino, P. Joosten, L.A.B., Netea, M.G., Fanucchi, S., Mhlanga, M.M.

Epigenetics of Infectious and Non-communicable Diseases ICGEB conference, 16-19 September 2019, Cape Town, South Africa, A chromatin-regulated biphasic circuit between *IL-1β* and *IL-37* coordinates inflammation and trained immunity. Fok, E.T., Moorlag, S., Negishi, Y., Groh, L.A., Dos Santos, J.C., da Cunha Jolvino, D.P., Migliorini, L. B., Neto, A.S., Severino, P. Joosten, L.A.B., Netea, M.G., Fanucchi, S., Mhlanga, M.M.

ABSTRACT

Inflammation provides broad immunological protection that is essential for our survival. This cellular response is characterised by a biphasic cycle consisting of an initial acute pro-inflammatory phase and a subsequent resolving anti-inflammatory phase. Underlying each of these phases are changes in the expression of hundreds of immune genes, which encode for inflammatory mediators called cytokines. Importantly, the biphasic nature of inflammation requires cytokine expression to be highly regulated and coordinated to different timescales during each phase of inflammation. For the initial pro-inflammatory response, cytokine expression needs to be rapid and robust to efficiently initiate host defence mechanisms and provide effective immunological protection. In contrast, the expression of anti-inflammatory cytokines is temporally delayed to ensure that anti-inflammation always follows pro-inflammation. In order to choreograph the expression of these cytokines during inflammation, numerous mechanisms within the cell serve to regulate and coordinate cytokine transcription.

Within the eukaryotic nucleus, multiple modes of transcriptional regulation function cooperatively to provide the regulatory capacity that is required for complex transcription patterns to emerge. These include the organisation of the genome, which confine cognate chromosomal contacts that are causal to transcription, and long-non coding RNAs (lncRNAs) that function to discretely fine tune transcriptional activity. Although many of the mechanisms that regulate transcription have been well described, their role in cytokine expression during inflammation remains largely unknown. In particular, the mechanisms that facilitate rapid and robust cytokine expression during pro-inflammation and the regulatory networks that coordinate the biphasic regulation of inflammation are unresolved.

In this work, two novel lncRNAs were discovered to transcriptionally regulate these key features of cytokine expression during inflammation. The first,

UMLILO (Upstream Master LncRNA of the Inflammatory chemokine LOcus), was found to emanate from the ELR+ CXCL chemokine TAD and regulate the transcriptional activation of the pro-inflammatory ELR+ CXCL chemokines (*IL-8*, *CXCL1*, *CXCL2* and *CXCL3*). By exploiting the pre-formed local 3D topology, UMLILO is able to epigenetically prime the chemokines for transcriptional activation. This involves the discrete deposition of H3K4me3 onto the promoters of the chemokines, which allows for the pre-loading of transcriptional machinery prior to their signal-dependent activation. This reveals a fundamental mechanism for the epigenetic priming and rapid activation of pro-inflammatory cytokine genes.

The second lncRNA, called AMANZI (A MAster Non-coding RNA antagoniZing Inflammation), was found to coordinate the transcription of two functionally opposed cytokines: the master pro-inflammatory IL-1β and the broad anti-inflammatory IL-37. AMANZI is encoded in the promoter of *IL-1β*, which results in its concomitant expression when *IL-1β* is transcriptionally active. Functionally, AMANZI mediates the formation of a dynamic chromosomal contact between *IL-1β* and *IL-37*. This leads to the delayed transcriptional activation of *IL-37* ensuring that the pro-inflammatory function of IL-1β precedes IL-37 mediated anti-inflammation. This revealed a novel biphasic circuit that coordinated the expression of *IL-1β* and *IL-37*, through the activity of AMANZI, to regulate the two functionally opposed states of inflammation. Clinical observations in healthy individuals revealed that a polymorphism occurring in AMANZI (rs16944) was able to augment the state of this genetic circuit and shift the relative levels of *IL-1β* and *IL-37* to influence an individual's inflammatory capacity. This affected the establishment of innate immunological memory, which is involved in the progression of many inflammatory conditions and the efficacy of certain vaccines.

The work described here uncovers novel mechanisms that transcriptionally regulate key features of the inflammatory response. Importantly, this work implicates the role of two novel lncRNAs in inflammation, essentially

contributing to the functional annotation to the genome and providing novel targets for the modulation of pathogenic inflammation.

ACKNOWLEDGEMENTS

I would most certainly not have been able to make it this far if it was not for the help and support of countless individuals. To everyone who was part of this journey in any way, I thank you. First and foremost, I would like to thank my supervisors Dr Musa Mhlanga and Dr Stephanie Fanucchi. Thank you for introducing me to a world of science that was previously unconceivable to me. Working with you has been inspirational and a privilege. I cannot thank you both enough for your mentorship over the years.

My gratitude also extends to all the members of the Mhlanga lab (past and present). Many of you have become great friends along the way. Thank you for everything, big and small! A specially thanks to Bianca Fowler who runs our lab. Thank you for taking care of us.

My thanks to the Netea lab, especially Simone Moorlag who performed all the experiments on the human samples described in this body of work.

I would also like to thank all members of the Scholefield lab. In particular I would like to thank Dr Janine Scholefield and Dr Jerolen Naidoo. I really don't think I would have made it this far without your support and friendship everyday.

My gratitude to the CSIR, as none of this would have been possible without their financial support. I would like to especially thank Dr Boitumelo Semete who, through her leadership capacity, endeavoured to see me through this journey.

I would also like to thank all my friends outside of the lab. Thank you for all the pity parties, the encouragement and your friendship.

And last, but most importantly, my parents. I cannot thank them enough for all they have done for me.

TABLE OF CONTENTS

LIST OF FIGURES

LIST OF TABLES

LIST OF ABBREVIATIONS

3C - Chromosomal conformation capture

AAV - Adeno-associated virus

ASO - Anti-sense oligonucleotide

ATAC-Seq - Assay for Transposase-Accessible Chromatin using Sequencing

ATP - Adenosine triphosphate

BCG - Bacille Calmette-Guérin

BET - Bromodomain and Extra-Terminal motif

BG - Beta-glucan

CAGE - Cap Analysis of Gene Expression

ChIA-PET - Chromatin Interaction Analysis by Paired-End Tag Sequencing

ChIP-Seq - Chromatin immunoprecipitation-sequencing

CTCF - CCCTC-binding factor

CTD - C-terminal domain

CXCL - C-X-C motif chemokine ligand

dCas9 - Deactivated Cas9

DMEM - Dulbecco's modified eagle medium

DNA - Deoxribonucleic acid

DNAse-Seq - DNaseI hypersensitive site sequencing

dNTP - Deoxyribonucleotide triphosphate

DRB - 5,6-Dichloro-1-β- d-ribofuranosylbenzimidazole

DSIF - DRB sensitivity-inducing factor

DTT - Dithiothreitol

EDTA - Ethylenediaminetetraacetic acid

EGM-2 - Endothelial Cell Growth Medium-2

ELISA - Enzyme-linked immunosorbent assay

ELR+ - Glutamic acid-leucine-arginine positive

ENCODE - Encyclopaedia of DNA Elements

eQTL - Expressed quantitative trait loci

eRNA - enhancer RNA

FANTOM - Functional Annotation of the Mammalian Genome

FBS - Foetal bovine serum

FISH - Fluorescent *in situ* hybridisation
GFP - Green fluorescent protein
gRNA - Genomic DNA
gRNA - Guide RNA
GSP - Gene specific primer
GWAS - Genome-wide association studies
HGP - Human Genome Project
HIF-1α - Hypoxia inducible factor-1α
HUVEC - Human umbilical vein endothelial cells
IFN-β - Interferon-β
IL-1 - Interlekin 1
IL-8 - Interleukin 8
IPL - Immune-gene Priming LncRNA
Kb - Kilobases
LLPS - Liquid-liquid phase separation
LNA - Locked nucleic acid
lncRNA - long non-coding RNA
LPS - Lipopolysaccharide
Mb - Megabases
miRNA - MicroRNA
MLL - Mixed Lineage Leukemia
mRNA - Messenger RNA
mTOR - Mammalian target of rapamycin
NABD - Nucleic-acid based drug
NELF - Negative elongation factor
NT - nucleotides
Oligos - oligonucleotide
P-TEFb - Positive-transcription elongation factor b
PBMC - Peripheral blood mononuclear cell
PBS - Phosphate buffered saline
PIC - Pre-initiation complex
PMA - Phorbol 12-myristate 13-acetate
Pol II - RNA polymerase II
PRC2 - Polycomb repressive complex 2

RACE - Rapid amplification of cDNA ends

RNA - Ribonucleic acid

RNA-Seq - RNA sequencing

RNAi - RNA interference

RPE1 - Retinal pigment epithelial 1

RT-qPCR - Reverse transcription quantitative polymerase chain reaction

shRNA - Short hairpin RNA

siRNA - Short interfering RNA

smFISH - Single molecule fluorescent in situ hybridisation

SNP - Single nucleotide polymorphism

T7E1 - T7 endonuclease I

TAD - Topologically associating domain

TAF3 - TATA box-binding protein 3

TFIID - Transcription factor II D

TNF - Tumour necrosis factor

TSS - Transcription start site

UMLILO - Upstream Master LncRNA of the Inflammatory chemokine Locus

WDR5 - WD repeat-containing protein 5

XIC - X chromosome inactivation centre

Chapter 1

INTRODUCTION

Complexity within the human genome

The genome carries the instruction for all cellular functions in an elegant quaternary code. When correctly deciphered, this produces proteins that express the encoded information. Our ability to read the deoxyribonucleic acid (DNA) sequence comprising our genome marked the beginning of the genomics era. Perhaps the most revered effort in this field is the Human Genome Project (HGP), which produced the first draft of the human genome as well as the complete genome sequence of various other model organisms commonly studied in biology (Fleischmann et al., 1995, Blattner et al., 1997, Consortium, 1998, Adams et al., 2000, Arabidopsis Genome, 2000, Lander et al., 2001).

Because proteins are considered the functional outputs of gene expression, the number of protein-coding genes encoded within a genome intuitively represents the functional capacity and complexity of an organism. The current version of the human genome sequence comprises of approximately 3 billion nucleotide pairs and is estimated to encode for a collection of 20 000 protein-coding genes (Venter et al., 2001, Willyard, 2018). Surprisingly, this accounts for only 2% of the human genome (Corces et al., 2018). Furthermore, organisms of seemingly lower complexity, such as worms and plants, are estimated to have an equivalent or richer gene content (Prasanth and Spector, 2007, Van Straalen and Roelofs, 2011). This revealed an unexpected disparity between gene content and the development of organismal complexity, giving rise to the G-value paradox (Hahn and Wray, 2002, Prasanth and Spector, 2007). How does such a relatively small repertoire of

protein-coding genes account for the wide range of cell phenotypes and specialised functions that define our species?

By definition, relative complexity is the minimum amount of information that is necessary for the operation of a system (Mattick, 2004). Increased protein-coding capacity, while necessary, does not always lead to improved organismal complexity. This is because a system that only expands in its functional capabilities will eventually tend towards chaos without the proper regulation (Mattick, 2004). This underscores the need for the co-evolution of regulatory mechanisms as the genome gained function. It has been predicted that the acquisition of these regulatory mechanisms scale quadratically to the number of genes in the network, suggesting that the complexity of a system arises from its regulation (Mattick, 2004).

The human genome is evolutionarily optimised to carry out all necessary functions using a library of approximately 20 000 proteins. Its complexity does not lie within this protein-coding potential, but rather the ability to regulate the expression of these genes in space and time. New paradigms in biology have indicated that organismal complexity arises from the expansion of the regulatory capacity within the non-coding regions of the genome (Mattick, 2004). As a result, this posed the greatest challenge since the production of the first draft of the human genome: to functionally annotate and decrypt the regulatory functions and networks embedded in this portion of the code.

In the last two decades, the protein-coding portion of the genome has been extensively studied. However, ascribing function to the non-coding genome has remained challenging and eluded biologists for a long time. It has become more apparent recently that this “dark matter” of the genome is replete with regulatory information that encodes for a large repertoire of mechanisms that cooperatively function to control gene expression. This ranges from higher order nuclear organisation of the genome to non-coding RNAs and the epigenetic regulation of transcription. Importantly, genome-wide association studies (GWAS) have revealed that the majority of single nucleotide

polymorphisms (SNPs) occur in the non-coding genome but are associated with changes in protein-coding gene expression (Maurano et al., 2012, Nishizaki and Boyle, 2017, van Arensbergen et al., 2019). This suggests that these SNPs are altering the regulatory functions found within these regions to generate divergent traits that are causal to health and disease. Despite the tremendous efforts in understanding the regulatory landscape of the genome, much of the function and regulation of the genome remains unknown. Therefore, modern day genomics continues to discover and characterise functional elements that regulate the expression of the genome in various biological processes.

The innate immune response

Amongst the many biological processes encoded within the genome, inflammation is a highly complex cellular response that is elicited by the innate immune system to provide broad immunological protection. Innate immunity is the first line of defence against microbial and viral infections and relies on regulatory programmes that dynamically choreograph changes in the expression of hundreds of immune genes (Rogatsky and Adelman, 2014).

A healthy inflammatory response is characterised by a biphasic cycle consisting initially of an acute pro-inflammatory phase, which serves to initiate host defence. This includes the remodelling of tissues, cell signalling for the recruitment of immune cells and the production of anti-microbial molecules, and the rewiring of cellular metabolism to redistribute energy and metabolite reserves to support pro-inflammation (Kornman, 2006). Together, these pro-inflammatory activities induce immense physiological stress which can be deleterious to the cell, if left unresolved (Medzhitov, 2008). Thus, downstream of pro-inflammation is an anti-inflammatory phase, which antagonises pro-inflammation, initiates tissue repair and restores basal cellular homeostasis (Figure 1.1) (Medzhitov, 2008, Rogatsky and Adelman, 2014). Each phase of inflammation is facilitated by a vast collection of immune genes which encode for inflammatory mediators called cytokines (Medzhitov, 2008, Rogatsky and

Adelman, 2014). Importantly, during the initial pro-inflammatory phase, pro-inflammatory cytokine expression has to be rapid, robust and dynamically responsive to the burden of infection in order to be effective. During the subsequent anti-inflammatory phase, the temporally delayed expression of anti-inflammatory cytokines is paramount for the self-regulatory biphasic nature of inflammation. Therefore, cytokine expression during inflammation has to be coordinated to different timescales, suggesting that multiple layers of regulation facilitate the execution of such an intrinsically complex and important process.

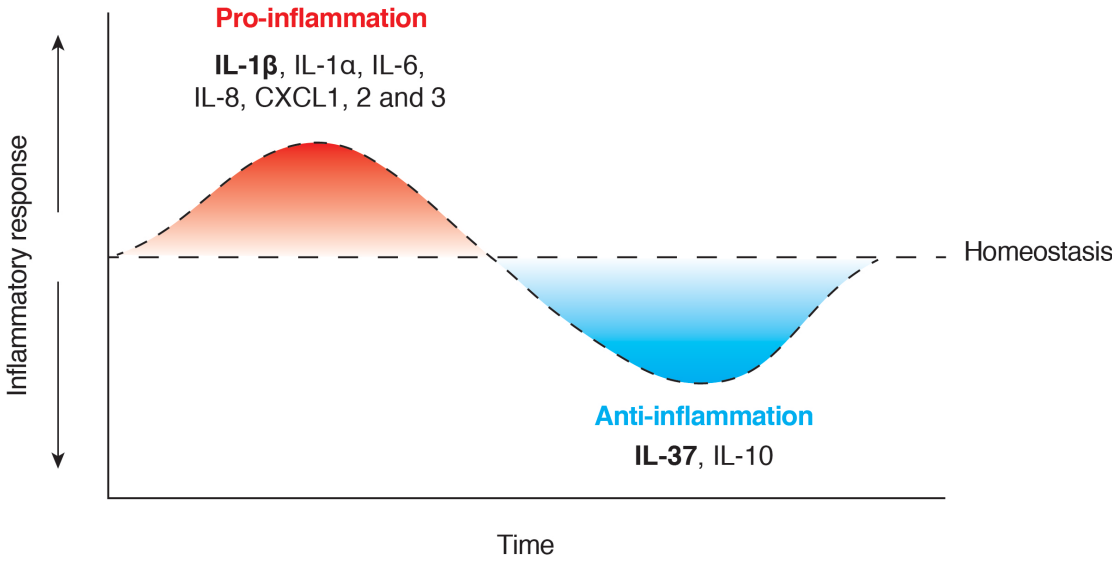

Figure 1.1: The biphasic nature of inflammation

The progression of inflammation follows a balanced biphasic cycle. During the initial pro-inflammatory phase, the transcription of pro-inflammatory cytokines is rapidly activated to effectively curb the progression of infection. This is subsequently resolved by the temporally delayed anti-inflammatory phase, which is characterised by the expression of anti-inflammatory mediators such as IL-37 and IL-10. This phase serves to antagonise the pro-inflammatory phase, initiate tissue repair and restore homeostasis.

Numerous mechanisms operating at the level of transcription, mRNA maturation, mRNA turnover and protein translation are integrated into complex networks to effectively regulate inflammation (Rogatsky and Adelman, 2014). However, various studies have indicated that regulation at the transcriptional level is particularly important in shaping the inflammatory

response (Escoubet-Lozach et al., 2011, Rabani et al., 2011, Bhatt et al., 2012). This is evident in the successive waves of coordinated immune gene activation and attenuation observed during inflammation (Amit et al., 2009). Furthermore, the dynamic range of innate immune gene transcription is extremely high (within 1000 fold) and is individually calibrated for each specific gene (Rogatsky and Adelman, 2014). This remarkable coordination and fine tuning of immune gene transcription indicates that highly sophisticated transcriptional programmes exist to regulate this process. Therefore, in order to understand the regulation of inflammation, it is important to understand how transcription is regulated in the human cell.

The basics of transcription

Transcription is the first step of gene expression and is thus fundamental to coordinating biological processes instructed by DNA. The products of this process are ribonucleic acid (RNA) molecules, which are functionally pervasive in biology, ranging from the transmission of genetic information from DNA to proteins (as messenger RNAs (mRNAs)) to the fine tuning of biological responses by a plethora of non-coding RNA species. The regulation of transcription is an essential control mechanism for orchestrating gene expression, ensuring that it is initiated in response to the correct developmental and environmental cues. As such, transcriptional regulation in multicellular higher-order organisms is complex and consists of numerous mechanisms of control.

Promoters

The most basic regulatory unit of transcription is the promoter (Johanson et al., 2019). This is a stretch of DNA that is proximally upstream of the transcriptional start site (TSS) and is embedded with transcription factor binding sites. This serves as a DNA docking platform for tissue-specific transcription factors that modulate the recruitment of RNA Polymerase II (Pol II). Pol II enzymatically drives transcription and undergoes the following 4

phases in a transcription cycle (Figure 1.2) (Hargreaves et al., 2009, Min et al., 2011, Rogatsky and Adelman, 2014):

1. **Recruitment:** The first step of the transcription cycle involves the assembly of the pre-initiation complex (PIC). This is facilitated by the loading of cognate transcription factors, transcriptional co-activators and Pol II to the promoter. In this complex, the C-terminal domain (CTD) of Pol II remains unphosphorylated.
2. **Initiation:** Serine 5 (Ser5) of the Pol II CTD is then phosphorylated to initiate transcription that pauses proximal to the promoter. This produces short RNA transcripts of 25-60 nucleotides (nt) in length. Pol II pausing is induced by the presence of the 5,6-Dichloro-1-β- d-ribofuranosylbenzimidazole (DRB) sensitivity-inducing factor (DSIF) and the negative elongation factor (NELF). In this state, Pol II is poised and ready for signal-dependent activation of transcription.
3. **Pause-release:** The recruitment of the positive-transcription elongation factor b (P-TEFb) phosphorylates DSIF, NELF, as well as Serine 2 (Ser2) of the Pol II CTD. This results in the dissociation of NELF from the protein complex, releasing Pol II from its suspended state. The recruitment of P-TEFb to the paused promoter generally occurs in a signal-dependent manner and is mediated by transcription factors such as NF-κβ, the Mediator complex or Bromodomain and Extra-Terminal motif (BET) proteins.
4. **Elongation:** The phosphorylation (Ser2/5) of the Pol II CTD allows for the binding of various RNA processing machinery and chromatin modifiers. These facilitate the elongation and maturation of a nascent RNA transcript during active transcription. Elongation will stop when Pol II traverses specific sequences that will terminate transcription and cause Pol II to dissociate from the DNA.

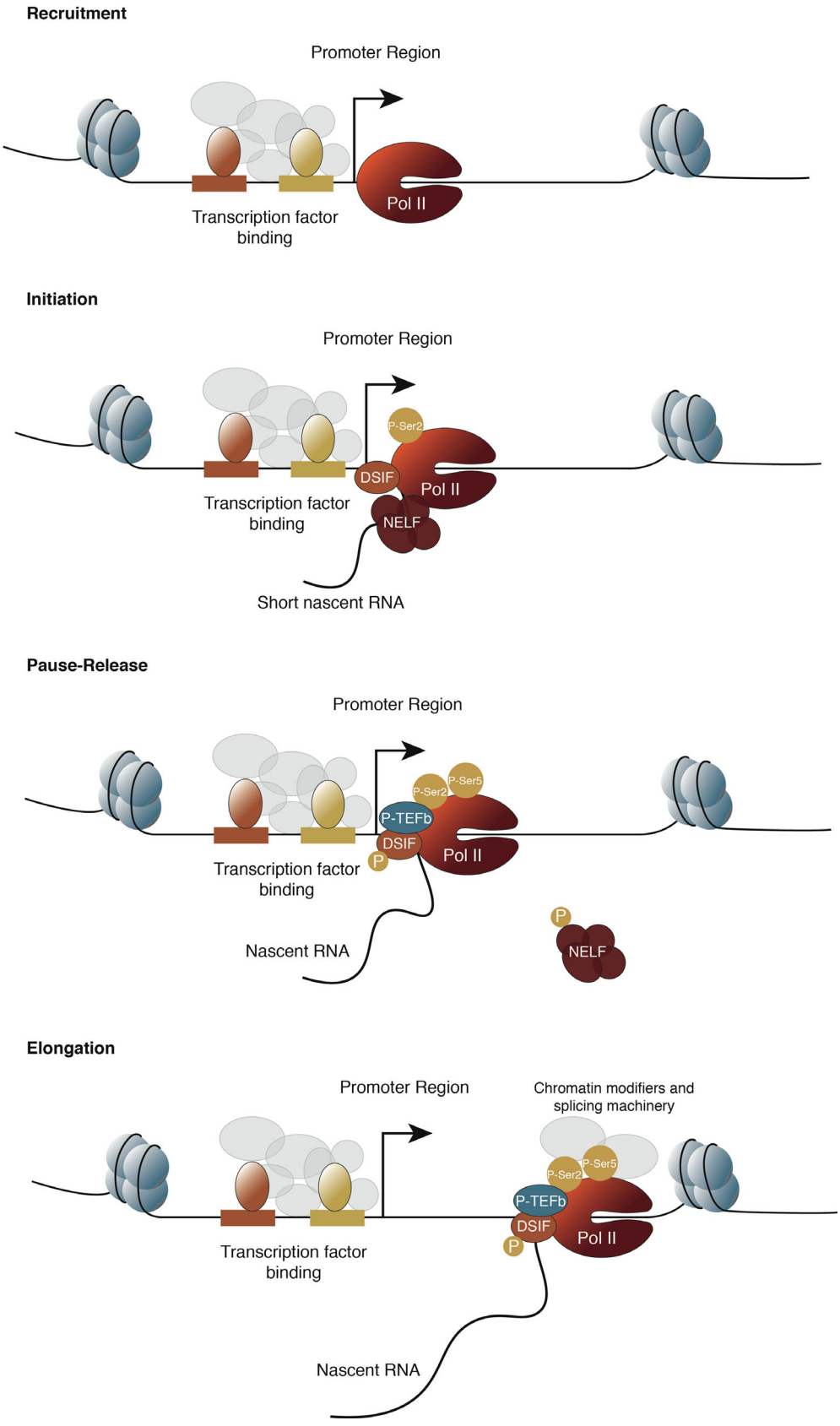

Figure 1.2: The phases of the transcription cycle

Transcription factors and Pol II are recruited to an accessible promoter region. Transcription is initiated with the phosphorylation of Ser2 on the Pol II CTD, leading to the production of a

short nascent transcript (25-60 nt). However, Pol II activity is paused by the presence of DSIF and NELF. The recruitment of P-TEFb by signal-dependent transcription factors results in the dissociation of NELF and the phosphorylation of DSIF and Pol II CTD Ser5, resulting in the pause-release of Pol II. With the help of chromatin modifiers and splicing machinery, Pol II is able to traverse the gene body and produce a nascent RNA transcript.

During a transcription cycle, the activity at a promoter can be regulated at two points: the recruitment of Pol II to the promoter and the pause-release of Pol II on the promoter. Primary response genes are rapidly induced in the absence of *de novo* protein synthesis (Fowler et al., 2011). These genes exist in a poised state whereby the PIC is assembled and Pol II activity is initiated prior to their transcriptional activation (Fowler et al., 2011). This allows for these genes to be regulated at the pause-release phase, resulting in fast transcriptional responses that resemble a digital kinetic profile (Fowler et al., 2011). Many pro-inflammatory immune genes exist in this state, allowing for their quick transcriptional activation in response to pathogens (Fowler et al., 2011, Rogatsky and Adelman, 2014). In contrast, secondary response genes are regulated at the level of Pol II recruitment and PIC assembly, introducing a temporal delay in the timeline of their activation (Fowler et al., 2011). Such responses may be more useful for the subsequent anti-inflammatory phase of inflammation.

While promoters can be regulated by modulating the activity of Pol II, the propensity for transcription factors and Pol II to bind promoters imbues these proximal *cis*-regulatory elements with inherent transcriptional activity. However, not all DNA binding sites are occupied by their cognate transcription factors and it is well established that only certain subsets of genes are transcribed in different human cell types and under different cellular conditions (Natoli, 2016). This indicates that not all the promoters in the genome are simultaneously active. Instead, cells of specialised function or under different cellular conditions make use of specific sets of transcriptional programmes.

Chromatin accessibility

The assignment of these transcriptional programmes is dictated by the accessibility of the encoding DNA to transcription factors and transcriptional machinery. By controlling the accessibility of the genetic code, only certain subsets of genes that drive the relevant biological functions are read and expressed.

Genomic DNA (gDNA) is coiled around histone octamers, forming nucleoprotein complexes (called nucleosomes) which serve as the basic units of the chromatin fibre. These nucleosomes play a fundamental role in the compaction of the DNA fibre in the confined space of the nucleus, but also affect gene transcription by regulating DNA accessibility (Felsenfeld and Groudine, 2003). Super-resolution microscopy has revealed that the chromatin fibre exists in clusters to form structures that are reminiscent of “beads on a string”. The size of these clusters are associated with the state of the chromatin, with smaller clusters being active and larger clusters being inactive (Ricci et al., 2015). These two functional states of chromatin are termed eu- or heterochromatin, respectively. The former assumes an “open” configuration which is accessible for transcription, while the latter is condensed and impenetrable to most transcription factors and transcriptional machinery (Felsenfeld and Groudine, 2003).

Techniques such as DNaseI hypersensitive site sequencing (DNase-Seq) (Boyle et al., 2008) or Assay for Transposase-Accessible Chromatin using Sequencing (ATAC-Seq) (Buenrostro et al., 2013) are able to map chromatin accessibility genome-wide and have revealed distinct chromatin accessibility profiles for different cell types and cellular functions (Buenrostro et al., 2015). Indeed, using a human cell line model for myeloid differentiation, overlaid ATAC-Seq and RNA Sequencing (RNA-Seq) showed that changes in the chromatin landscape were correlated to distinct gene expression profiles that were associated with the specialised function of distinct cell-types (Ramirez et

al., 2017). Thus, the modulation of promoter accessibility significantly contributes to transcriptional regulation (Buenrostro et al., 2015).

The establishment of this regulatory landscape involves the local remodelling of chromatin in response to developmental and environmental cues. This can occur through the activity of chromatin remodelling complexes, such as SWI/SNF, which can reposition nucleosomes or eject histones to create accessible nucleosome-free regions (Eberharter and Becker, 2004). Chromatin accessibility can also be directed by epigenetic histone modifications. Post-translational modifications, such as acetylation and methylation to protruding histone tails, can alter their affinity to DNA. For example, the acetylation of lysine residues neutralises the positive charge of the histone tail, thus weakening the interaction with negatively charged DNA. This loosens the entire nucleosome complex providing improved accessibility to the DNA (Bannister and Kouzarides, 2011). It is therefore common to observe the acetylation of lysine 27 of histone 3 (H3K27Ac) at active promoter elements (Klemm et al., 2019). Active promoters are also decorated with tri-methylated lysine 4 of histone 3 (H3K4me3) (Soares et al., 2017). It is thought that H3K4me3 increases the local hydrophobicity of chromatin, allowing specific transcription factors to engage more favourably with DNA in the aqueous environment of the nucleus (Su et al., 2016). Indeed, H3K4me3 promoter occupancy is associated with the recruitment of histone acetyltransferases (HATs) (such as p300/CBP) as well as positive transcriptional regulators, which consolidate nucleosome accessibility and promote transcriptional activity, respectively (Crump et al., 2011, Lauberth et al., 2013, Soares et al., 2017). Therefore, the composition and epigenetic histone modifications of nucleosomes affect the functional state of chromatin by regulating DNA accessibility to control transcription.

Enhancers

Despite promoters being regulated by chromatin accessibility and the availability of unique combinations of transcription factors, they are not

sufficiently complex to give rise to the intricate gene expression patterns observed in humans (Johanson et al., 2019). Promoters alone do not have the regulatory capacity to process the diverse signals underlying human cell function, suggesting that additional regulatory elements exist to increase the dimensionality of transcriptional regulation.

In metazoans, additional regulatory elements called enhancers are distributed throughout the non-coding genome (Robson et al., 2019). These are distal *cis*-regulatory elements which recruit transcription factors and co-activators to aid the signal-dependent activation of transcription at cognate promoters (Figure 1.3) (Levine et al., 2014, Robson et al., 2019). Similar to promoters, the activity of an enhancer is dictated by changes in chromatin accessibility. Active enhancers are regions free of nucleosomes and enriched for H3K4me1 and H3K27Ac occupancy (Calo and Wysocka, 2013, Pradeepa, 2017). These regions are typically identified by chromatin immunoprecipitation-sequencing (ChIP-Seq) signatures and functionally validated for enhancer activity by sub-cloning the genomic region into reporter systems (Arnold et al., 2013) or through genetic perturbations that disrupt their regulatory activity (Canver et al., 2015, Diao et al., 2016).

It is now apparent that enhancers far outnumber protein-coding genes and their promoters (Levine et al., 2014). In macrophages, the chromatin remodeller PU.1 has been found to shape the enhancer landscape of these cells and give rise to approximately 45 000 identified enhancer regions (Natoli et al., 2011). This large number of enhancers allows for redundant layers of regulation that ensure transcriptional robustness. Furthermore, many of these enhancers are activated by diverse stimuli to regulate a single promoter, increasing the signal diversity that a promoter can respond to (Figure 1.3). Conversely, multiple promoters can be regulated by a single enhancer, enabling multiplexed gene regulation. This suggests that through the complex combinatorial usage of enhancers, the regulatory capacity of the genome is significantly increased to allow for precise spatiotemporal and tissue-specific gene expression.

Strikingly, unlike the proximal nature of promoters, the regulatory information encoded within enhancer regions are distal to the TSS (Robson et al., 2019). Genomic mapping of enhancers have revealed that they are found at vast distances from the genes that they regulate (Johanson et al., 2019). The most well studied promoter-enhancer interaction is the locus control region (LCR) that regulates the transcription of *β-globin*, which is positioned 50 kilobases (kb) away (Tolhuis et al., 2002). Through the formation of chromosomal loops, the distance between these two genomic regions is collapsed, allowing for the LCR to physically contact the *β-globin* promoter and activate transcription (Tolhuis et al., 2002). Forced looping of the LCR to the *β-globin* locus induced ectopic *β-globin* expression, confirming that chromatin contact was essential for transmitting regulatory information from distal enhancers to promoters (Deng et al., 2012). Similarly, live-cell imaging of enhancers, promoters and nascent transcription in Drosophila have also shown that transcriptional bursting corresponds to the proximity of these elements (Chen et al., 2018, Lim et al., 2018). Together, this highlights the importance of genome organisation in regulating active promoter-enhancer contacts for transcription.

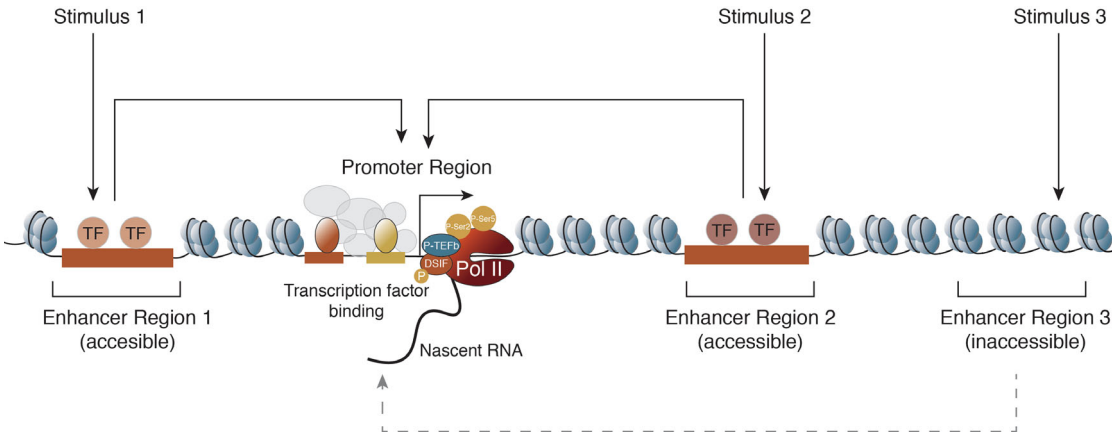

Figure 1.3: The interplay between proximal and distal *cis*-regulatory elements in transcription

Transcription is regulated by proximal (promoter) and distal (enhancer) *cis*-regulatory elements. The functional state of these regulatory elements is governed by the local accessibility of the chromatin to transcription factors and transcription machinery. Promoters primarily serve as docking platforms for transcription machinery at the TSS, while accessible

enhancers recruit transcription factors in a stimulus dependent manner to aid in the loading and activation of Pol II at promoters. Through combinatorial enhancer usage, the regulatory capacity of the genome is significantly increased to allow for transcription to occur in a tissue- and stimulus-specific manner. In the schematic above, this is illustrated as enhancer region 1 and 2 being active (accessible), thus allowing for the activation of the cognate promoter by either stimulus 1 and 2. However, enhancer region 3 is inaccessible in this state, preventing the promoter from responding to stimulus 3. This highlights how transcription is shaped by the enhancer landscape.

In summary, the hallmark of transcriptional activation is the accessibility of the regulatory elements, which include proximal promoter elements as well as distal enhancer elements. Chromatin remodellers and epigenetic histone modifications are able to dynamically shape this landscape for different genes to be permissive for transcription. Furthermore, the combinatorial use of accessible enhancers and promoters provide the computational logic required for complex multicellular functions. The regulation of such promoter-enhancer permutations is coordinated by long-range chromosomal contacts, suggesting that genome organisation provides higher order modalities of transcriptional control.

Nuclear architecture

The eukaryotic nucleus is a dense cellular compartment that houses the genome. In order to fit into this confined space, gDNA is highly condensed at different scales of length. At the smallest, the DNA helix is coiled around nucleosomes to form the chromatin fibre. This undergoes further volumetric compaction through the extensive formation of chromatin loops which constitute entire chromosomes. Over the last two decades, microscopy studies and chromosomal conformation capture (3C) technologies have provided many insights into the principles of genome organisation, including the non-random compaction and positioning of chromosomes and genes, the formation of functionally distinct homotypic chromatin compartments and spatially segregated intra-chromosomal domains. Importantly, it has become evident that these architectural features are imperative for providing higher-

order regulation of gene expression by guiding long-range cognate promoter-enhancer interactions.

The first evidence of nuclear organisation came from microscopy studies which revealed that uncondensed interphase chromosomes occupied discrete nuclear volumes, known as chromosome territories (Figure 1.4) (Cremer and Cremer, 2001). The advent of unbiased genome-wide chromosomal contact maps, generated using Hi-C, showed that that these territories were further sub-divided into two large compartments (5-10 megabases (Mb)) that reflected the functional state of chromatin (Figure 1.4) (Lieberman-Aiden et al., 2009). The A (active) compartment consisted of euchromatin and actively transcribed regions near the nuclear interior, while the B (inactive) compartment was heterochromatised and transcriptionally inactive at the nuclear periphery (Gibcus and Dekker, 2013, Wijchers et al., 2016). Imaging approaches have confirmed that homotypic compartments interact and co-localise in concordance with Hi-C maps (Boettiger et al., 2016). Importantly, spatial segregation according to chromatin state is linked to gene expression and can be dynamically modulated in response to various biological processes. For example, mapping of these compartments in human embryonic stem cells revealed substantial genome reorganisation and compartment switching during lineage specification (Dixon et al., 2015).

At the sub-chromosome level, Hi-C maps revealed that the chromatin fibre is segmented into discrete regions enriched with self-associating chromosomal loops called topologically-associating domains (TADs) (Figure 1.4) (Dixon et al., 2012). The existence of these structures have been corroborated by direct visualisation of chromosome conformation using Oligopaint-labelled DNA fluorescent *in situ* hybridisation (FISH) and super-resolution microscopy (Szabo et al., 2018). With 90% of the genome configured as conserved TADs across different cell-types, these are considered to be ubiquitous 3D units of genome organisation (Finn et al., 2019, Johanson et al., 2019).

Size

Chromosome territories and Comparments

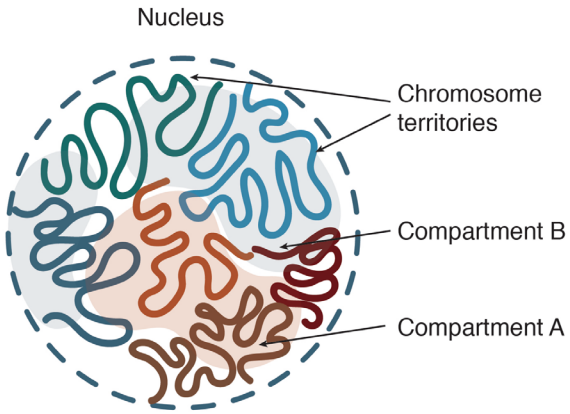

Topologically Associating Domains (TADs)

HiC TAD maps:

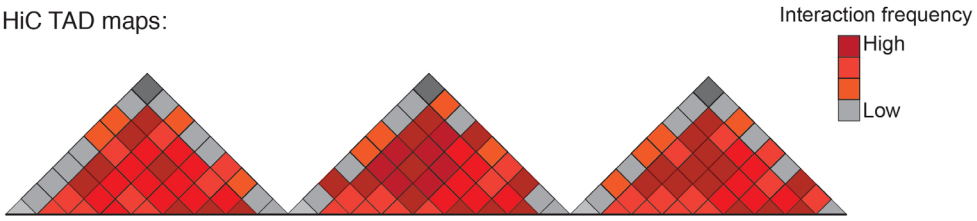

Chromatin fibre:

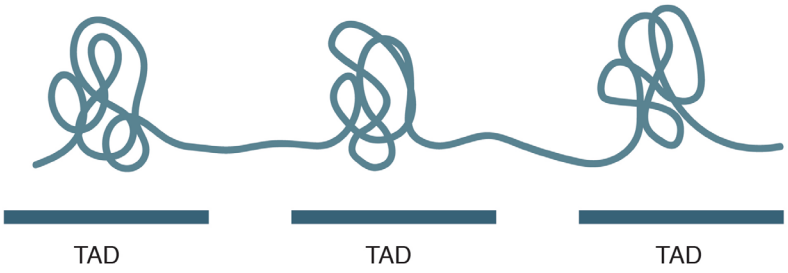

Multi-gene complex/Phase-separated condensate

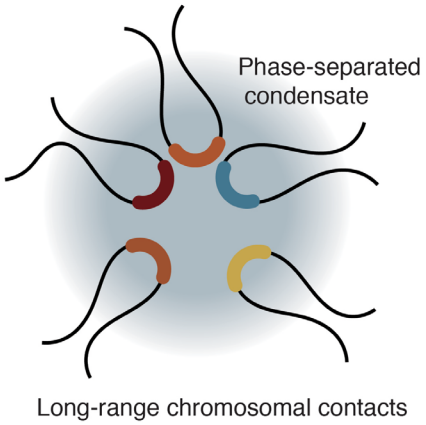

Figure 1.4: The different scales of genome organisation

In the interphase nucleus, uncondensed chromosomes occupy distinct areas in the nucleus called chromosome territories. These territories are further sub-divided into two sub-compartments according to the functional state of the chromatin: the active A compartment of the inactive B compartment. Homotypic compartments tend to cluster together and form chromosomal interactions. At the sub-chromosome level, genome-wide mapping of chromosomal contacts using Hi-C have revealed that the chromatin fibre is segregated into distinct regions enriched for chromosomal contacts, called topologically-associating domains (TADs). Through the formation of chromosomal loops, TADs bring distal regulatory elements and promoters into close spatial proximity. Within this confined space, these genetic elements can interact to engage in multi-gene complexes by forming phase-separated liquid condensates. This facilitates long-range cognate promoter-enhancer interactions which are causal to transcription.

The formation of TADs is dependent on the extrusion and maintenance of chromosomal loops. This process is facilitated by architectural proteins such as CCCTC-binding factor (CTCF) and cohesin. It is thought that cohesin serves as the motor protein that traverses along the DNA and physically extrudes the DNA to form a loop, while convergent CTCF-bound sites serve to delimit the boundaries of the loops that constitute TADs (Sanborn et al., 2015, Ganji et al., 2018). In doing so, genes and regulatory elements that may be separated by large linear genomic distances are able to access each other in 3D space to form multi-gene complexes that can be transcriptionally co-regulated and coordinated (Lupianez et al., 2016). Conversely, this compartmentalised architecture can insulate transcriptional activity by serving as a physical barrier that segregates genes and regulatory elements (Lupianez et al., 2016, Gong et al., 2018).

Numerous genome editing experiments have demonstrated the importance of this organisation, with the loss of TAD boundaries and chromosomal loops resulting in the re-wiring of promoter-enhancer contacts and the ectopic expression of genes. For example, the deletion of a CTCF demarcated boundary at the X chromosome inactivation centre (XIC) resulted in the partial fusion of adjacent TADs and aberrant gene activation (Nora et al., 2012). Large scale genomic rearrangements, such as inversions and duplications,

across TAD boundaries of a region encoding developmental genes, resulted in the disruption of TAD structures and the development of severe limb malformations in mice (Lupianez et al., 2015). CTCF binding sites are also sensitive to DNA methylation, which can compromise CTCF occupancy and loop demarcation. Indeed, targeted CTCF motif methylation using deactivated Cas9 (dCas9) fused to the DNMT3a DNA methyltransferase, disrupted loop configurations that insulated transcriptional activity (Liu et al., 2016). The loss of this insulation capacity has been shown to be causal to many diseases, including gliomas, where gain-of-function mutations that result in the hyper-methylation of DNA, such as at CTCF sites, drive insulator dysfunction and oncogene activation (Flavahan et al., 2016). These examples show that the 3D genomic organisation is imperative for the regulation of transcription by facilitating or limiting genome-wide promoter-enhancer contacts through chromosomal looping and TAD demarcation.

While the formation of TADs facilitate cognate promoter-enhancer contacts, recent evidence has indicated that the physical interaction is coordinated by liquid-liquid phase separation (LLPS) (Figure 1.4). Multivalent proteins or proteins with intrinsically disordered domains can form phase-separated liquid condensates when locally concentrated in the cell. Strikingly, various nuclear-resident proteins, such as transcription factors, proteins from the Mediator complex and Pol II have been observed to form such condensates (Strom et al., 2017, Boija et al., 2018, Cho et al., 2018, Chong et al., 2018, Sabari et al., 2018). Importantly, homotypic condensates are able to interact and mix while excluding other biochemically incompatible biomolecules. This suggests that genomic loci bound by proteins of homotypic biochemistry are able to interact with complementary condensates and create compartments that facilitate specific chromosomal interactions within TADs. In support of this, the assembly of artificial condensates on specific loci resulted in their physical interaction, demonstrating that the mixing of phase-separated liquid condensates can generate mechanical forces that are sufficient to shape chromosomal interactions (Shin et al., 2018).

LLPS and the formation of “transcriptional condensates” provides a more granular understanding of promoter-enhancer contacts. Enhancers (specifically large stretches of enhancers known as super-enhancers) and promoters can serve as nucleation sites for LLPS by recruiting and concentrating various transcription factors and co-activators on chromatin (Robson et al., 2019). Transcription can then be induced when promoter condensates mix with compatible enhancer condensates to form a transcriptional hub that specifies cognate promoter-enhancer interactions (Robson et al., 2019). This would provide highly precise control for the establishment of chromosomal contacts that are causal to transcription within TADs.

It has become clear that the organisation of the genome is non-random, but rather intricately arranged to provide high-order regulation of transcription. Through different scales of organisation, specific promoter-enhancer contacts are facilitated by the formation of increasingly smaller compartments for the sequential minimisation of their genomic search space (Figure 1.4). Numerous immune genes have been found to occupy the same TADs, suggesting that their regulation is coordinated through compartmentalised chromosomal looping events (Jin et al., 2013).

While there are numerous single case studies supporting this model of genomic confinement and function, a recent study done in Drosophila challenged this paradigm (Ghavi-Helm et al., 2019). Using heterozygous mutants that carried a wild-type set of chromosomes as well as a mutant set containing extensive genomic rearrangements, the investigators were able to map and compare the topology and gene expression patterns in an allele-specific manner genome-wide. Remarkably, they found that widespread topological variations only affected a small fraction of nearby gene expression. This suggested that genome topology was uncoupled from gene expression. While this study does not debase the enormous body of work that supports the role of genome organisation in the regulation of gene expression, it does highlight our incomplete understanding of how the genome is

regulated and suggests that there may be other collaborative mechanisms that facilitate the complexity of transcription and gene expression (Finn and Misteli, 2019, Ghavi-Helm et al., 2019).

Long non-coding RNAs (lncRNAs)

Deep sequencing of the transcriptome has revealed that the human genome is pervasively transcribed. However, less than 2% of these transcripts encode for proteins, while the remaining fraction of non-coding transcripts mostly emanates from the "dark" regions of the genome and is largely uncharacterised (Lander et al., 2001, Bertone et al., 2004, Kapranov et al., 2007, Quinn and Chang, 2016). As a result, it was thought that many of these non-coding transcripts were biologically functionless and the result of transcriptional noise. However, through extensive characterisation of the transcriptome over the last two decades, it has emerged that non-coding RNAs play important roles in almost every biological process (Quinn and Chang, 2016).

Small non-coding RNAs (such as transfer RNAs, Piwi-associated RNAs and microRNAs (miRNAs)) are highly conserved and their biological roles have been appreciated for a long time (Kung et al., 2013). In contrast to this, the function of long non-coding RNAs (lncRNAs) have remained elusive and controversial because of their low abundance and poor conservation (Mercer et al., 2011, Kung et al., 2013). Furthermore, they are not easily amenable to study by classical methods developed for mRNAs, thus requiring the development of more specialised tools (Fok et al., 2017). Despite this, there are now numerous examples of well characterised lncRNAs that clearly show their participation in the regulation and fine tuning of gene expression (Wang and Chang, 2011, Quinn and Chang, 2016).

LncRNAs are generally transcribed by Pol II and can arise from promoters and enhancers as well as regions intervening or from within protein-coding genes (Quinn and Chang, 2016). These transcripts often undergo post-

transcriptional modifications including 5′ capping, splicing and 3′ polyadenylation (Quinn and Chang, 2016). Mature lncRNAs assume specific secondary and higher-order conformations which often imbue these transcripts with their functionality. By providing binding sequences and structural domains for interaction with other biomolecules, lncRNAs can essentially serve as the interface between DNA, RNA and proteins (Mercer and Mattick, 2013). With the current catalogue, lncRNAs are curated into four different classes according to their mode of function (Figure 1.5):

Decoys

LncRNAs can function as molecular decoys that competitively sequester transcription factors and miRNAs to regulate gene expression. For example, Lethe is a pseudogene lncRNA that negatively regulates NF-κβ signalling. Lethe is able to interact with and titrate away RelA, a subunit of NF-κβ, preventing the binding and activation of NF-κβ regulated genes (Rapicavoli et al., 2013). Similarly, the pseudogene *PTEN1* was found to bind regulatory miRNAs that target the tumour suppressor gene *PTEN*. In doing so, it sequesters silencing miRNAs away from *PTEN* mRNA, allowing for the expression of *PTEN* to proceed unencumbered (Poliseno et al., 2010).

Scaffolds

LncRNAs can also serve as platforms for the assembly of multi-component biomolecular structures, thereby coordinating diverse functions in space and time. These lncRNAs are able to bind multiple effector partners which can be transcriptionally activating or repressive. In embryonic stem cells, many genes exist in a state of “quantum superposition" by having functionally ambivalent histone marks, such as methylated H3K4 (active) as well as methylated H3K27 (inactive). This state needs to be collapsed during differentiation, so that the chromatin either assumes the active or inactive histone methylation form (Tsai et al., 2010). The lncRNA HOTAIR is able to resolve this ambivalent chromatin state at the HOXD locus, by recruiting both the polycomb

repressive complex 2 (PRC2) as well as LSD1 (Rinn et al., 2007, Tsai et al., 2010). Functionally, this allows for the multiplexing of two distinct histone modifications, as PRC2 methylates H3K27 and the LDS1/CoREST/REST complex demethylates H3K4. Overall, this results in the onset of an inactive chromatin state that represses transcription (Tsai et al., 2010). Thus, HOTAIR functions as a scaffold to recruit two different histone modification complexes to provide combinatorial epigenetic histone alterations that together, suppress gene expression at the HOXD locus.

Guides

A subset of lncRNAs can spatially direct their activity to specific loci in the genome, in *cis* or *trans*. This provides highly specific, spatially regulated control of gene expression. LncRNA activity can be constrained to their site of transcription by Pol II tethering or traverse long-range distances to function at distal sites defined by sequence, structural or biochemical interfaces that confer some kind of specificity (Wang and Chang, 2011). HOTTIP is expressed from the HOXA gene cluster and serves to regulate homeotic gene expression in *cis* during development. It recruits the WD repeat-containing protein 5/Mixed Lineage Leukemia (WDR5/MLL) protein complex to deposit local histone methylation marks, which maintain an active chromatin state across its target genes (Wang et al., 2011). Conversely, HOTAIR is transcribed from the HOXC locus on chromosome 12, but transcriptionally silences genes at the HOXD locus on chromosome 2 by targeted locus-specific recruitment fo the PRC2 silencing complex (Rinn et al., 2007).

Enhancer RNAs (eRNAs)

Owing to the advances in sequencing technologies, such as the development of Cap Analysis of Gene Expression (CAGE), it was found that enhancer regions are actively transcribed (Andersson et al., 2014). Transcription of enhancers occurs bi-directionally to generally produce unspliced and non-polyadenylated transcripts of approximately 300-400 nt in length, termed

eRNAs (Andersson et al., 2014). Early experiments showed that the depletion of eRNAs led to the loss of transcription of nearby genes, while the tethering of eRNAs to reporter genes led to enhanced transcription. These studies provided the first evidence that eRNAs were functional as transcriptional activators (Lai et al., 2013, Lam et al., 2013, Li et al., 2013, Melo et al., 2013). eRNAs are now known to interact with the Mediator complex and facilitate chromosomal looping of enhancers to cognate promoters to activate transcription (Lai et al., 2013). Importantly, the transcription of different eRNAs was found to be cell-type specific and responsive to a variety of developmental and cellular contexts, allowing for them to aid in the precise spatiotemporal and tissue-specific regulation of gene expression (Lai et al., 2013, Andersson et al., 2014).

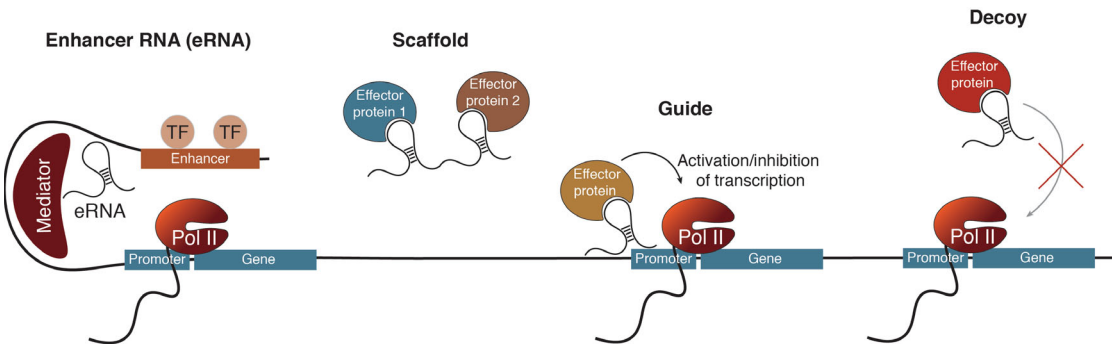

Figure 1.5: The different molecular mechanisms of lncRNA function in the regulation of transcription

LncRNAs emanating from enhancer regions (eRNAs) interact with the Mediator complex to facilitate chromosomal looping of enhancers to their cognate promoters for transcriptional activation. LncRNAs can also serve as scaffolds for multiple protein complexes, allowing them to exhibit multi-function capabilities in regulating transcription. They can also function as guides that target transcriptional regulators to particular loci or act as decoys that titrate proteins and RNAs (such as miRNAs) away to modulate transcription.

Currently, lncRNAs constitute 70% of the transcriptome, but only a small fraction of these have been well studied. As technologies continue to advance, the catalogue of lncRNAs will only grow, widening the gap in our knowledge. By developing our understanding of the role of these diverse molecules in various biological processes, they might emerge as novel drug

targets for the next generation of therapeutics. Such therapeutic modalities will function at the transcriptional level and may prove to be more efficacious than the current post-translational modulators, which often rely on a mechanism of protein titration.

Aims

While inflammation provides essential immunological protection, its dysregulation is also a major contributor to many diseases, including diabetes, atherosclerosis, gout and rheumatoid arthritis (Netea et al., 2017). In order to develop novel therapies that can modulate pathogenic inflammation more effectively, it is paramount that a clear understanding of the mechanisms that regulate inflammation is established. For example, novel insights into the role of tumour-associated macrophages have revealed that these immune cells are reprogrammed by the tumour microenvironment to become immunosuppressive of the T-cell mediated anti-tumour response. As a result, this allows for the tumour to evade immune surveillance and continue its progression uninhibited (Aras and Zaidi, 2017). Therapeutics that can reverse the immunosuppressive state of the macrophages have been shown to be beneficial in delaying tumour growth (Tian et al., 2013, Liu et al., 2015). Other methods involve the inhibition of this negative immune regulation by disrupting receptor-ligand interactions that are causal to T-cell dysfunction (Seidel et al., 2018). By reactivating and exploiting the immune response, these immunotherapies have proven to be a highly effective form of treatment for certain cancers and driven the tremendous growth in the industry seen in recent years. In contrast, sepsis is caused by the severe dysregulation of the inflammatory response and is the leading cause of hospital-related deaths worldwide. Despite this, treatment options have remained severely limited and archaic (Hotchkiss et al., 2009, Waterhouse et al., 2018). This is because no new treatments for sepsis have successfully been introduced in the last 25 years due to the poor understanding of the pathogenic mechanisms underlying sepsis (Hotchkiss et al., 2009, Waterhouse et al., 2018).

These examples highlight the pervasive role of innate immunity in maintaining health and driving disease. They also underscore the need to gain deeper insights into the fundamental processes that regulate the inflammatory response, in order effectively modulate its function. Transcription has been implicated as a key regulator of the inflammatory response (Escoubet-Lozach et al., 2011, Rabani et al., 2011, Bhatt et al., 2012). It is clear that the eukaryotic cell is replete with regulatory mechanisms that cooperatively function to govern the precise transcription of the genomic code. These include the organisation of the genome to coordinate specific promoter-enhancer contacts and the role of lncRNAs to fine tune locus-specific transcription. While there is a good working model that describes the many facets of transcriptional regulation in the nucleus, many of the molecular mechanisms and networks that regulate transcription specifically during the inflammatory response remain poorly understood. Therefore, the broad aim of this work was to dissect the molecular mechanisms and genetic circuitry that regulate some of the fundamental aspects of inflammation:

1. The rapid and robust transcriptional activation of the innate immune genes
2. The coordination of pro- and anti-inflammatory cytokine transcription for the biphasic regulation of inflammation
3. The role of these molecular mechanisms in regulating innate immunological memory (trained immunity)

Chapter 2

A LONG NON-CODING RNA PRIMES IMMUNE GENE EXPRESSION IN THE ELR+ CXCL CHEMOKINE TAD

Introduction

The initial phase of inflammation is characterised by the transcriptional activation of various pro-inflammatory cytokines and chemokines, which are involved in cellular signalling and chemotaxis, respectively (Rogatsky and Adelman, 2014). Importantly, the rapid and robust transcriptional activation of these immune genes is fundamental to the success of this pro-inflammatory phase. In order to meet the fast transcriptional kinetics required, the promoters of many pro-inflammatory immune genes exist in a primed state (Fowler et al., 2011, Bhatt et al., 2012). This allows for their rapid activation by signal-dependent transcription factors (Bhatt et al., 2012).

Tumour necrosis factor (TNF) can induce the pro-inflammatory response through the rapid transcriptional induction of immune genes (Paulsen et al., 2013). Hi-C studies have shown that numerous TNF-responsive genes co-occupy TADs, suggesting their potential co-regulation (Jin et al., 2013). Remarkably, mapping of these chromosomal contacts revealed that TNF-responsive promoter-enhancer contacts were pre-formed in the unstimulated state (Jin et al., 2013). Intuitively, pre-formed chromosomal loops reduce the stochasticity of transcription by creating insulated compartments from which co-regulated genes can be primed and robustly transcribed. In contrast, the slower transcriptional kinetics associated with the dynamic formation of promoter-enhancer contacts may subvert the effectiveness of pro-inflammatory immune gene transcription. Thus, the 3D organisation of innate

immune genes may play an important role in aiding the rapid and robust transcription of pro-inflammatory genes.

Within the TNF-responsive immune gene TADs, TNF induction of transcription was shown to be independent of SWI/SNF chromatin remodelling (Ramirez-Carrozzi et al., 2009). This suggests that the chromatin of rapidly responsive immune genes is accessible prior to stimulation. In contrast, interferon-β (IFN-β)-induced transcription is dependent on SWI/SNF activity, and as a result has slower activation kinetics (Ramirez-Carrozzi et al., 2009). The accessible state of TNF-responsive genes allows for their regulation at the level of Pol II pause-release (Adelman et al., 2009). This means that the promoters of these immune genes exist in a poised state, where the PIC is pre-assembled and Pol II activity has been paused on the promoter (Figure 1.2). This allows for these promoters to be rapidly activated by signal-dependent transcription factors which recruit P-TEFb to release Pol II from its suspended state upon stimulation (Hargreaves et al., 2009).

At the promoters of these rapidly inducible genes, dense CpG islands and epigenetic histone modifications, such H3 and H4 acetylation and H3K4me3, maintain the euchromatin state and instruct the pre-loading of transcriptional machinery, respectively (Ramirez-Carrozzi et al., 2009, Fenouil et al., 2012, Rogatsky and Adelman, 2014). In particular, H3K4me3 is a prominent histone mark that has been shown to epigenetically prime promoters and direct the assembly of the PIC (Lauberth et al., 2013). The loading of Pol II during PIC assembly is mediated by the general transcription factor II D (TFIID), which is responsible for core promoter recognition and binding (Thomas and Chiang, 2006, Juven-Gershon et al., 2008). In two seminal studies, TFIID was found to selectively bind H3K4me3 via the TATA box-binding protein 3 (TAF3) subunit, thus allowing for the selective assembly of the PIC at H3K4me3 marked genes (Vermeulen et al., 2007, Lauberth et al., 2013). In support of this, it is thought that H3K4me3 increases the local hydrophobicity of chromatin and assists with the cooperative binding of transcription factors to DNA in the aqueous nucleoplasm (Su et al., 2016). Further functional studies have

demonstrated that H3K4me3 is causal to transcription (Cano-Rodriguez et al., 2016). Using the histone methyltransferase PRDM9 fused to dCas9, targeted local H3K4me3 deposition at promoter regions induced the expression of transcriptionally silenced genes (Cano-Rodriguez et al., 2016). Therefore, H3K4me3 is instructive of transcription and is predictive of the transcriptional responsiveness and strength of a promoter (Lauberth et al., 2013, Saeed et al., 2014). While it is clear that this epigenetic histone modification is essential for establishing the primed state of rapidly responsive genes, such as the pro-inflammatory genes, the preceding molecular mechanisms that spatially direct the discrete deposition of H3K4me3 at these specific promoters have remained unknown.

In a recent study, our laboratory described the discovery and function of a novel family of lncRNAs, called Immune-gene Priming LncRNAs (IPLs) (Fanucchi et al., 2019). These were found to epigenetically prime the transcriptional response of innate immune genes. Using a bespoke bioinformatic pipeline that integrated chromosomal contact (from Hi-C and Chromatin Interaction Analysis by Paired-End Tag Sequencing (ChIA-PET)), CAGE and ChIP-Seq datasets, it was revealed that an IPL emanated from within each of the TADs containing primed TNF-responsive genes. Classification of these TADs revealed sub-classes where (1) an IPL made chromosomal contact with a single primed TNF-responsive gene or (2) an IPL made chromosomal contacts with multiple primed TNF-responsive genes. In depth mechanistic studies demonstrated that the IPLs interacted with the WDR5/MLL1 complex to direct local H3K4me3 accumulation. By exploiting the 3D genome architecture, the IPLs were able to spatially direct H3K4me3 deposition on the promoters of TNF-responsive immune genes and prime their transcriptional activity.

One candidate IPL, called UMLILO (Upstream Master LncRNA of the Inflammatory chemokine LOcus), was found to emanate from the glutamic acid-leucine-arginine positive (ELR+) CXCL chemokine TAD and made chromosomal contacts with *interleukin-8* (*IL-8*), (C-X-C motif chemokine

ligand 1) *CXCL1*, *CXCL2* and *CXCL3* (Fanucchi et al., 2019). The expression of these chemokines are responsible for the induction of neutrophil chemotaxis, which is essential for amplifying the pro-inflammatory response and initiating offensive measures, such as phagocytosis, the release of anti-microbials and the production of neutrophil extracellular traps (Kobayashi, 2008, Amulic et al., 2012). It was hypothesised that this lncRNA functioned as a typical IPL to regulate the transcriptional priming and activity of these chemokines.

In this chapter UMLILO was functionally validated for IPL activity. This included the depletion of UMLILO and measuring the effect on the transcription, chromosomal contacts and H3K4me3 accumulation on neighbouring chemokine genes. The results presented here demonstrate that UMLILO exploits the local 3D topology to access neighbouring chemokine genes and regulate their transcription through the discrete deposition of H3K4me3 at their promoters.

Materials and Methods

Bioinformatic analysis

Previously unpublished Hi-C data was analysed and the interaction heat map was generated by Maxim Imakaev as previously described (Imakaev et al., 2012). ChIA-PET data from TNF treated primary human umbilical vein endothelial cells (HUVECS) enriched for Pol II (Ser2/5) mediated chromosomal contacts was obtained from the National Centre for Biotechnology Information (accession number: GSE41553) (Papantonis et al., 2012). Recovered PETs were processed and analysed by Maxim Imakaev as described by Fanucchi et al., 2019. ChIP-Seq data made use of the Encyclopaedia of DNA Elements (ENCODE) database and was visualised using the UCSC Genome Browser (https://genome.ucsc.edu). CAGE data was from the Functional Annotation of the Mammalian Genome 5 (FANTOM 5) database and visualised using the Zenbu Browser (http://fantom.gsc.riken.jp/zenbu).

Cell culture

HUVECs (Lonza) were grown using the Endothelial Cell Growth Medium-2 (EGM-2) Bullet Kit (Lonza) containing Endothelial Basal Medium, vascular endothelial growth factor (concentration not specified by EGM-2 kit) and 2% foetal bovine serum (FBS). Cells were cultured in T25 flasks in a humidified incubator with 5% CO_2 at 37˚C until 80% confluent (as determined by inspection using a light microscope) before sub-culturing. To dissociate the cells, the cell culture medium was discarded, the cells were washed with 1X phosphate buffered saline (PBS) (Thermo Fisher Scientific) and treated with 1 ml TrypLE Express (Thermo Fisher Scientific). After 2-3 minutes of incubation at 37˚C, 1 ml of complete cell culture medium was added to neutralise the TrypLE. Repeat pipetting was performed to dissociate the cells into a single-cell suspension, after which 80% of the cell suspension was discarded.

Complete cell culture medium was then added to make up a final volume of 5 ml.

HeLa cells (Sigma-Aldrich) were cultured in Dulbecco's Modified Eagle Medium (DMEM) (Thermo Fisher Scientific) containing 1% GlutaMAX (Thermo Fisher Scientific) and 10% FBS (Thermo Fisher Scientific). HeLa cells were sub-cultured in the same way as described for HUVECs.

HUVEC stimulation with TNF and reverse transcription quantitative PCR (RT-qPCR)

$2x10^5$ HUVECs were seeded into a 24-well plate and serum starved (HUVEC medium with 0.5% FBS) for 24 hours. The cells were then treated with 10 ng/ml of TNF (Sigma-Aldrich) for 30 minutes. RNA was extracted from these cells according to the instructions of the Direct-zol RNA Miniprep Kit (Zymo) (Appendix A2.1). 1 μg of this RNA was then converted to cDNA using the SuperScript IV First-Strand Synthesis System according to the manufacturer's instructions (Appendix A2.2) (Thermo Fisher Scientific). qPCR was performed using the CFX Real-Time PCR Detection System (Bio-Rad) and the following reaction was set up as technical duplicates: 1 μl of the cDNA library, 0.25 μM forward primer, 0.25 μM reverse primer, 5 μl of the Sso Advanced Universal SYBR Green Supermix (Bio-Rad) and made up to a final volume of 10 μl with water. Reactions were subject to the following cycle conditions: initial denaturation of 95˚C for 3 mins, and 45 cycles of denaturation at 95˚C for 10 seconds, primer annealing at 55˚C for 10 seconds, extension at 72˚C for 20 seconds. Amplicons were verified by melt curve analysis (ramp up from 65-95˚C at 0.5˚C increments). Relative expression levels were calculated according to the delta delta Ct method using *HPRT* as the house-keeping gene. Relative fold changes were then calculated by normalising relative expression values to the control condition of each experiment. Primer sequences are provided in Table 1.1.

Table 1.1: List of primers used for RT-qPCR

Primer Name	Sequence (5′ - 3′)
UMLILO F	ACATGTGGAGATTAAGACCCATAA
UMLILO R	TGGAGTGTTGCTGCGAGAAT
IL-8 F	AGGGCCAAGAGAATATCCGA
IL-8 R	GGACTTGTGGATCCTGGCTA
CXCL1 F	AGCTTGCCTCAATCCTGCAT
CXCL1 R	CCTCCTCCCTTCTGGTCAGT
CXCL2 F	CACAGTGTGTGGTCAACATTTCTC
CXCL2 R	ACACAGAGGGAAACACTGCATAA
CXCL3 F	TCTGGAATCCGAGACGATGG
CXCL3 R	GACAGGAAAGGCACGACTTC
ANKRD17 F	AATGTTGCCACCACTCTTCC
ANKRD17 R	TGCAGCTGTGCATTCTTTTC
HPRT F	GATTAGCGATGATGAACCAGGTT
HPRT R	CCTCCCATCTCCTTCATGACA

siRNA depletion of UMLILO

A siRNA pool targeting UMLILO (Table 1.2) (Dharmacon) was delivered into HUVECs by electroporation using the Neon Transfection System (Thermo Fisher Scientific). $1.5x10^5$ HUVECs were prepared according to the instructions provided by the Neon Transfection System (Appendix A2.3) and were electroporated with 20 nM of the siRNA pool in a 10 μl tip according to the following parameters: 1 pulse of 1 350 V for 30 ms. The electroporated cells were immediately seeded in a 24-well plate with 0.5 ml of complete HUVEC medium per well for the cells to recover. After 24 hours, the medium was replaced with HUVEC medium containing 0.5% FBS to serum starve the cells for 24 hours. 48 hours post-electroporation, the cells were then stimulated with 10 ng/ml TNF for 30 minutes prior to RNA extraction, cDNA synthesis and qPCR (as described above).

Table 1.2: List of siRNA sequences used to target UMLILO

siRNA Sequence (5′ - 3′)
AUC UUA AAU UAG AGG CGA AUU
CAU ACA AAU UCU CGC AGC AUU
AAG AGU UGG UAC ACG GUG AUU
GCA UAU UAA CCC UAC AAG UUU

3C

3C was performed following the protocol described by Hagege et al., with minor modifications (Hagege et al., 2007). Briefly, $8x10^6$ singlet HeLa cells were resuspended in 10% (v/v) FBS/PBS and crosslinked with 1% formaldehyde for 10 minutes at room temperature. The formaldehyde was quenched with 0.125 M cold glycine and incubated for 5 minutes on ice. The fixed cells were harvested by centrifugation at 225 g for 8 minutes at 4°C and lysed in 3C lysis buffer (Appendix A3.1) for 30 minutes. To aid this lysis, the cell suspension was dounce homogenized with pestle B. The nuclei were then collected by centrifugation at 400 g for 5 minutes at 4°C. The pellet was resuspended in 1.2X Buffer R (Thermo Fisher Scientific) with 0.3% SDS. This was incubated at 37°C for 1 hour with gentle shaking. 2% Triton X-100 was added and incubated at 37°C for 1 hour to sequester the SDS. 550 units of HindIII (Thermo Fisher Scientific) was incubated with the mixture at 37°C overnight and gentle shaking. The following day, 1.3% of SDS was added and incubated at 65°C for 20 minutes to stop the digestion. 6.125 ml of 1.15X T4 ligation buffer (Thermo Fisher Scientific) and 20% Triton X-100 was then added and incubated for 1 hour at 37°C with gentle shaking. 100 U of T4 ligase (Thermo Fisher Scientific) was added to the reaction and incubated at 16°C for 4 hours with gentle shaking, followed by 30 minutes at room temperature. 300 µg of Proteinase K (Thermo Fisher Scientific) was added to reverse the crosslinks. This was incubated at 65°C overnight. RNA was then digested with 300 µg of RNAse A and incubated at 37°C for 30 minutes. The remaining genomic DNA was then purified by phenol/chloroform extraction

and precipitated using isopropanol. 3C reactions were mixed with an equal volume of phenol-chloroform and mixed vigorously. These were decanted into a Maxtract tube (Qiagen) and centrifuged at 1 800 g for 10 minutes at room temperature. The DNA in the recovered supernatant was then precipitated by adding an equal volume of isopropanol, 10% (of original volume) 3M sodium acetate and 5 μl Glycoblue. The mixture was vortexed and then incubated at -80˚C for 1 hour. Precipitated DNA was recovered by centrifugation at 3 000 g for 30 minutes at 4˚C. DNA pellets were washed twice with 500 μl of ice cold 70% ethanol. Recovered 3C libraries were resuspended in 50 μl TE buffer (Appendix A3.2).

Proximity ligated DNA products were detected using unidirectional primers (Table 1.3) and qPCR. These primers were designed by mapping all HindIII sites within this region and simulating proximity ligation products in Snapgene. Using these chimeric products as templates, Primer Blast (https://www.ncbi.nlm.nih.gov/tools/primer-blast/) was used to identify primers that had a uniform annealing temperature and were specific to the 3C ligation product. The function of each primer was tested in combination with the universal anchor primer by PCR. Resultant amplicons were visualised by agarose gel electrophoresis (Appendix A1.1). Primer amplification efficiency was determined by performing qPCR on a dilution series of a control 3C library (Appendix A1.1). Primers that were efficient and specific when annealed at 58˚C were chosen for the assay.

qPCR to measure interaction frequencies was performed on the CFX Real-Time PCR Detection System (Bio-Rad) and the following reaction was set up as technical triplicates: 1 μl 3C library, 0.25 μM anchor primer, 0.25 μM test primer, 5 μl Sso Advanced Universal SYBR Green Supermix (Bio-Rad) and made up to a final volume of 10 μl with water. qPCR reactions were carried out with an initial denaturation of 95˚C for 3 mins, and 35 cycles of denaturation at 95˚C for 10 seconds, primer annealing at 58˚C for 10 seconds, extension at 72˚C for 20 seconds. Amplicons were verified by melt curve analysis (ramp up from 65-95˚C at 0.5˚C increments). A putative

interacting genomic region (*GAPDH*) was used to normalise for variation between 3C library preparations. Interaction frequencies were further normalised to random interaction frequencies as determined by a 3C library prepared from a bacterial artificial chromosome (RP11-68O13, Empire Genomics) containing the genomic region of interest.

In order to deplete UMLILO prior to assaying chromosomal contacts by 3C, siRNAs (20 nM) were delivered by RNAiMax (Thermo Fisher Scientific) transfection, according to the manufacturer's protocol (Appendix A2.4), into the HeLa cells 48 hours before harvesting their cell nuclei.

Table 1.3 List of primers used for 3C-qPCR

Primer Name	Sequence (5′ - 3′)
Anchor	TCCTCTGACATAATGAAAAGATGAGGGTGC
Primer 1	AAAATAGAAACCCTGAATGTACCGGTAACA
Primer 2	TCAAATCCGTGATCAGCATTACCAAGCCAT
Primer 3	ATTGGAAGGCTAAATATACTTACATGGC
Primer 4	TTTTAAAAGCAGCACTAGTGTATCCGG
Primer 5	AAAGAGCTCAATGTGTGTTACTAAAGAATG
Primer 6	AAAGGTAAGCAATAATTGGCCCATATCTC
Primer 7	AAAAGTGATACATGTTCATTGCATTTAAAC
Primer 8	CGTAAGGCTGGTCAAGGTATGCTGAG
Primer 9	TTCTTCATTATGCTAGTGTTGTGTATTGTG
Primer 10	TGAAATTAGAGAAAAACATGTACTTAGGGA
Primer 11	CACCCCGCCCATTTGATGAACTGTTT
Primer 12	ACTTCAAACTCCAAACTCCACCGATTTG
Primer 13	CCAACATCACTGAAGCAAAGAAACTTGGAG
Primer 14	TCTGCTTGTACGTAGGTATGTAGATT
Primer 15	GCTAGCAACCAACTCTTTAAGAATACAGCC
Primer 16	AGAAACACAACGATACAATGTGAAA
Primer 17	AGTGTGACTCCAAATAACCTAGTTTGCTA

Primer 18	ACACAGTCATAATCACAACCCCAGTC
Primer 19	TCAGACTCATGGGCTCAGTTGATTC
Primer 20	GGCTGACACATTATGGTCTCCCACTAAATA
Primer 21	GAAACATGTCAAGAGGCCGTGGACATTT
Primer 22	AGTGTGAAACAAAACGAGAAGGGAAG
Primer 23	AAATTATTTGCTTTAGGAAGGGAAGTAGAA
Primer 24	CATAGGAGAGACTGCGACAGAAATTCCATT
Primer 25	TTACAACTCCTACAACCGTGCTTGGTACAT
GAPDH control F1	TGCCAATCTCCTTGTTTTCTAATG
GAPDH control F2	TATTCCCCCAGGTTTACATGTTC

ChIP-qPCR:

$1x10^6$ HUVECs were fixed with 3.7% formaldehyde for 10 minutes at room temperature. The cells were washed with cold PBS three times, after which 0.125 mM of cold glycine was added and incubated for 5 minutes at room temperature with gentle shaking. The cells were then washed twice with 10 ml cold PBS, resuspended in 5 ml of PBS and centrifuged at 1000 g for 5 minutes. The pellet was resuspended in FA lysis buffer (Appendix A3.3) and sonicated using the Covaris S220 Sonicator to generate DNA fragments between 500 - 1000 bp in size. The sonicated material was collected by centrifugation at 8 000 g for 30 seconds at 4°C. 50 µl of each sample was reserved to serve as an input control to normalise for DNA concentration. Each immunoprecipitation reaction contained 25 µg of protein, 1:10 RIPA buffer (Appendix A3.4) and 1 µg of the appropriate ChIP-grade antibody (anti-H3K4me3 (ab8580; Abcam), MED12 (A300–774A; Bethyl Laboratories), anti-RNA Pol II (Ser5) (ab5131; Abcam), anti-WDR5 (ab56919; Abcam). A mixture of protein A and G magnetic beads (Resyn Biosciences) was prepared by pre-absorbing with sonicated single-stranded salmon sperm DNA (1.5 µg per 20 µl beads) and incubated with the reactions at 4°C overnight with rotation. Magnetically capture beads were washed three times with 1 ml wash buffer (Appendix A3.5) and then once with final wash buffer (Appendix A3.6). The

captured DNA was eluted from the beads by adding 120 µl elution buffer (Appendix A3.7) and incubating at 37°C for 15 minutes with rotation. The DNA was then purified using phenol/chloroform extraction and precipitated as previously described. Pelleted DNA libraries were resuspended in 50 μl TE buffer (Appendix A3.2). qPCR primer sequences are provided in Table 1.4. qPCR was performed as previously described for 3C. Percentage of input was calculated using the following: $2^{-(\text{experiment ct - input ct})}$

Table 1.4: List of primers for ChIP-qPCR

Primer Name	Sequence (5′ - 3′)
IL-8 F	TGGGCCATCAGTTGCAAATC
IL-8 R	AGTGAGATGGTTCCTTCCGG
CXCL1 F	ACGTGGGTCTAAGGGATCTG
CXCL1 R	GGGTCTGACTGTCTTGCGTA
CXCL2 F	CTGTGGTGGTTCTCAGGGAT
CXCL2 R	TGGACTCTGAGACTCTGGGA
CXCL3 F	TCTGGAATCCGAGACGATGG
CXCL3 R	GACAGGAAAGGCACGACTTC
ANKRD17 F	AATGTTGCCACCACTCTTCC
ANKRD17 R	TGCAGCTGTGCATTCTTTTC

Results

UMLILO emanates from the ELR+ CXCL chemokine TAD

The 3D organisation of the genome is essential for mediating specific chromosomal contacts which are causal to transcription (Deng et al., 2012, Fanucchi et al., 2013, Morgan et al., 2017). Genome-wide chromosomal contact maps, such as those generated by Hi-C or ChIA-PET can help identify target genes that are regulated by specific distal elements. Analysis of previously unpublished Hi-C data indicated that the ELR+ CXCL chemokine genes (*IL-8*, *CXCL1*, *CXCL2* and *CXCL3*) co-occupy the same TAD on chromosome 4 (Figure 2.1A). UMLILO, a previously uncharacterised multi-exonic lncRNA that is 575 nt in length, emanated from this TAD.

In order to gain better resolution of specific chromosomal contacts within this region, publicly available ChIA-PET data generated from HUVECs was examined (Papantonis et al., 2012). PETs recovered by this method are enriched by immunoprecipitation of a particular chromatin-interacting protein of interest, thus retrieving very specific contacts (Fullwood et al., 2009). We examined the dynamics of chromosomal contacts within the ELR+ CXCL chemokine TAD that were mediated by actively transcribing Pol II Ser2/5 in response to TNF stimulation. Prior to TNF exposure, very few Pol II-mediated contacts were observed within the TAD, as the genes were transcriptionally inactive in this unstimulated state. Numerous Pol II-mediated contacts emerged after 30 minutes of TNF stimulation (Figure 2.1 B). Importantly, there was an enrichment of these contacts specifically between UMLILO and the ELR+ CXCL chemokine genes, suggesting the formation of a multi-gene complex by chromosomal looping during active transcription.

Next, ChIP-Seq data from ENCODE was analysed to determine the chromatin state of the genes in unstimulated primary HUVECs and HeLa cells. The chemokine genes in contact with UMLILO were enriched for active epigenetic histone marks (H3K4me1, H3K4me2, H3K4me3 and H3K27Ac) (Figure 2.1C).

Specifically, the enrichment of H3K27Ac indicated that each of these genes were accessible prior to stimulation. The lack of H3K36me3 (a mark of active transcription) and the enrichment of H3K4me3 confirmed that these genes were not being actively transcribed in the unstimulated state, but rather primed for transcriptional activation (Sims and Reinberg, 2009). This appeared to be true for all the chemokine genes in this TAD, with the exception of *CXCL1* in the HeLa dataset.

CAGE is a highly sensitive genome-wide method for detecting the 5′ end of transcripts and the mapping of TSSs (Shiraki et al., 2003). CAGE data available from the FANTOM consortium corroborated previous RNA-Seq annotations of UMLILO. It confirmed that UMLILO was transcribed in the sense (forward) direction and expressed in multiple cells types, including professional immune cells such as macrophages and neutrophils, as well as non-immune cells such HUVECs and HeLa (Figure 2.1D). Importantly, UMLILO was detected in immune challenged and unchallenged cells, albeit at significantly lower levels in the resting cells. This indicated that UMLILO was transcribed at a basal level in unstimulated cells.

Taken together, UMLILO emerges from the ELR+ CXCL chemokine TAD containing *IL-8*, *CXCL1*, *CXCL2* and *CXCL3*. These genes are epigenetically primed prior to their activation and specifically engage in chromosomal contacts with UMLILO during active transcription. This suggests that these genes may be co-regulated by UMLILO.

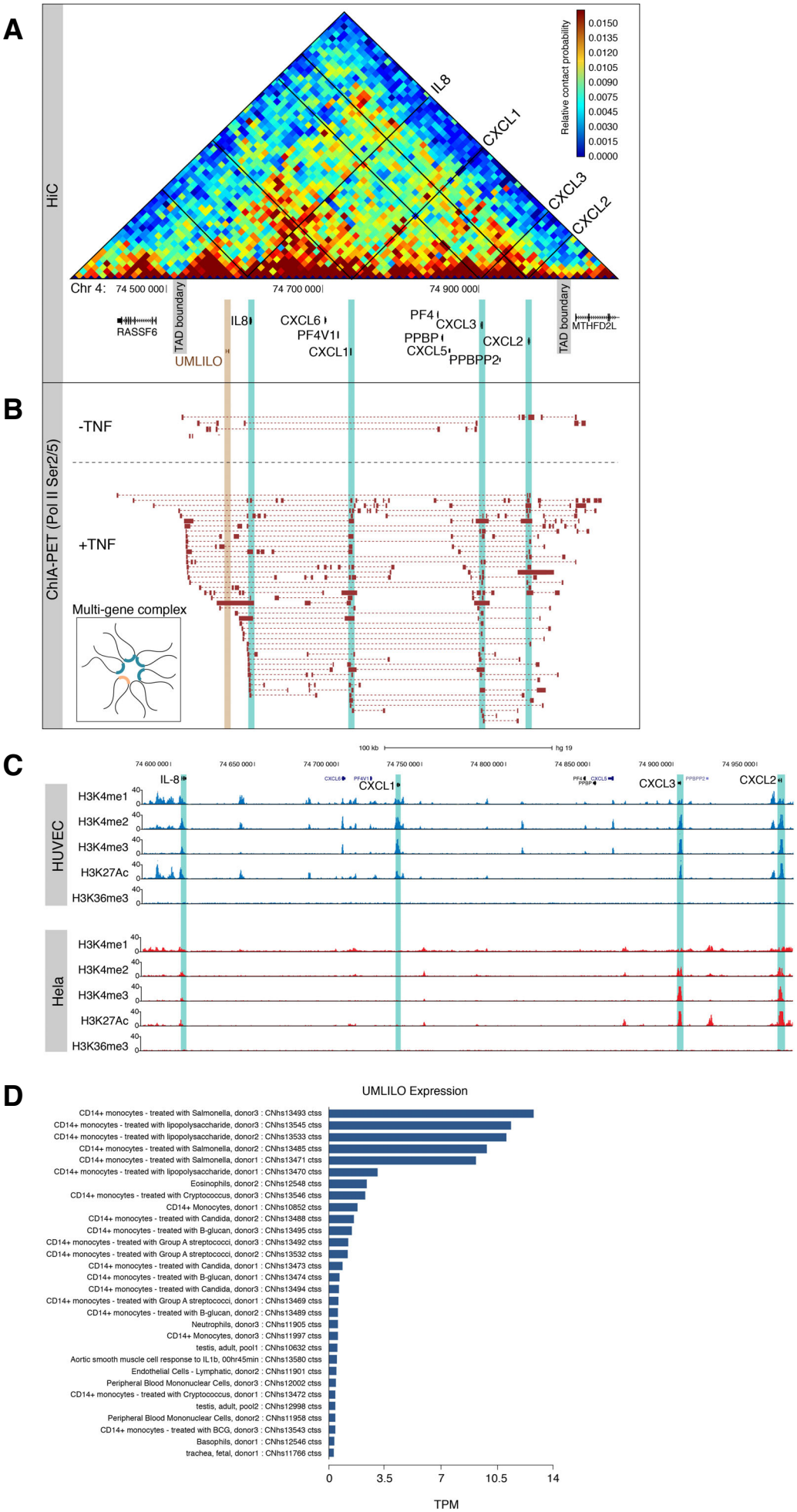
A
HiC
Relative contact probability
0.0150
0.0135
0.0120
0.0105
0.0090
0.0075
0.0045
0.0030
0.0015
0.0000
IL8
CXCL1
CXCL3
CXCL2
Chr 4: 74 500 000 74 700 000 74 900 000
RASSF6
TAD boundary
UMLILO
IL8
CXCL6
PF4V1
CXCL1
PF4
CXCL3
PPBP
CXCL5
PPBPP2
CXCL2
TAD boundary
MTHFD2L
B
ChIA-PET (Pol II Ser2/5)
-TNF
+TNF
Multi-gene complex
C
100 kb
hg 19
74 600 000
74 650 000
74 700 000
74 750 000
74 800 000
74 850 000
74 900 000
74 950 000
IL-8
CXCL1
CXCL3
CXCL2
HUVEC
H3K4me1
H3K4me2
H3K4me3
H3K27Ac
H3K36me3
Hela
H3K4me1
H3K4me2
H3K4me3
H3K27Ac
H3K36me3
D
UMLILO Expression
CD14+ monocytes - treated with Salmonella, donor3 : CNhs13493 ctss
CD14+ monocytes - treated with lipopolysaccharide, donor3 : CNhs13545 ctss
CD14+ monocytes - treated with lipopolysaccharide, donor2 : CNhs13533 ctss
CD14+ monocytes - treated with Salmonella, donor2 : CNhs13485 ctss
CD14+ monocytes - treated with Salmonella, donor1 : CNhs13471 ctss
CD14+ monocytes - treated with lipopolysaccharide, donor1 : CNhs13470 ctss
Eosinophils, donor2 : CNhs12548 ctss
CD14+ monocytes - treated with Cryptococcus, donor3 : CNhs13546 ctss
CD14+ Monocytes, donor1 : CNhs10852 ctss
CD14+ monocytes - treated with Candida, donor2 : CNhs13488 ctss
CD14+ monocytes - treated with B-glucan, donor3 : CNhs13495 ctss
CD14+ monocytes - treated with Group A streptococci, donor3 : CNhs13492 ctss
CD14+ monocytes - treated with Group A streptococci, donor2 : CNhs13532 ctss
CD14+ monocytes - treated with Candida, donor1 : CNhs13473 ctss
CD14+ monocytes - treated with B-glucan, donor1 : CNhs13474 ctss
CD14+ monocytes - treated with Candida, donor3 : CNhs13494 ctss
CD14+ monocytes - treated with Group A streptococci, donor1 : CNhs13469 ctss
CD14+ monocytes - treated with B-glucan, donor2 : CNhs13489 ctss
Neutrophils, donor3 : CNhs11905 ctss
CD14+ Monocytes, donor3 : CNhs11997 ctss
testis, adult, pool1 : CNhs10632 ctss
Aortic smooth muscle cell response to IL1b, 00hr45min : CNhs13580 ctss
Endothelial Cells - Lymphatic, donor2 : CNhs11901 ctss
Peripheral Blood Mononuclear Cells, donor3 : CNhs12002 ctss
CD14+ monocytes - treated with Cryptococcus, donor1 : CNhs13472 ctss
testis, adult, pool2 : CNhs12998 ctss
Peripheral Blood Mononuclear Cells, donor2 : CNhs11958 ctss
CD14+ monocytes - treated with BCG, donor3 : CNhs13543 ctss
Basophils, donor1 : CNhs12546 ctss
trachea, fetal, donor1 : CNhs11766 ctss
0
3.5
7
10.5
14
TPM

Figure 2.1: UMLILO emanates from the ELR+ CXCL chemokine TAD and engages in specific chromosomal contacts with the chemokine genes

(A) Hi-C analysis showed that UMLILO emanates from a TAD containing TNF-responsive ELR+ CXCL chemokine genes.

(B) ChIA-PET interactions showing the dynamics of Pol II-mediated (ser2/5) chromosomal contacts in HUVECs, before and after TNF stimulation. Prior to TNF treatment, very few active Pol II-mediated contacts were recovered as the genes were transcriptionally inactive. Upon stimulation, a large number of Pol II-mediated contacts emerged, specifically between UMLILO, *IL-8*, *CXCL1*, *CXCL2* and *CXCL3*, to form a multi-gene complex.

(C) ChIP-Seq analysis in unstimulated HUVECs and HeLa cells from the ENCODE database. All the chemokines that UMLILO interacted with were enriched for active chromatin marks (H3K4me1, H3K4me2, H3K4me3 and H3K27Ac). The lack of H3K36me3 (active transcription) and the enrichment of H3K4me3 indicated that these genes were not actively transcribed prior to stimulation, but were primed for transcriptional activation, respectively.

(D) CAGE data from the FANTOM 5 database showed that UMLILO was transcribed in profession immune cells as well as non-immune cells. UMLILO levels were highest in immune challenged cells, but basal levels of UMLILO were detected in unstimulated cells too.

UMLILO is required for chemokine transcription

In order to determine the transcriptional response of UMLILO and its associated chemokines, HUVECs were stimulated for 30 minutes with TNF and gene expression was quantified using RT-qPCR. Chemokine transcription was strongly induced by TNF (ranging from 15-20 fold increase) and this was accompanied by a 2.5 fold increase in UMLILO expression from basal levels (Figure 2.2A). The expression of ANKRD17 was used as a negative control, as it is non-responsive to TNF and occupies a neighbouring TAD. To determine whether UMLILO was required for this transcriptional activation, RNA interference (RNAi) was used to deplete UMLILO in HUVECs. A pool of small interfering RNAs (siRNAs) were targeted to UMLILO and observed to efficiently knockdown UMLILO by approximately 80% (Figure 2.2B). siRNAs targeting the green fluorescent protein (GFP) was used as a negative control (siGFP). Strikingly, depletion of UMLILO 48 hours prior to TNF stimulation

significantly abrogated the transcriptional activation of the chemokines compared to the negative control (Figure 2.2B). Importantly, the effect of UMLILO silencing was confined to the chemokines within this TAD, as ANKRD17 remained unaffected. These data demonstrated that UMLILO is a bonafide functional lncRNA that is essential for the co-regulated transcription of *IL-8*, *CXCL1*, *CXCL2* and *CXCL3* in response to TNF stimulation.

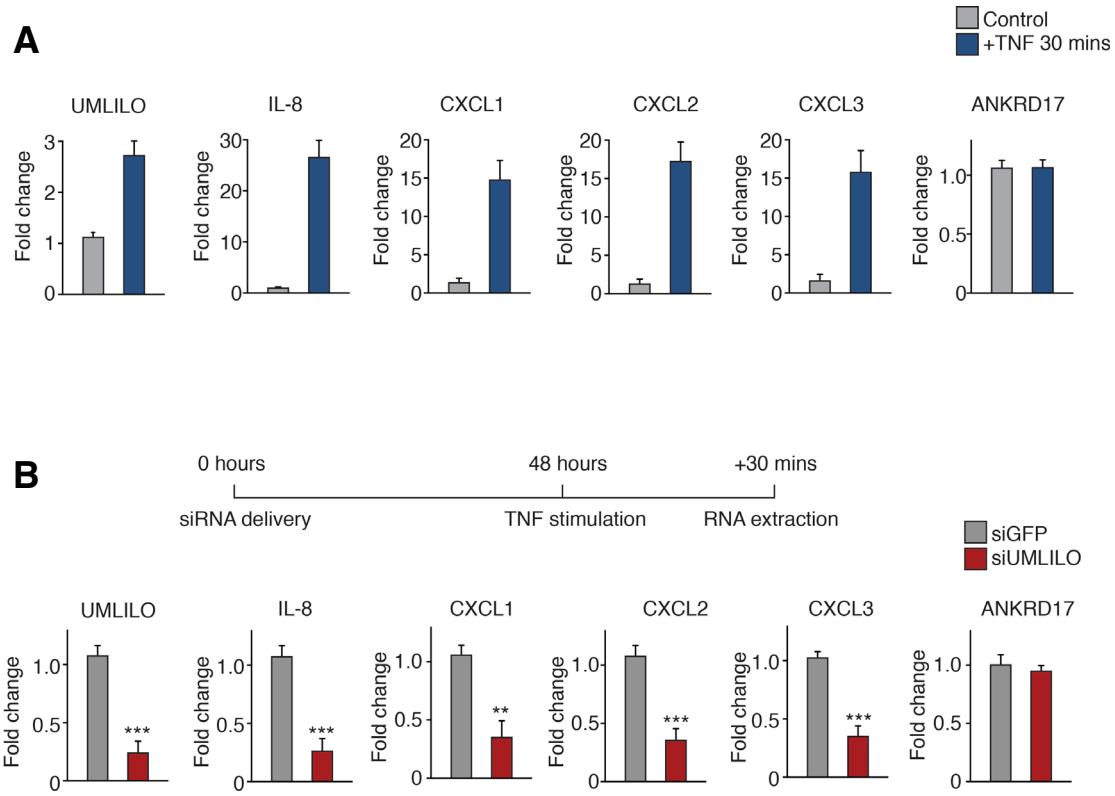

Figure 2.2: UMLILO is essential for co-regulated chemokine transcription

(A) RT-qPCR measurements showed that TNF stimulation induced the transcription of UMLILO and its associated chemokines in HUVECs. ANKRD17, a gene in a neighbouring TAD, was unaffected by TNF treatment. (n=3)

(B) Knockdown of UMLILO using siRNAs in HUVECs significantly abrogated chemokine transcription in response to TNF compared to the siGFP control. ANKRD17 expression remained unaffected by the loss of UMLILO. (n=3)

Data are represented as mean±SEM. n=number of independent experiments. p values were calculated using the Student's t-test. **p<0.01, ***p<0.001

Chromosomal contacts with UMLILO are pre-formed

From Hi-C contact maps, it is clear that UMLILO and the ELR+ CXCL chemokines occupy the same TAD (Figure 2.1A) and are likely to participate in chromosomal contacts. The ChIA-PET data supports this by showing that UMLILO was in contact with these genes during active transcription via Pol II-mediated interactions (Figure 2.1B). However, with the limited resolution of Hi-C and the selection bias of ChIA-PET for Pol II-mediated contacts, it remained unclear whether UMLILO specifically engages with the chemokine genes in the unstimulated state.

In order to study the dynamics of the chromosomal contacts between UMLILO and the ELR+ CXCL chemokine genes, 3C was performed on HeLas to generate a high resolution interaction map across this TAD, before and after TNF stimulation (Figure 2.3 A). *IL-8* was used as an anchor point and primers were designed across the TAD to test for chromosomal interactions. Primers targeting regions outside of the TAD were used as negative controls. In the unstimulated state, it was observed that UMLILO engaged in chromosomal contacts with all the chemokine genes, corresponding to the PETs recovered from Pol II Ser2/5 ChIA-PET. After 30 minutes of TNF activation, the frequency of these contacts largely remained unchanged. This suggested that UMLILO and the chemokine genes existed in a pre-formed multi-gene complex, which may be significant for the priming of the chemokine promoters prior to their activation and their co-regulated expression.

UMLILO does not mediate the chromosomal contacts in the ELR+ CXCL chemokine TAD

Through the recruitment of the Mediator complex, eRNAs are able to facilitate precise chromosomal contacts that are causal to transcription (see section entitled *Enhancer RNAs*). From the previous results, the transcription of the chemokine genes was dependent on UMLILO and engaged in chromosomal contacts (Figure 2.2B and Figure2.3A). In order to determine whether

UMLILO played a role in the formation and maintenance of these contacts, which are likely to be causal to the co-regulated transcription pattern of the chemokines, the basal levels of UMLILO were depleted by siRNA prior to performing 3C on the locus. Previously validated siRNAs were delivered into HeLa cells and 3C was carried out on unstimulated cells 48 hours later using the same primer sets as before. Knockdown of UMLILO did not affect the earlier described pre-formed contacts compared to the negative control siGFP (Figure 2.3B). This indicated that the formation of the multi-gene complex was not dependent on UMLILO, suggesting that this lncRNA did not function like an eRNA to coordinate chromosomal loops and mediate the transcription of the chemokine genes.

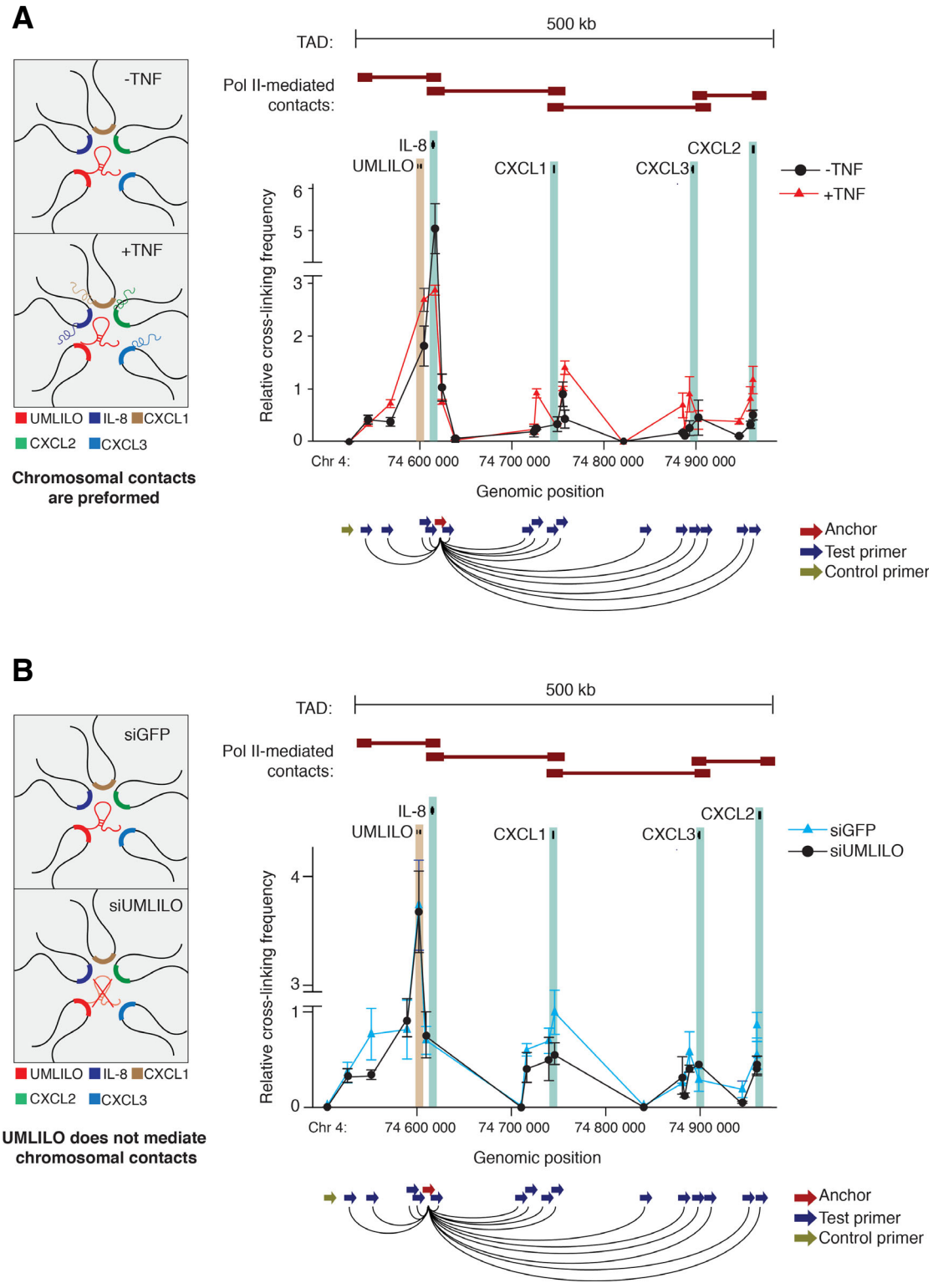

Figure 2.3: UMLILO does not mediate the pre-formation of chromosomal contacts

(A) 3C across the chemokine TAD in HeLas revealed that there were no significant changes in chromosomal contacts between UMLILO and the chemokine genes before and after TNF stimulation. This suggests that these contacts are pre-formed prior to stimulation (inset). *IL-8* was used as an anchor point and a primer set designed to target a region outside the TAD was used as a control. (n=3)

(B) Depletion of baseline UMLILO levels using siRNAs (siUMLILO) in HeLas did not alter the chromosomal contacts (as measured by 3C) in this region compared to the siRNA targeting the GFP sequence (siGFP) control. This indicated that UMLILO does not mediate the formation and maintenance of this pre-formed architecture (inset). (n=3)

Data are represented as mean±SEM. n=number of independent experiments.

UMLILO is required for H3K4me3 and Pol II occupancy at the chemokine promoters

H3K4me3 is causal to transcription by facilitating transcription factor binding and the assembly of the PIC (Vermeulen et al., 2007, Lauberth et al., 2013, Cano-Rodriguez et al., 2016). H3K4me3 deposition is carried out by the MLL family of histone methyltransferases (Wang et al., 2012). Importantly, it associates with WDR5, which functions as an adaptor protein which can bind RNA (Yang et al., 2014). It has been found that the WDR5/MLL1 complex can associate with lncRNAs such as NeST and HOTTIP, to spatially direct the deposition of H3K4me3 at their target genes (Wang et al., 2011, Gomez et al., 2013).

As previously observed, UMLILO engages in chromosomal contacts with the ELR+ CXCL chemokine genes, which are H3K4me3 primed prior to TNF activation. In order to test whether UMLILO was regulating H3K4me3 deposition at the promoters of these chemokine genes, UMLILO was knocked down and ChIP-qPCR was performed. Using the same siRNAs as before, UMLILO was efficiently depleted (Figure 2.2B) 48 hours prior to TNF stimulation in HUVECs. siGFP was used as a comparative control. The promoter DNA of *IL-8*, *CXCL1*, *CXCL2* and *CXCL3* were pulled down using an anti-H3K4me3 antibody and quantified using qPCR. Compared to the siGFP control, the loss of UMLILO resulted in the significant loss of H3K4me3 occupancy across all the chemokine promoters (Figure 2.4A). This demonstrated that UMLILO was essential for H3K4me3 deposition at the promoters of these chemokines. Accompanying the loss of H3K4me3 was the significant loss of Pol II occupancy (Figure 2.4B). qPCR on libraries prepared

using an anti-WDR5 antibody also showed significant loss in WDR5 occupancy at the chemokine promoters (Figure 2.4C), suggesting that UMLILO was recruiting MLL1 to this multi-gene complex via WDR5. All these effects of UMLILO knockdown were not observed on the control gene, ANKRD17. Furthermore, all ChIP-qPCR experiments were accompanied by a control library prepared using an IgG antibody in order to determined background DNA pull down.

Taken together, these results revealed the UMLILO was required for the deposition of H3K4me3 at the chemokine genes within this TAD. As a result, UMLILO indirectly facilitated Pol II loading, which is essential for transcription. Furthermore, UMLILO was able to do this via the recruitment of WDR5, which interacts with MLL1 to catalyse the deposition of H3K4me3 at the promoters of this chemokine multi-gene complex.

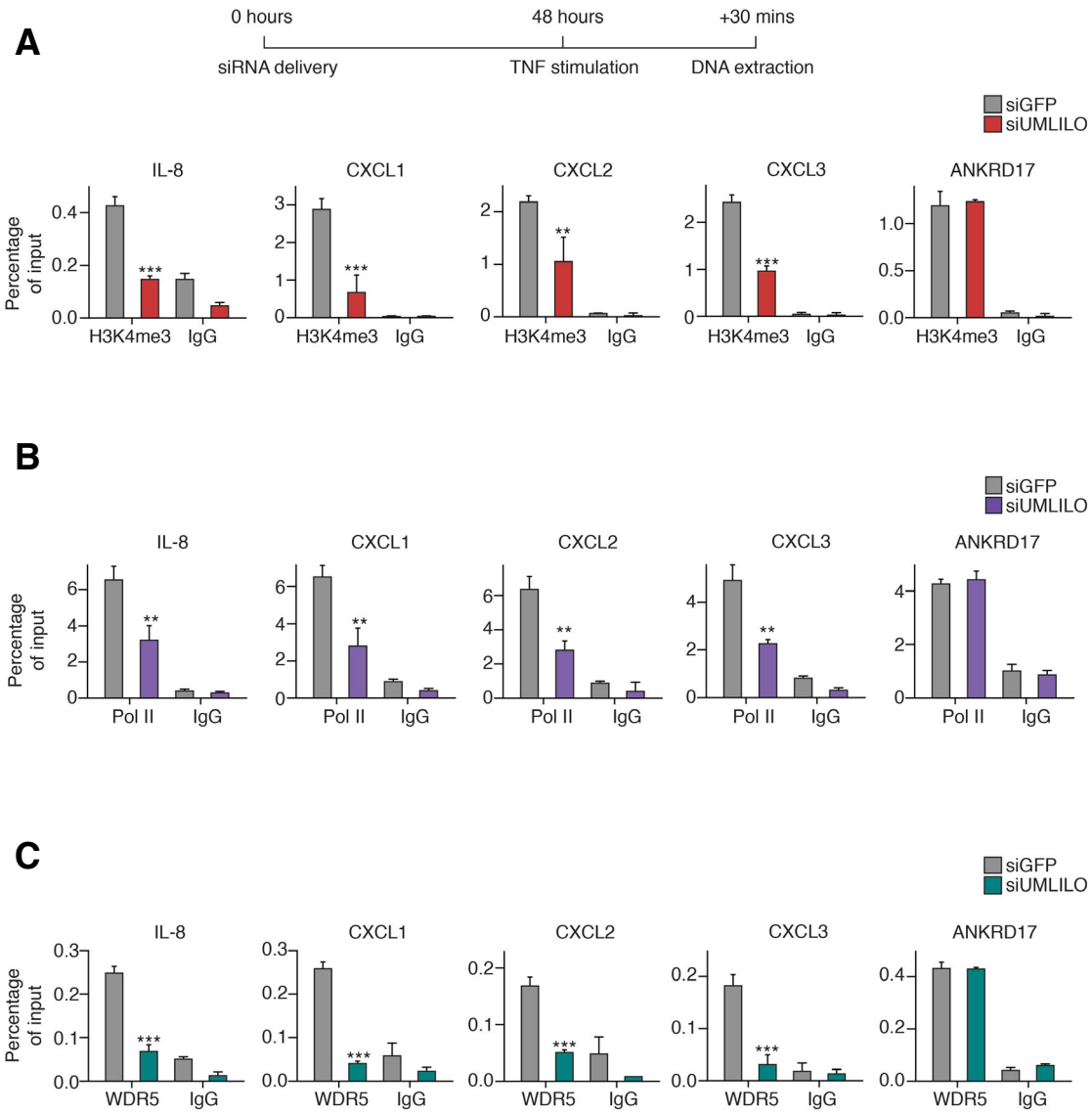

Figure 2.4: UMLILO mediates H3K4me3 and Pol II occupancy at the chemokine promoters by recruiting WDR5

(A) ChIP-qPCR showed that the depletion of UMLILO using siRNAs in HUVECs, prior to TNF stimulation, resulted in the loss of H3K4me3 at the chemokine promoters (siUMLILO vs siGFP control). (n=3)

(B) Accompanying the loss of H3K4me3 was the loss of Pol II occupancy at the chemokine promoters. (n=3)

(C) UMLILO knockdown modulated the locus-specific recruitment of WDR5, which interacts with the MLL1 histone methyltransferase responsible for the catalysis of H3K4me3 deposition. (n=3)

Data are represented as mean±SEM. n=number of independent experiments. p values were calculated using the Student's t-test. **p<0.01, ***p<0.001

Discussion

Rapid and robust transcriptional activation of pro-inflammatory immune genes is essential for providing effective immunological protection. Therefore, many of these immune genes exist in a primed state (Fowler et al., 2011, Bhatt et al., 2012). H3K4me3 occupancy is central for establishing this primed state, as it marks the genes for the pre-loading of transcriptional machinery onto their promoters (Lauberth et al., 2013). This allows for these genes to be regulated by signal-dependent transcription factors which release paused Pol II for active transcription (Fowler et al., 2011, Bhatt et al., 2012).

In this chapter, the data presented shows that a previously uncharacterised lncRNA, UMLILO, was essential for the H3K4me3 priming of the ELR+ CXCL chemokines. Indeed, the loss of UMLILO resulted in the loss of H3K4me3 and Pol II occupancy at the promoters of these genes. This corresponded with the well known role of H3K4me3 for Pol II loading at promoters (Lauberth et al., 2013). Furthermore, this revealed the causal mechanism underlying the loss of chemokine transcription when UMLILO was depleted. Chromatin interaction mapping by 3C revealed that UMLILO and the chemokine genes were engaged in a pre-formed multi-gene complex. UMLILO did not play a role in the establishment or maintenance of these chromosomal contacts, suggesting that UMLILO does not have architectural abilities like eRNAs. Taken together, it appears that UMLILO rather exploits the 3D topology and is able to recruit the WDR5/MLL1 complex to the promoters of the chemokines and direct discrete local H3K4me3 deposition prior to immune activation (Figure 2.5).

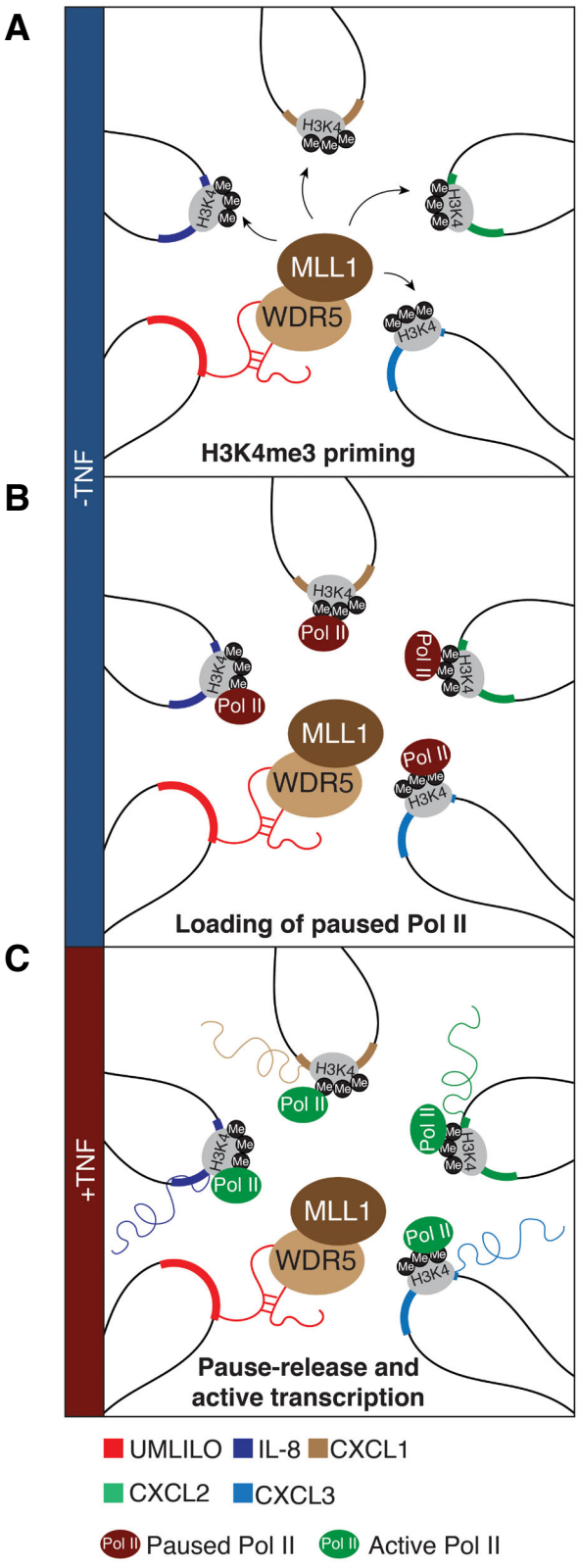

Figure 2.5: A schematic showing the functional mechanism of UMLILO

(A) UMLILO engages in specific chromosomal contacts with the ELR+ CXCL chemokine genes to form a multi-gene complex. Within this compartment, UMLILO recruits WDR5 which interacts with the histone methyltransferase, MLL1. This allows for the discrete

deposition of H3K4me3 on the promoters of the chemokine genes, priming them for transcriptional activation.

(B) H3K4me3 priming facilitates the assembly of the PIC and the pre-loading of paused Pol II.

(C) Upon TNF activation, signal-dependent transcription factors recruit P-TEFb to release the paused Pol II from its suspended state. This results in the active co-transcription of the chemokine genes, in a rapid and robust manner.

By establishing a pre-formed multi-gene complex, the stochasticity associated with transcriptional activation is significantly reduced, allowing for the robust and coordinated co-transcription of the chemokine genes (Cavalli and Misteli, 2013). Within this multi-gene complex, the H3K4me3 epigenetic priming by UMLILO changes the ground state of these genes into a poised state, allowing for the fast kinetic responses required. Therefore, the superimposition of these two layers of regulation (structural and epigenetic) underly the rapid and robust transcriptional responses required by pro-inflammatory genes.

Chromosomal contacts observed by Hi-C and 3C, however, represent static snapshots derived by averaging contact frequencies across an entire cell population. Using imaging-based single cell analysis and polymer modelling, the collective data from Hi-C experiments can be deconvolved to reveal a repertoire of genomic configurations, highlighting the probabilistic nature of genome organisation (Giorgetti et al., 2014). Furthermore, single cell Hi-C experiments and FISH-based imaging have demonstrated extensive heterogeneity in chromosomal contacts across a cell population (Flyamer et al., 2017, Fudenberg and Imakaev, 2017, Finn et al., 2019). Contributing to this inter-cellular variation, recent studies have suggested that TADs and chromosomal loops are dynamic structures (Hansen et al., 2018). Such variation may subvert the effectiveness of UMLILO to prime the chemokine genes and lead to variegated gene expression across the cell population (Noordermeer et al., 2011). This may undermine the ability of a cell to mount a sufficiently powerful pro-inflammatory response to effectively combat a pathogen. The emergence of rare “jackpot” cells, which happen to be in a configuration that supports the transcription of specific genes and display

increased levels of expression, may be able to compensate for the silent neighbouring cells. However, using intronic RNA single molecule FISH (smFISH), the ELR+ CXCL chemokine genes were observed to be robustly transcribed in the majority of TNF stimulated cells, refuting the role of rare “jackpot” cells in directing the inflammatory response (Fanucchi et al., 2019).

Recent studies have demonstrated that the turnover of TADs and chromosomal loops is highly dynamic and are lost and re-formed within minutes (Hansen et al., 2018). This could reconcile the disparity between the fluid nature of TADs and the ability for robust transcription. Due to the high frequency of chromosomal loop assembly and disassembly, UMLILO could function cyclically on its cognate chemokine genes during the assembled phase of the multi-gene complex. In doing so, even when the complex is temporarily dissolved, the chemokine genes will be in a primed state and ready for transcriptional activation. This would explain the robust transcription patterns of these chemokines observed in single cells, despite the extensive inter-cellular variation in genome organisation (Fanucchi et al., 2019, Finn et al., 2019).

In order for UMLILO to prime the chemokine genes, its activity must occur in resting cells, prior to immune activation. Although it is transcriptionally responsive to TNF treatment, CAGE data and our own have indicated that there are basal levels of UMLILO in unstimulated cells. This means that UMLILO is able to prime the chemokine genes during homeostatic conditions, suggesting that basal UMLILO transcription is independent of TNF activation. Furthermore, RNA smFISH experiments have shown that UMLILO transcripts are not distributed widely across the nucleus, but rather remain localised near the chemokine genes (Fanucchi et al., 2019). RNA-Seq experiments have also demonstrated that the function of UMLILO is restricted to the ELR+ CXCL chemokine TAD (Fanucchi et al., 2019). These findings suggest that there are mechanisms that retain UMLILO within the multi-gene complex after its transcription. Such mechanisms are currently unknown, but we can speculate that UMLILO is able to recruit WDR5/MLL1 while being transcribed

and tethered by Pol II, form DNA-RNA R-loops or recruit other proteins that keep UMLILO localised to its site of transcription (Long et al., 2017).

While it is clear that UMLILO interacts with the WDR5/MLL1 complex to execute its function (Fanucchi et al., 2019), some aspects describing the protein complex associated with UMLILO may also be incomplete. It is possible that UMLILO function may not be limited to histone methyltransferase activity, but rather serve as a scaffold for expanded functional capabilities. There are numerous examples of histone modifiers in complex with metabolic enzymes (Kera et al., 2013, Matsuda et al., 2016). This is because cellular metabolism is closely linked to histone modifications, as it provides the substrates for the deposition of these epigenetic marks (Fok et al., 2018). For example, methionine adenosyltransferase, which is responsible for the synthesis of the methyl donor, *S*-adenosylmethionine, exists in a complex with the H3K9 methyltransferase, SETDB1 (Kera et al., 2013). Together, this complex epigenetically regulates COX2 gene expression through the local production of the methyl donor, which is essential for the deposition of the repressive H3K9me3 mark (Kera et al., 2013). It is possible that UMLILO can recruit metabolic enzymes to locally produce the metabolites required for H3K4me3 deposition. By doing so, stricter spatial limitations are imposed for the highly specific and discrete priming of genes. Thus, it might be worthwhile in future studies to characterise the ribonucleoprotein complex more fully to elucidate any other potential functions.

In summary, the discovery and characterisation of UMLILO and the IPLs illuminate a novel mode of transcriptional regulation of the innate immune genes during inflammation (Fanucchi et al., 2019). This provides a novel class of drug target candidates that can be modulated to attenuate inflammatory responses, highlighting the importance of this work, as many diseases are caused by excessive inflammation (Netea et al., 2017). Furthermore, numerous other genes within the genome respond in a similarly rapid and robust signal-dependent manner, suggesting that other “IPL-like” lncRNAs exist to direct the H3K4me3 priming of these genes. By applying the

bioinformatic pipeline described by Fanucchi et al., it is possible to discover these lncRNAs, which may function pervasively in human biology and provide novel ways for manipulating biological processes.

Chapter 3

A CHROMATIN-REGULATED BIPHASIC CIRCUIT COORDINATES *IL-1β* AND *IL-37* TRANSCRIPTION DURING INFLAMMATION

Introduction

Inflammation is characterised by a biphasic cycle consisting initially of an acute pro-inflammatory phase, which is subsequently resolved by anti-inflammatory processes (Medzhitov, 2008, Rogatsky and Adelman, 2014). During the first stage, the induction of the pro-inflammatory immune genes needs to occur rapidly in order to initiate host defences and curb the progression of infection. The subsequent activation of the anti-inflammatory phase is temporally delayed and serves to attenuate pro-inflammation, initiate tissue repair and restore the basal cellular state (Medzhitov, 2008, Rogatsky and Adelman, 2014). The dysregulation of this response generally manifests as a state of hyper-inflammation or immunosuppression, both of which are major contributors to the pathogenesis of many diseases, including sepsis, atherosclerosis and cancer (Hotchkiss et al., 2009, Grivennikov et al., 2010, Back and Hansson, 2015). Therefore, inflammation is a careful balancing act between pro- and anti-inflammation, with shifts that tilt this balance being deleterious to human health. Each phase of the inflammatory response is directed by the coordinated transcription of key cytokines, suggesting that their regulation is intimately linked. However, the molecular mechanisms that orchestrate this coordinated gene expression remain poorly understood.

The interleukin-1 (IL-1) family of cytokines and receptors constitute one of the main signalling routes of inflammation and have long been implicated in modulating this host response (Dinarello, 2013, Mantovani et al., 2019). The

IL-1 family is functionally diverse and consists of seven pro-inflammatory agonists (IL-1α, IL-1β, IL-18, IL-33, IL-36α, IL-36βɣ and IL-36ɣ), one anti-inflammatory cytokine (IL-37) and three receptor antagonists (IL-1Ra, IL-36Ra and IL-38) (Mantovani et al., 2019). Phylogenetic analysis of the IL-1 family revealed that pro-inflammatory function co-evolved with anti-inflammatory capabilities 420 million years ago, highlighting the evolutionary significance for developing a balanced inflammatory response (Rivers-Auty et al., 2018). By encompassing both pro- and anti-inflammatory function, the coordinated induction of the IL-1 family can contribute to the different stages of an inflammatory cycle.

Interleukin-1 beta (IL-1β) is a master cytokine positioned at the apex of inflammation (Kornman, 2006). It is one of the first genes to be transcriptionally activated in the face of immune challenge and is predominantly expressed in monocytes, macrophages and dendritic cells (Kornman, 2006, Moorlag et al., 2018). The expression of IL-1β induces powerful pro-inflammatory functions, including the induction of other pro-inflammatory cytokines, such as IL-6 and TNF-α, and the consolidation of glycolytic metabolism (Jung et al., 2003, Cheng et al., 2014). Overproduction of IL-1β is detrimental and contributes to many hyper-inflammatory diseases, such as rheumatoid arthritis, gout, atherosclerosis and other auto-inflammatory syndromes (Dinarello, 2011). Blocking of IL-1β has proven to be a highly effective way to attenuate pro-inflammation and control these diseases, highlighting the critical and hierarchical role of IL-1β in the inflammatory response (Dinarello, 2011).

Due to the powerful upstream pleiotropic function of IL-1β, its expression is tightly regulated by a two-factor activation mechanism. The first step occurs at the level of IL-1β transcription, which produces a mRNA sequence that encodes for the inactive pro-IL-1β protein. The second level of regulation involves the conversion of pro-IL-1β into its active form by intracellular inflammasome-associated proteases, such as caspase-1, or extracellular inflammatory proteases (Moorlag et al., 2018). Despite this regulation, human

blood monocytes constitutively express activated caspase-1, essentially removing the post-translational regulation of IL-1β (Netea et al., 2009). This suggests that in these cells, which are a major source of IL-1β, the transcriptional regulation of IL-1β is particularly important in shaping a calibrated inflammatory response.

Genome wide association studies (GWAS) have revealed that the non-coding genome is replete with polymorphisms that affect coding gene function (Nishizaki and Boyle, 2017). As such, polymorphisms in the promoter region of *IL-1β* have been shown to regulate inflammatory responses by altering *IL-1β* transcription (Wen et al., 2006). In particular, the rs16944 polymorphism (G>A) influences susceptibility to multiple immune-related diseases and is highly prevalent worldwide, with approximately a third of the global population being homozygous for this variation (Genomes Project et al., 2015) (Figure 3.1A). Importantly, strong associations have been made between this pervasive polymorphism and many inflammatory disease states, including periodontitis (Wu et al., 2015), systemic sclerosis (Huang et al., 2016), pancreatitis (Li et al., 2015a) and lethal sepsis (Jimenez-Sousa et al., 2017). Furthermore, the rs16944 polymorphism is also associated with enhanced risk and severity of infectious diseases, such as those caused by Mycobacterium tuberculosis (Awomoyi et al., 2005), hepatitis B virus (Fan et al., 2017) and fungal infections (Wojtowicz et al., 2015) (Figure 3.1B). Although the precise mechanism by which this SNP affects *IL-1β* transcription remains unknown, its influence in multiple inflammatory conditions provides strong correlative evidence that the correct transcriptional regulation of *IL-1β* is imperative for a successful immune response.

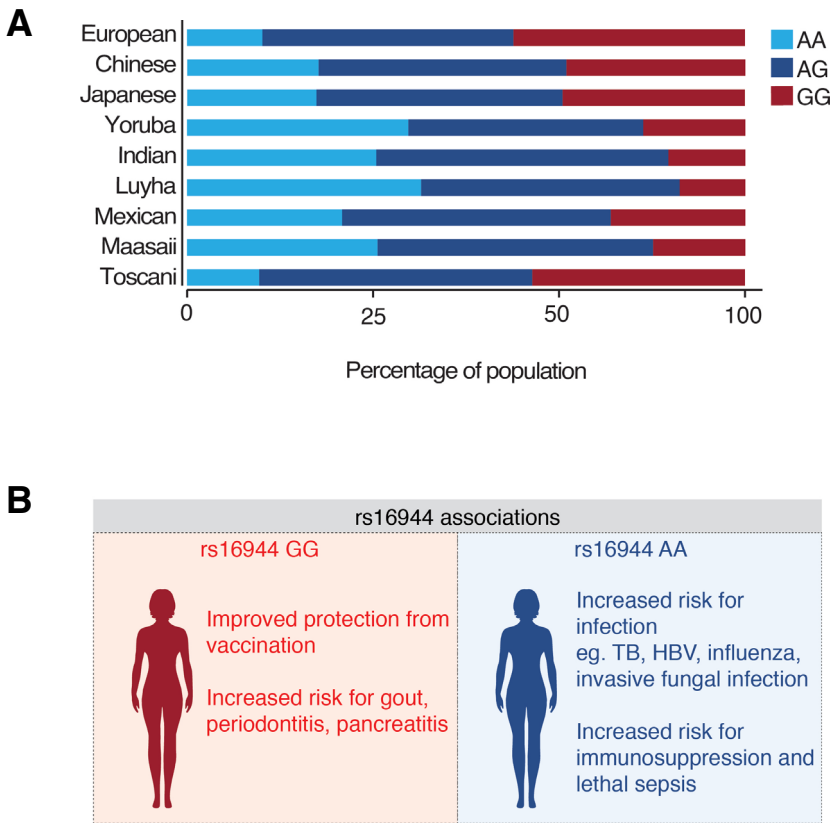

Figure 3.1: The global distribution of the rs16944 SNP genotypes and the associated phenotypes

(A) The rs16944 SNP occurs in the promoter region of *IL-1β* (G>A) and has approximately 50/50 allelic distribution worldwide. This means that a third of the global population is either homozygous AA or homozygous GG.

(B) The rs16944 SNP has been extensively studied and homozygous phenotypes are strongly correlated with highly divergent inflammatory responses. rs16944 GG individuals display improved protection from vaccination but are predisposed to hyper-inflammatory conditions. Conversely, rs16944 AA individuals are at risk for infection and have and increased likelihood for developing immunosuppressive disorders.

While it is clear that IL-1β plays an important role in driving the pro-inflammatory component of inflammation, the compensatory role of IL-37 as a powerful and broad anti-inflammatory cytokine has only recently emerged (Nold et al., 2010, Li et al., 2015b, Li et al., 2019). More specifically, functional studies have shown that IL-37 can inhibit innate immunity by effectively modulating IL-1β production (Nold et al., 2010). Furthermore, although no murine homolog of *IL-37* exists, several studies using IL-37 expressing transgenic mice have shown that the human protein is functional in the

mouse, and have revealed that IL-37 plays a protective role in the suppression of pathogenic inflammation (Nold et al., 2010).

Mechanistically, IL-37 can function intracellularly to down regulate the transcription of pro-inflammatory cytokines or extracellularly through IL-1R8 and IL-18R signalling to induce inhibitory signals (Sharma et al., 2008, Nold et al., 2013, Nold-Petry et al., 2015). The latter is associated with the inhibition of the inflammasome, which is important for IL-1β maturation (Moretti et al., 2014). IL-37 can also activate AMP-activated protein kinase (AMPK), which serves as a key metabolic sensor that regulates energy homeostasis (Hardie et al., 2012, Cavalli et al., 2017). By doing so, IL-37 reverses the glycolytic state of the cell during pro-inflammation and restores the normative oxidative phosphorylation (Cavalli and Dinarello, 2018). These functions of IL-37 diametrically oppose key activities of IL-1β, suggesting that IL-37 is a strong candidate able to modulate IL-1β-mediated responses (Figure 3.2A and B).

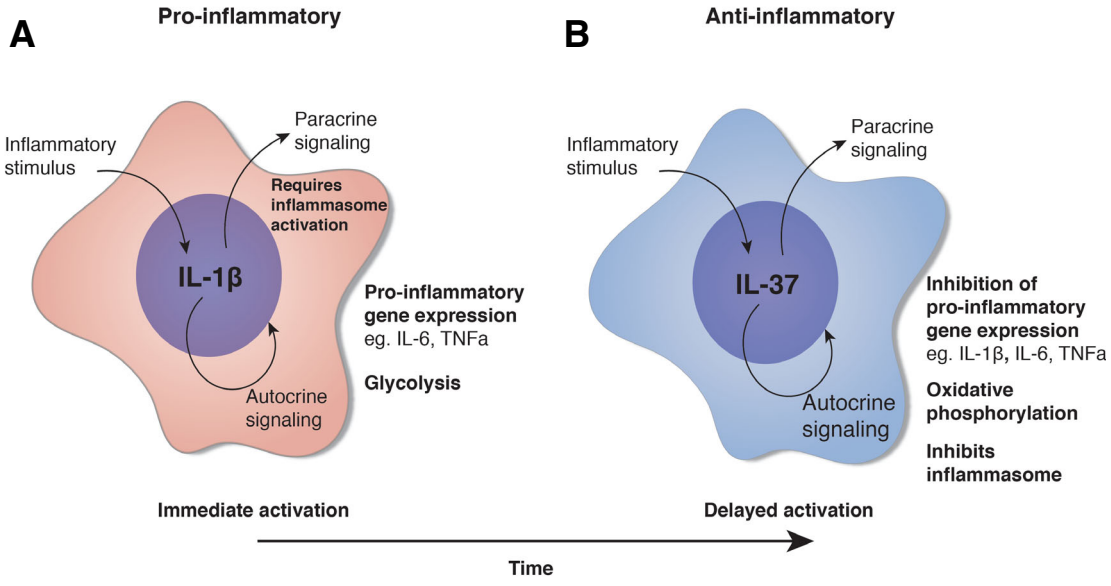

Figure 3.2: A schematic summarising the diametrically opposed functions of IL-1β and IL-37

(A) *IL-1β* is one of the first cytokines to be transcriptionally activated in a cell under immune challenge (macrophage depicted here). The maturation of IL-1β usually requires the caspase-1 activity associated with the inflammasome. In human circulating monocytes, activated caspase-1 is constitutively expressed, negating the regulatory role of this post-translational regulation and emphasising the regulatory role of transcription. Mature IL-1β

can signal in an autocrine and paracrine manner to induce the expression of other pro-inflammatory cytokines as well as shift the cellular metabolism of the cell towards glycolysis.

(B) IL-37 diametrically opposes the functions of IL-1β and serves as a broad inhibitor of pro-inflammation. IL-37 can also function in an autocrine or paracrine manner, in order to inhibit pro-inflammatory gene expression and inflammasome function, as well as reverse glycolytic metabolism by restoring oxidative phosphorylation. Importantly, the expression of IL-37 is delayed and occurs downstream of IL-1β.

Many diseases with an inflammatory basis are accompanied by the dysregulation of IL-37 (Xu et al., 2015). Polymorphisms in *IL-37* have been shown to be expressed quantitative trait loci (eQTLs) for *IL-1β* (Offenbacher et al., 2018). This suggests that the transcriptional regulation of *IL-1β* and *IL-37* are linked, and potentially participate in balancing the functionally opposed biphasic nature of inflammation. However, the mechanism describing how *IL-1β* and *IL-37* may be transcriptionally coordinated remains unknown.

Within the eukaryotic nucleus, multiple layers of transcriptional regulation, such as chromosomal loops and lncRNAs, work cooperatively to coordinate and control transcription (see Chapter 1). Such mechanisms are essential for the regulation of immune gene expression during inflammation (see Chapter 2). Interestingly, the functionally opposed *IL-1β* and *IL-37* are located within the same TAD. However, the significance of this architecture and the role of lncRNAs in the regulation and coordination of their transcription, during inflammation, currently remains unclear.

In this chapter, the genetic circuitry and molecular mechanisms that coordinate the transcription of the functionally opposed *IL-1β* and *IL-37* were dissected. Assessment of the region surrounding the rs16944 SNP uncovered a novel lncRNA that was transcribed from the *IL-1β* promoter. Functional experiments implicated this lncRNA in the transcriptional activation of *IL-37* through the formation of dynamic chromosomal contacts. Importantly, IL-37 is a negative regulator of IL-1β, revealing a chromatin-regulated feedback circuit

that coordinated *IL-1β* and *IL-37* transcription to follow the biphasic progression of pro- and anti-inflammation.

Materials and Methods

Bioinformatic analysis

Hi-C sequencing data generated by (Rao et al., 2014) was visualised using an online Hi-C browser (http://promoter.bx.psu.edu/hi-c/view.php). Capture Hi-C from (Javierre et al., 2016) was visualised using the online Capture Hi-C Plotter (https://www.chicp.org). Publicly available ChIP-Seq datasets were examined using the UCSC Genome Browser. The traces shown here are from the BLUEPRINT project and the ENCODE consortium. CAGE data was from the FANTOM 5 database and visualised using the Zenbu browser.

Cell culture

The THP-1 cell line was kindly donated by Susan Malfeld from the National Institute of Communicable Diseases. These cells were grown in RPMI 1640 medium (Thermo Fisher Scientific) supplemented with 10% FBS (Thermo Fisher Scientific), 1% GlutaMAX (Thermo Fisher Scientific) and 50 nM 2-mercaptoethanol (Thermo Fisher Scientific). When the cells reached a density of approximately $1x10^6$ cells/ml, 70% of the cell culture was discarded and the volume was replaced with fresh complete culture medium. THP-1 monocytes were differentiated using 100 ng/ml 12-myristate 13-acetate (PMA) for 24 hours. PMA-differentiated THP-1 macrophages were then allowed to rest for another 24 hours in PMA-free medium prior to being used. HEK293T cells (Sigma-Aldrich) were cultured in DMEM (Thermo Fisher Scientific) containing 1% GlutaMAX (Thermo Fisher Scientific) and 10% FBS (Thermo Fisher Scientific). HEK293T cells were sub-cultured in the same way as described in the *Cell Culture* section of Chapter 2. The retinal pigment epithelial 1 (RPE1) cell line (ATCC) was cultured in DMEM/F12 (Thermo Fisher Scientific) containing 1% GlutaMAX (Thermo Fisher Scientific) and 10% FBS (Thermo Fisher Scientific). RPE1 cells were sub-cultured in the same way as described in the *Cell Culture* section of Chapter 2. HeLa cells were grown as previously described in the *Cell Culture* section of Chapter 2.

THP-1 stimulation with LPS and RT-qPCR

To isolate primer sets that could detect AMANZI transcription, qPCR primers were designed to overlap and tile the entire putatively transcribed AMANZI region (primer sequences provided in Table 2.1). 2.5x10^5 THP-1 monocytes were seeded per well in a 24-well plate and treated with 10 ng/ml lipopolysaccharide (LPS) (Sigma-Aldrich) for 60 minutes, after which RNA was extracted, cDNA was synthesised and qPCR was carried out as described in *HUVEC stimulation with TNF and RT-qPCR* in Chapter 2.

To compare the transcription pattern of *IL-1β* and AMANZI in response to LPS stimulation, THP-1 monocytes, THP-1 macrophages and RPE1 cells were stimulated with 10 ng/ml LPS for 24 hours. THP-1 monocytes were stimulated as described above. For THP-1 macrophages, 2.5x10^5 THP-1 monocytes were PMA-differentiated prior to stimulation with 10 ng/ml LPS. For the RPE1 cells, 7.5x10^4 were seeded and allowed to adhere for 24 hours before LPS (10 ng/ml) stimulation. After LPS stimulation, RNA was extracted, cDNA was synthesised and qPCR was carried out (using Primer set 6 from Table 2.1) as described in *HUVEC stimulation with TNF and RT-qPCR* in Chapter 2.

Table 2.1: List of overlapping primers tiling AMANZI

Primer Name	Sequence (5′ - 3′)
Primer set 1 F	TGCCAGTTTCTCCCTCGCTG
Primer set 1 R	ATTAGTCCCCTCCCCTAAGAAGC
Primer set 2 F	GGAAAGGGGAAAAGAGTATTGGTGG
Primer set 2 R	AATGTGTCATAGTTTGCTACTCCTTGC
Primer set 3 F	TTCATGGAAGGGCAAGGAGTAGC
Primer set 3 R	GGACATCAACTGCACAACGA
Primer set 4 F	CTGACAATCGTTGTGCAGTTG
Primer set 4 R	TGTCTTCCACTTTGTCCCACA
Primer set 5 F	ATATGTGGGACAAAGTGGAAGACAC
Primer set 5 R	GGGCTATTGGCCCTTCATTGTAC

Primer set 6 F	CCTCCCTGTCTGTATTGA
Primer set 6 R	GCATACCGTATGTTCTCTG
Primer set 7 F	ATACGGTATGCAGGGTTCAGGC
Primer set 7 R	GCAGAGCTCATCTGGCATTGATC
Primer set 8 F	AACCAGATCAATGCCAGATGAGC
Primer set 8 R	ACTTTGCTGGTGTCTCGGTTAAAG
Primer set 9 F	TTTAACCGAGACACCAGCAAAGTGC
Primer set 9 R	AGGCAAAGGAGGGTGTTCCTAC

3′ RACE

RNA was extracted from 2.5x10^5 THP-1 monocytes using the Direct-zol RNA Miniprep Kit (Zymo) (Appendix A2.1). 500 ng of RNA was converted to cDNA using the SuperScript IV First-Strand Synthesis System (Thermo Fisher Scientific) as per the manufacturer's instructions (Appendix A2.2), with the exception of using the bespoke 3′ RACE polydT_adapter R primer instead of the provided primers in the kit. This produced a 3′ adapter-tagged cDNA library. A nested PCR approach was used to amplify the 3′ end of AMANZI. In the first round of amplification, PCR1 was set up to contain 10 μl 5x Q5 Buffer (NEB), 0.2 mM deoxyribonucleotide triphosphate (dNTP) mix, 0.5 μM 3′ RACE F1, 0.25 μM 3′ RACE adapter R (binds to the adapter sequence on the 3′ end of the cDNA), 1 μl cDNA template, 0.25 μl Q5 Polymerase (NEB) and water to make up the reaction to a final volume of 50 μl. PCR1 was subject to the following conditions: an initial cycle of 98˚C for 30 seconds, 98˚C for 10 seconds, 65˚C for 10 seconds, 72˚C for 10 minutes followed by 35 cycles of 98˚C for 10 seconds, 65˚C for 10 seconds, 72˚C for 1 minute and a final extension of 72˚C for 2 minutes. 5 μl of PCR1 was visualised on a 1% TAE (Appendix A3.8) agarose gel stained with 1 μg/ml ethidium bromide. PCR2 contained 10 μl 5x Q5 Buffer (NEB), 0.2 mM dNTP deoxynucleotide triphosphate (dNTP) mix, 0.5 μM 3′ RACE F2, 0.5 μM 3′ RACE adapter R, 1 μl of PCR1 (1:300), 0.25 μl Q5 Polymerase (NEB) and was made up to a final volume of 50 μl with water. Cycling conditions were as follows for PCRs: 98˚C

for 30 seconds, followed by 30 cycles of 98˚C for 10 seconds, 65˚C for 10 seconds, 72˚C for 30 seconds and a final extension of 72˚C for 2 minutes. The entire volume of PCR2 was visualised on a 1% TAE (Appendix A3.8) agarose gel stained with 1 μg/ml ethidium bromide. Bands of interest were gel extracted using to the GeneJet Gel Extraction Kit (Thermo Fisher Scientific) according to the manufacturer's protocol (Appendix A2.5). PCR amplicons were ligated into pUC19 according to a 6:1 molar ratio, after KpnI and EcoRI digestion. Plasmid clones were transformed (Appendix A2.7) into chemically competent Stbl3 *E.coli* and 5 colonies representing each band on the gel were sent for Sanger Sequencing at Inqaba Biotec. Returned sequences were analysed using the sequence alignment tool from Snapgene. Primer sequences are presented in Table 2.2.

Table 2.2: List of primer sequences for 3′ RACE

Primer Name	Sequence (5′ - 3′)
3' RACE F1	ATACGGTATGCAGGGTTCAGGC
3' RACE F2	AACCAGATCAATGCCAGATGAGC
3' RACE polydT_adapter R	GACTCGAGTCGACATCGAGGTACCTTTTT TTTTTTTTTTTT
3' RACE adapter R	GACTCGAGTCGACATCG

Locked nucleic acid (LNA) delivery in THP-1 monocytes

LNA GapmeRs (Exiqon) were electroporated into THP-1 monocytes using the Neon Transfection System. 2.5x10^5 THP-1 monocytes were harvested and prepared according to the Neon Transfection System protocol (Appendix A2.3). 200 nM LNA GapmeR was introduced into these cells by using 3 pulses at 1 600 V and 10 ms in a 10 μl tip. LNA sequences are provided in Table 2.3. After 24 hours, the cells were then stimulated with 10 ng/ml LPS for 24 hours prior to RNA extraction and transcriptional analysis by RT-qPCR (as described in *HUVEC stimulation with TNF and RT-qPCR* in Chapter 2) (see Table 2.4 for primer sequences). For 3C and ChIP, the same protocol was

carried out, with the exception of using the 100 μl tip to accommodate the larger cell numbers and the appropriate upscaled volume of reagents.

Table 2.3: List of LNA GapmeR sequences

LNA Name	Sequence (5′ - 3′)
AMANZI LNA	CCAAGAAAGGTCAATT
IPL-IL-1β LNA	AGGTAAAGAGAGTCAG

Table 2.4: List of RT-qPCR primers for *IL-1β* TAD genes

Primer Name	Sequence (5′ - 3′)
IL-1β F	GATCGTACAGGTGCATCGTGC
IL-1β F	GACAAGCTGAGGAAGATGCTGG
AMANZI F	CCTCCCTGTCTGTATTGA
AMANZI R	GCATACCGTATGTTCTCTG
IL-1α F	AGTAGCAACCAACGGGAAGG
IL-1α R	AAGGTGCTGACCTAGGCTTG
IL-37 F	GGAGTTTTGTCTCTACTGTGACAAGG
IL-37 R	GCAGGAGGTGCAGATGAACCATC
IL-1β eRNA F	GTGAGGTCCAAGGTTAGGGC
IL-1β eRNA R	ACATTAGTCGGCTTGCTCCC
HPRT F	GATTAGCGATGATGAACCAGGTT
HPRT R	CCTCCCATCTCCTTCATGACA

CRISPR guide RNA (gRNA) design and cloning

gRNAs were designed using the online CRISPOR tool (http://www.crispor.tefor.net). Three gRNA candidates targeting each end of the AMANZI “safe” deletion region were chosen based on predicted cleavage efficiency and off-target activity. Complementary oligonucleotides (oligos) encoding the target regions (see Table 2.5) were annealed in a 10 μl reaction containing 10 μM oligo F, 10 μM oligo R, 1 μl 10X T4 ligation buffer (Thermo

Fisher Scientific), 0.5 μL T4 polynucleotide kinase and made up to the final volume with water. The reaction was incubated in a thermocylcer at 37˚C for 30 minutes and then heated to 95˚C for 5 minutes followed by a slow ramp down to 25˚C at 0.1˚C/second. The pX330 (Addgene #42230) CRISPR/Cas9 expression plasmid was digested as follows: 1 μg of plasmid, 1 μl FastDigest BbsI (10 U/μl) (Thermo Fisher Scientific), 2 μl 10X FastDigest Buffer and water to make up a final volume of 20 μl. The reaction was incubated for 1 hour at 37˚C and resolved on a 1% TAE (Appendix A3.8) agarose gel stained with 1 μg/ml ethidium bromide. Successfully linearised plasmid was gel extracted using the GeneJet Gel Extraction Kit (Appendix A2.5). The annealed oligos were then ligated into the linearised pX330 backbone in a 10 μl reaction containing 50 ng of digested BbsI, 1 μl of the annealed oligos diluted 1:300, 1 μl of T4 ligation buffer (Thermo Fisher Scientific), 10 U of T4 ligase and water. The ligation reaction was incubated at 22.5˚C for 60 minutes before 4 μl was transformed into Stbl3 *E. coli* (Appendix A2.7). Two clonal colonies for each construct were then picked for plasmid extraction using the QIAprep Spin Miniprep Kit (Appendix A2.8) (Qiagen).

Table 2.4: List of CRISPR gRNA oligonucleotides

Primer Name	Sequence (5′ - 3′)
sgRNA 1 F	GACCCTCAATACAGACAGGGA
sgRNA 1 R	TCCCTGTCTGTATTGAGGGTC
sgRNA 2 F	GCCACACCCTCAATACAGACA
sgRNA 2 R	TGTCTGTATTGAGGGTGTGGC
sgRNA 3 F	GCACCCTCAATACAGACAGGG
sgRNA 3 R	CCCTGTCTGTATTGAGGGTGC
sgRNA 4 F	GTGTGATTACAAGCTGAACGA
sgRNA 4 R	TCGTTCAGCTTGTAATCACAC
sgRNA 5 F	GTTGCCGCATAAAGACTCTG
sgRNA 5 R	CAGAGTCTTTATGCGGCAAC
sgRNA 6 F	GATTACAAGCTGAACGAAGG
sgRNA 6 R	CCTTCGTTCAGCTTGTAATC

T7 endonuclease 1 (T7E1) assay

To validate the DNA cleavage activity of the CRISPR clones, the T7E1 assay was carried out using HeLa cells. 24 hours prior to transfection, $7.5x10^4$ HeLa cells per well were seeded in a 24-well plate. On the day of transfection, the cell culture medium was replaced with 0.5 ml fresh medium. 500 ng of plasmid DNA was mixed with 2 μl Lipofectamine 2000 (Thermo Fisher Scientific) and made up to 50 μl with DMEM. The reaction was incubated for 5 minutes at room temperature and added drop-wise to a well of cells. 48 hours post-transfection, gDNA was extracted using QuickExtract (Lucigen). To do this, the cells were dissociated as described in the *Cell culture* section of Chapter 2. Cells were collected by centrifugation at 300 g for 3 minutes. The supernatant was discarded and 200 μl QuickExtract (Lucigen) was used to resuspend the cell pellet. The cell suspension was then incubated at 65˚C for 6 minutes, mixed by vortexing for 15 seconds and incubated at 98˚C for 2 minutes. The gDNA was then used as a template to amplify the gRNA target regions using a PCR containing 10 μl 5x Q5 Buffer (NEB), 0.2 mM dNTP deoxynucleotide triphosphate (dNTP) mix, 0.5 μM Primer F, 0.5 μM Primer R, 50 ng gDNA, 0.5 μl Q5 Polymerase (NEB) and water to make up a final volume of 50 μl. PCR cycling conditions were as follows: 98˚C for 30 seconds, followed by 30 cycles of 98˚C for 10 seconds, 65˚C for 10 seconds, 72˚C for 30 seconds and a final extension of 72˚C for 2 minutes. Amplicons were then column purified using the GeneJet PCR Purification Kit (Thermo Fisher Scientific) (Appendix A2.6). Heteroduplexes were formed by melting and reannealing (95˚C for 5 minutes and ramp down to 25 ˚C at 0.1˚C per second) 600 ng DNA in 2 μl 10X DreamTaq Buffer (Thermo Fisher Scientific) and water to make a final reaction volume of 20 μl. The heteroduplexes were then digested with T7E1 in a reaction containing 10 μl of the heteroduplex reaction, 0.6 μl of T7E1 (NEB), 2 μl of 10X T7E1 buffer and water to make up a final volume of 20 μl. The entire reaction was resolved on an 8% polyacrylamide gel stained with 1 μg/ml ethidium bromide. Band density was analysed using Fiji (ImageJ) and cleavage efficiency was calculated as described by (Ran et al., 2013). T7E1 primer sequences are presented in Table 2.5.

Table 2.5: List of primer sequences for T7E1 PCR

Primer Name	Sequence (5′ - 3′)
5' cut F	CTGACAATCGTTGTGCAGTTG
5' cut R	GCATACCGTATGTTCTCTG
3' cut F	CTCTCTCCTAGACAGGATCTACCTTTATC
3' cut R	GAAGCTCAAGGTTTCTGACCTGTATC

Construction of TRISPR vectors

The reagents for the TRISPR system were developed and kindly donated by the D. Grimm laboratory. The system allows for three gRNAs to be expressed from independent RNA Pol III promoters (U6, H1 and 7SK) from a single AAV particle. Two TRISPR constructs were generated, with each containing three guides to target the 5´ and 3´ regions of AMANZI to induce a deletion. Individual gRNAs were first ligated downstream of either a U6, H1 or 7SK expression plasmid using Golden Gate Assembly by setting up the following reaction: 40 fmol expression plasmid, 1μl of annealed oligos from the *CRISPR guide RNA (gRNA) design and cloning* section above diluted 1:200, 1 μl FastDigest BsmBI (10 U/μl) (Thermo Fisher Scientific), 1 μl 10X FastDigest Buffer (Thermo Fisher Scientific), 30 U T4 ligase (Thermo Fisher Scientific), 1 mM adenosine triphosphate (ATP), 1 mM dithiothreitol (DTT) and water to make up a final volume of 10 μl. The reaction was incubated for 20 cycles of digestion and ligation at 37˚C for 3 minutes and 20˚C for 5 minutes followed by 80˚C for 20 minutes. 3 μl of the assembled DNA was transformed into chemically competent Stbl3 *E. coli* (Appendix A2.7). Colonies were picked and cultured at 30˚C for 24 hours for plasmid extraction using the QIAprep Spin Miniprep Kit (Appendix A2.8). To assemble the CRISPR multiplex vectors, a subsequent Golden Gate Assembly reaction containing 20 fmol triplex expression plasmid, 20 fmol U6 gRNA expression plasmid, 20 fmol, H1 gRNA expression plasmid, 20 fmol 7SK gRNA expression plasmid, 0.5 μl FastDigest BbsI (10 U/μl) (Thermo Fisher Scientific), 1 μl 10X FastDigest Buffer (Thermo Fisher Scientific), 15 U T4 ligase (Thermo Fisher Scientific), 1 mM adenosine

triphosphate (ATP), 1 mM dithiotheitol (DTT) and water to make up a final volume of 10 *µ*l was set up. Reaction conditions were the same as the first Golden Gate Assembly reaction. 8 *µ*l of the reaction was used to transform chemically competent Stl3 *E.coli*. Colonies were screened by Sanger Sequencing using the AAV triplex expression plasmid sequencing primer: GTATGTTGTGTGGAATTGTGAG. Positive clones were bulk cultured and plasmid DNA was extracted using the NucleoBond Xtra Maxi Kit (Macherey-Nagel) according to the provided instructions (Appendix A2.9).

AAV packaging

Crude AAV stocks were produced by performing a triple transfection in HEK293T cells in 6-well plates. $3.5x10^5$ cells in 4 ml of medium per well were seeded 24 hours prior to transfection. Transfection was carried out using Lipofectamine 2000 according to the manufacturer's protocol. A triple plasmid mixture consisting of 1.3 µg of each plasmid (the AAV helper plasmid (encoding *rep* and *cap*), the adenovirus helper plasmid and the triplex gRNA or SpCas9 expression plasmid) was used for each transfection. The *cap* variant used produced the AAV6 serotype. 72 hours post-transfection, the cells were harvested by centrifugation at 300 g for 10 minutes and resuspended in 300 µl PBS. These cells were then subjected to five freeze-thaw cycles by incubating at 37˚C and then immersing in liquid nitrogen. The cell debris was then cleared by centrifugation at 3 000 g for 10 minutes and the supernatant containing the released AAV particles was stored at -80˚C until use.

THP-1 macrophage transduction with AAVs

48 hours prior to AAV transduction, $2x10^5$ THP-1 monocytes per well were seeded in a 24-well plate and differentiated with 100 ng/ml of PMA. 24 hours after PMA differentiation, the PMA medium was removed and the cells were allowed to recover in normal culture medium for 24 hours. On the day of AAV transduction, the medium on the THP-1 macrophages was removed and

replaced with 13.3 μl of AAV6-5′ cut, 13.3 μl of AAV6-3′ cut, 13.3 μl of AAV6-Cas9 and 160 μl of complete culture medium. The cells were incubated for 24 hours after which 0.5 ml of complete culture medium was added to each well of cells. Fresh culture medium was added every 3 days and after 7 days, the cells were harvested for analysis.

3C

3C was carried out using THP-1 monocytes as described in the *3C* section of Chapter 2. Primer sequences are presented in Table 2.6 and the RP11-68O13 BAC clone was used (Thermo Fisher Scientific). Primer testing data are presented in Appendix A1.2

Table 2.6: List of primer sequences for 3C-qPCR

Primer Name	Sequence (5′ - 3′)
Primer 1	CCCTTCTGCCATGATGTGTTTCCTGAGTCC
Primer 2	GAGAGGATTTCATATTCGTGCAGACAG
Primer 3	CTAAAACTTAGTGCCAAATGCTGAGGAG
Primer 4	TTAAAACATGGAGAATTAGCAAGCTGCC
Primer 5	CTCAGCCCTTTATTTTTCAGATGAGGTC
Primer 6 (Bait)	TATGGCTTTCAAAAGCAGAAGTAGGAG
Primer 7	TTATTCCATTACACTCACCAGACAAAAC
Primer 8	GAGCAACTGTAAATCACTTGAGGTTCTG
Primer 9	AGGCCGTAACTCCTTCATTAGTATTCTC
Primer 10	GAAAGGTTTAATTCACCAGAAAGACAC
Primer 11	GGTTCTAAGCATCATGGCTGTATTTCAC
Primer 12	CAGTTGAAATTGGAAACCACAGCATTAAG
Primer 13	TTAAAAATGCAGTCCTAGTCAGGTGGAG
Primer 14	CCTGTGTCCAGAGATAGATCCTACTGGTGG
Primer 15	GCCAAAGTGTAATTCCTAGAGCAGAAC

Primer 16	GCCATGCCACTCAAAGGGTGTCTTCAGACC
Primer 17	TGTGTGTTTTAAGAAGTTTATAAGTATGCC
Primer 18	AGATGCAAATTTGTTGACACTTATCCC
Primer 19	CAGCTTGAGTTGACATCCATTTGTATAGG
GAPDH control F1	TGCCAATCTCCTTGTTTTCTAATG
GAPDH control F3	TATTCCCCCAGGTTTACATGTTC

ChIP-qPCR

ChIP-qPCR was performed using THP-1 monocytes as described in the section *ChIP-qPCR* of Chapter 2. Primer sequences are presented in Table 2.7.

Table 2.7: List of primer sequences for ChIP-qPCR

Primer Name	Sequence (5′ - 3′)
IL-37 promoter F	CCCGTGTGTTAGCACTGTGA
IL-37 promoter R	GCAACCAGAAAGGCACCAAG

Results

A novel lncRNA called AMANZI emanates from the *IL-1β* promoter region

The rs16944 polymorphism is equally distributed across the global population by allelic frequency and is strongly associated with numerous inflammatory conditions (Figure 3.1A and B). Strikingly, alternate homozygous genotypes are correlated with highly divergent phenotypes, with rs16944 GG individuals being at risk for hyper-inflammation and rs16944 AA individuals being at risk for immunosuppressive conditions. The rs16944 SNP is located 511 bp upstream of the TSS of *IL-1β*, in the putative promoter region (Figure 3.3). In order to gain deeper insights to the role of this SNP in modulating inflammation, ChIP-Seq data from ENCODE was examined (Figure 3.3).

We hypothesised that the SNP could be altering transcription factor binding motifs in the *IL-1β* promoter to alter its activity and modulate the inflammatory response. Surprisingly, transcription factor ChIP-Seq analysis revealed that there was no transcription factor enrichment at the location of the SNP (Figure 3.3A). Instead, a transcription factor rich region was identified upstream of the rs16944 polymorphism. Importantly, PU.1 and CEBPB, which are transcription factors that were previously shown to be essential for *IL-1β* activation, did not coincide with the position of the SNP (Toda et al., 2002). This suggested that the rs16944 SNP did not interfere with transcription factor binding at the promoter to alter *IL-1β* transcription.

ChIP-Seq for epigenetic histone modifications showed that the position of the SNP coincided with signals for H3K4me1 and H3K27Ac in CD14+ monocytes (Figure 3.3B). This particular epigenetic histone signature is characteristic of active enhancer regions in the genome (see section entitled *Enhancers*), suggesting that the region surrounding the rs16944 polymorphism may be transcribed into a regulatory lncRNA that functions as an eRNA. Indeed, FANTOM CAGE data showed that the region was being transcribed, from approximately 100 bp upstream of the SNP, to produce a previously

unannotated lncRNA which we named AMANZI (Figure 3.3C). Interestingly, transcription of AMANZI occurred in the forward (sense) direction, which was opposite to the direction of *IL-1β* transcription, revealing a bidirectional transcription pattern at the *IL-1β* promoter. Furthermore, active transcription of this region selectively occurred in activated CD14+ monocytes, which are a major source of IL-1β. Taken together, this data showed that rs16944 was unlikely to modulate transcription factor recruitment to the promoter of *IL-1β*. However, a novel transcript (AMANZI), resembling an eRNA, does emanate from this region and could potentially be involved in the transcriptional regulation of *IL-1β*.

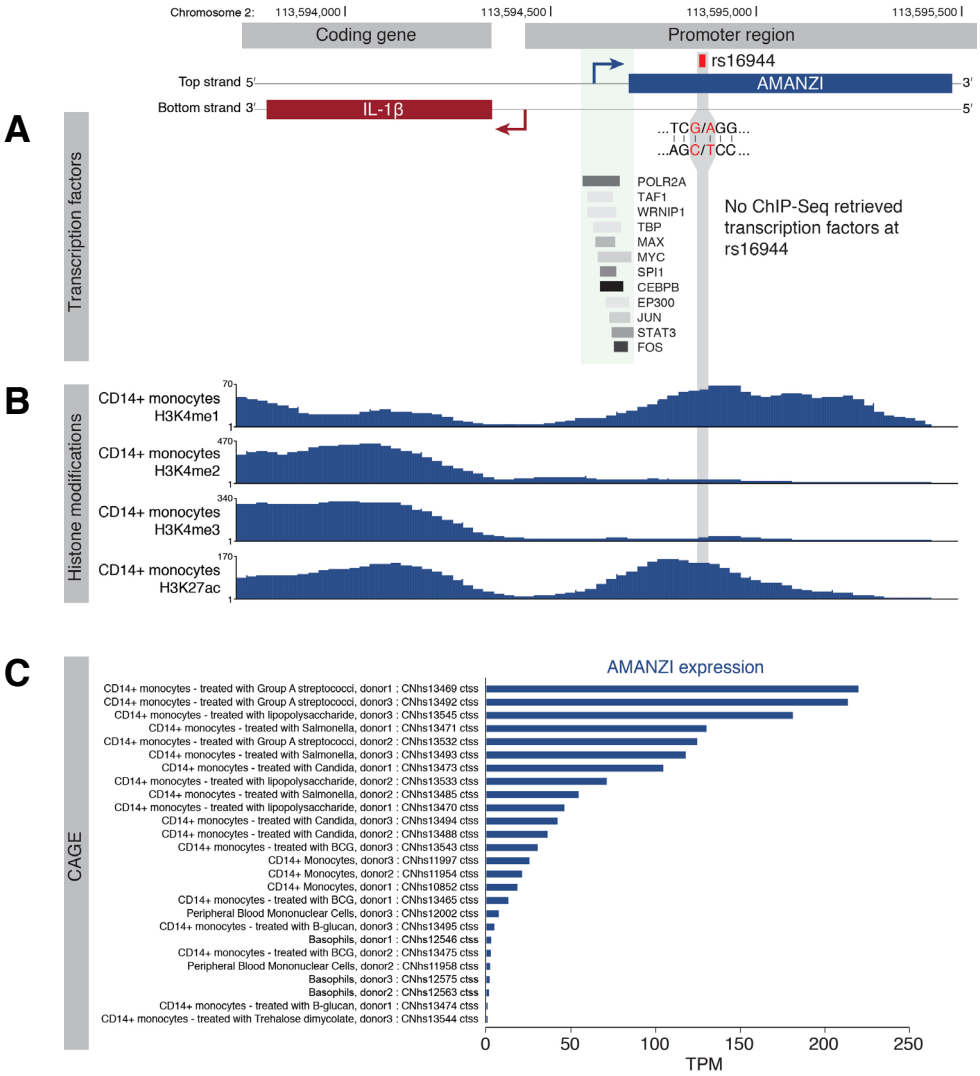

Figure 3.3: The promoter region surrounding the rs16944 SNP is actively transcribed in monocytes to produce a novel lncRNA called AMANZI

(A) The rs16944 SNP falls within the promoter region of *IL-1β* but does not coincide with any ChIP-Seq validated transcription factor binding sites that are relevant for the regulation of *IL-1β* transcription.

(B) ChIP-Seq of epigenetic histone modifications showed that the SNP was located in an active enhancer region (enriched for H3K4me1 and H3K27Ac).

(C) Analysis of CAGE data revealed that this enhancer was transcribed, predominantly in activated monocytes, to produce a novel eRNA (AMANZI). AMANZI was transcribed in the forward direction, opposite to the direction of *IL-1β* transcription (reverse), revealing a bidirectional transcription pattern at the *IL-1β* promoter region.

AMANZI can be detected by RT-qPCR and 3′ RACE

In order to isolate primer pairs that could recover the non-coding transcript that emerged from this region by RT-qPCR, an array of primers were designed to tile along the genomic locus downstream of the CAGE annotated TSS (Figure 3.4A). This encompassed the entire enhancer region as demarcated by H3K4me1 and H3K27Ac ChIP-Seq peaks. cDNA libraries were prepared from RNA harvested from the monocytic-like cell line, THP-1. Primer sets designed downstream of the AMANZI TSS (primer set 4-9) showed high levels of AMANZI expression (1.5 - 10 fold increase) after 60 minutes of stimulation with bacterial LPS, with the exception of primer set 5 (Figure 3.4B). Signal from primer set 5 after LPS stimulation resembled the poor signal from primers that targeted upstream of the TSS (primer sets 1-3), which represented an untranscribed region (Figure 3.4B). The low signal of primer set 5 could be the result of poor primer efficiency or the loss of the corresponding primer target region as a result of AMANZI being spliced. From these experiments, primer set 6 was chosen for the detection and quantification of AMANZI in subsequent experiments.

CAGE data provided the coordinates of the TSS, allowing for the 5′ end of AMANZI to be mapped. However, the 3′ end of AMANZI remained unknown. 3′ rapid amplification of cDNA ends (RACE) is a commonly used technique to discriminate the terminal end of a transcript. This requires capturing the transcript by the 3′ polyA tail found on mRNAs. In order to determine whether the non-coding AMANZI transcript was polyadenlyated, primer set 6 was used to detect AMANZI from a cDNA library constructed using a polydT primer (Figure 3.4C). AMANZI could be retrieved from this polyA captured cDNA library, albeit less frequently compared to using a random hexamer cDNA library. This indicated that AMANZI was indeed polyadenylated and amenable for interrogation by 3′ RACE.

3′ RACE was performed in LPS stimulated and unstimulated conditions, using a nested PCR approach. In the first round of PCR (PCR1), gene specific

primer 1 (GSP1) and the polydT primer were used to amplify a larger region of the transcript. This yielded multiple products, ranging from 200 - 800 bp in length, as observed by agarose gel electrophoresis (Figure 3.4D). Controls for this PCR included a library that did not contain any reverse transcriptase (-RT) and a water control. These control reactions were devoid of any amplification products, indicating that there was no residual gDNA or exogenous contaminants in the reactions. As only a single GSP was used in PCR1, it was expected that the specificity of the reaction would be poor. Therefore, a second round of PCR (PCR2) with GSP2 and the polydT primer was used to amplify a smaller region of AMANZI from within the products of PCR1. Observation of the resulting amplicons showed a significantly improved PCR specificity (Figure 3.4D). Despite this, there were still multiple products being amplified. However, these were considered as possible on-target products that could be describing variants of AMANZI length. Therefore, each of these bands were cloned and sent for Sanger sequencing. The result of this revealed that the DNA fragments that were around the 500 bp mark on the agarose gel of PCR2, mapped back to the AMANZI region, while the fragments that were 100 bp or 1 000 bp in length were non-specific. Taking into consideration the CAGE annotated TSS, AMANZI was found to be approximately 1 kb in length irrespective of LPS stimulation (Figure 3.4E).

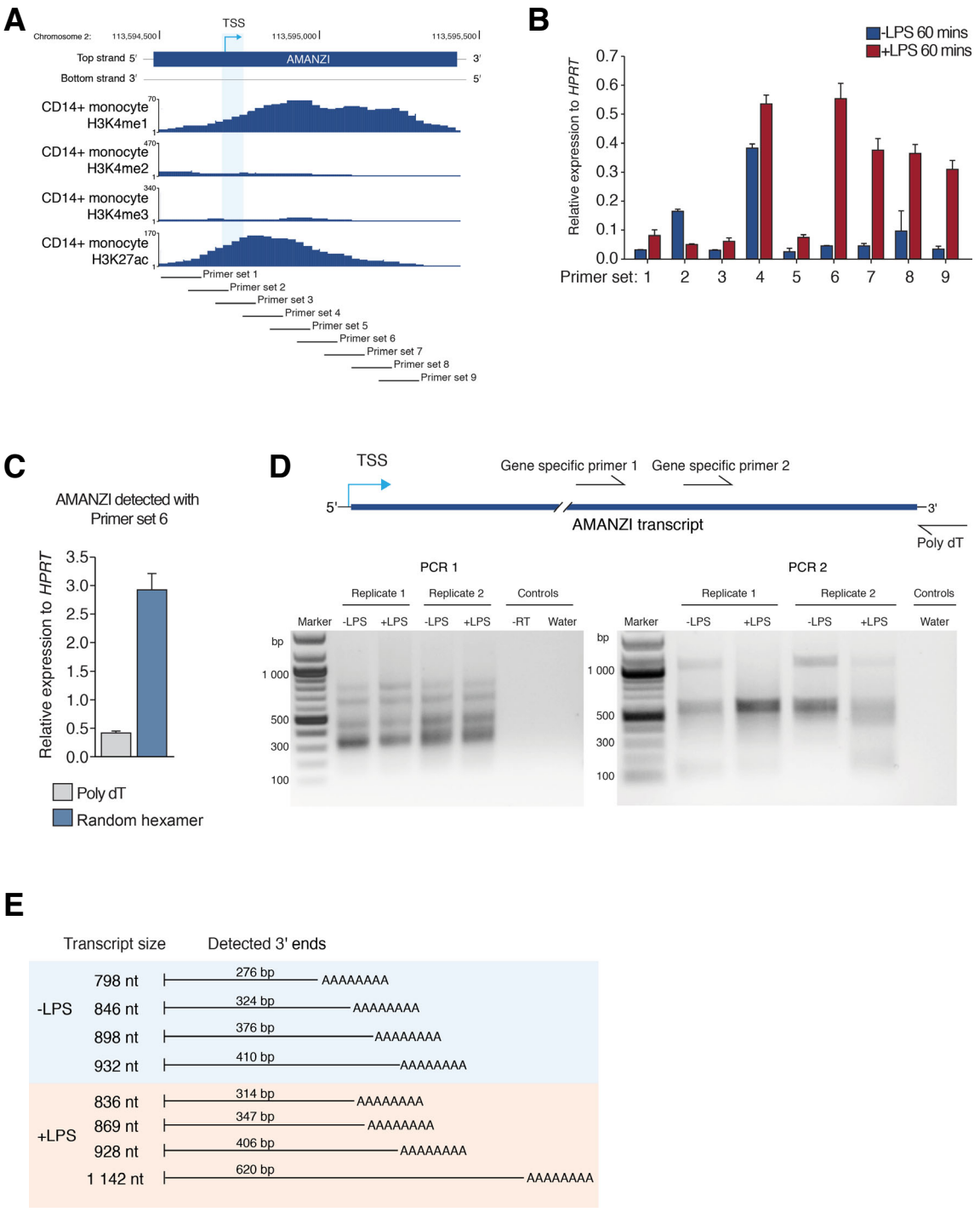

Figure 3.4: AMANZI is detectable by RT-qPCR and 3′ RACE in THP-1 monocytes

(A) A schematic showing the position of overlapping primer sets that were designed to tile the entire enhancer region as demarcated by H3K4me1 and H3K27Ac ChIP-Seq peaks.

(B) RT-qPCR was performed on unstimulated and LPS stimulated THP-1 monocytes to isolate primer sets that could detect AMANZI. Primer sets 4-9 bound downstream of the CAGE peak, whereas primer sets 1-3 bound upstream of the CAGE peak. Primer set 6 showed the most robust signal and was chosen for subsequent experiments.

(C) RT-qPCR using primer set 6 was performed on cDNA libraries made using a polydT primer or random hexamer. Recovery of AMANZI from the polydT library indicated that AMANZI was polyadenylated and conducive for 3′ RACE.

(D) A nested PCR approach was used to amplify and map the 3′ end of AMANZI (3′ RACE). PCR products were visualised by gel electrophoresis and showed that the nested PCR approach significantly improved the specificity of AMANZI recovery. Amplicons from PCR2 were cloned and identified by Sanger sequencing.

(E) A summary of the 3′ ends recovered by 3′ RACE after Sanger sequencing. These results revealed that AMANZI was approximately 1 kb in length.

AMANZI is a negative regulator of *IL-1β* transcription

The close proximity of AMANZI to *IL-1β* suggested that the two genes (coding and non-coding) would be co-transcribed when the shared *IL-1β* promoter was activated. To confirm this, RT-qPCR was used to measure the transcriptional response of AMANZI and *IL-1β* in THP-1 monocytes and PMA differentiated macrophages stimulated with LPS for 24 hours (Figure 3.5A). In both cell types, it was observed that the increase in *IL-1β* transcription in response to LPS stimulation, was accompanied by the significant increase in AMANZI transcription. This confirmed a co-transcriptional response between *IL-1β* and AMANZI. A similar response was also observed in the non-immune RPE1 cell line, however, the levels of *IL-1β* and AMANZI were much lower in these cells.

It was possible that the emergence of AMANZI from the promoter region of *IL-1β* may have been the result of transcriptional noise that accompanied *IL-1β* expression. In order to determine whether AMANZI was a bonafide functional lncRNA that regulates gene transcription, interfering LNAs were delivered into THP-1 monocytes 24 hours prior to LPS stimulation (Figure 3.5B). *IL-1β* and AMANZI transcripts were then measured by RT-qPCR in cells that were LPS stimulated for 1 hour or 24 hours. At both time points, a modest, but significant, knockdown efficiency (~65%) was observed compared to a negative control LNA (Figure 3.5B). Surprisingly, this loss of

AMANZI resulted in the over expression of *IL-1β* by 2.5 and 4.5 fold after 1 hour and 24 hours of LPS stimulation, respectively (Figure 3.5B).

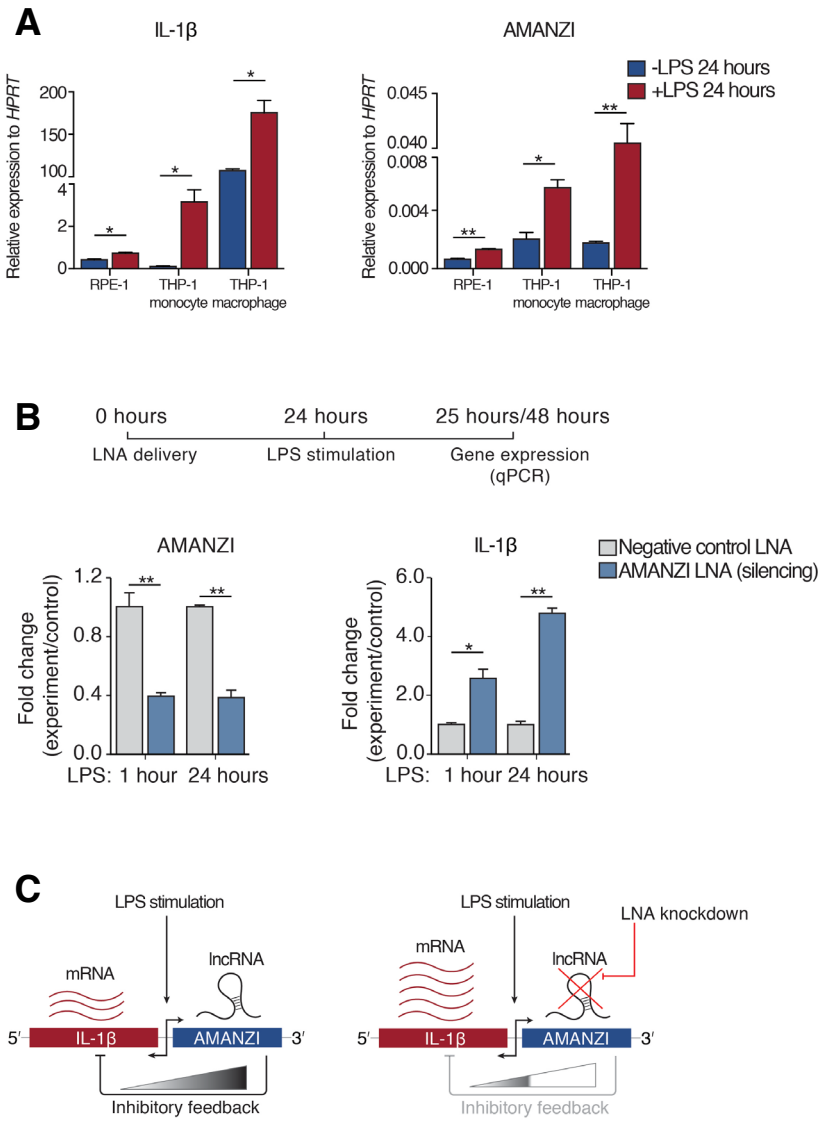

Figure 3.5: AMANZI is a negative regulator of *IL-1β* transcription

(A) RT-qPCR showed that *IL-1β* transcription was accompanied by the production of AMANZI in THP-1 monocytes and PMA differentiated macrophages, as well as the non-immune RPE1 cells, after 24 hours of LPS stimulation. (n=3)

(B) Modest depletion of AMANZI using interfering LNAs resulted in the over expression of *IL-1β* in THP-1 monocytes after 1 hour and 24 hours of LPS stimulation, compared to a negative control LNA. (n=3)

(C) Schematic of the negative feedback circuitry showing AMANZI functioning as a negative regulator of *IL-1β* transcription.

Data are represented as mean±SEM. n=number of independent experiments. p values were calculated using the Student's t-test. *p<0.05, **p<0.01, ***p<0.001.

From the epigenetic histone modification signature of this region and the close proximity of AMANZI to *IL-1β*, it was originally hypothesised that AMANZI functioned as an eRNA that activated *IL-1β* transcription. In contrast to this, these data presented here shows that AMANZI functions as a negative regulator of *IL-1β* transcription, which when depleted results in *IL-1β* transcription progressing uninhibited (Figure 3.5C). For this reason, this transcript was named A MAster Non-coding RNA antagoniZing Inflammation (AMANZI).

AMANZI and *IL-1β* co-occupy the same TAD as *IL-37*

TADs are regarded as the fundamental units of chromosomal organisation and gene regulation (see section entitle *Nuclear architecture*). In order to delineate the interaction network of *IL-1β*/AMANZI with other genes in 3D space, the *IL-1β* TAD was mapped using publicly available Hi-C data. This analysis revealed that other members of the IL-1 family, including *IL-1α* and *IL-37*, co-occupied this TAD with *IL-1β* and AMANZI (Figure 3.6A). Importantly, it was observed that the TAD was functionally bisected into two distinct sub-TADs (sub-TAD A and sub-TAD B), which segregated the pro-inflammatory cytokines (*IL-1α* and *IL-1β*) from the anti-inflammatory cytokine, *IL-37*. A CTCF binding site, which generally marks TAD boundaries and facilitates chromosomal loop formation (see section entitle *Nuclear architecture*), was found to be positioned between sub-TAD A and sub-TAD B and presumably mediated the formation of the two sub-loops within the main TAD. In order to gain higher resolution of the physical interactions within this TAD, publicly available Promoter Capture Hi-C data was examined. This data specifically enriches for genome-wide interactions between promoters, thus giving a more granular view of the interaction network between genes. This data revealed that there were several chromosomal contacts across the sub-TAD boundary, between the *IL-1β* promoter (from which AMANZI emanates) and *IL-37* (Figure 3.6B). Interestingly, these contacts were enriched in M1

(pro-inflammatory) macrophages. Taken together, these data suggested that these genes could be transcriptionally co-regulated through chromosomal looping events.

AMANZI is required for *IL-37* transcription

To determine whether AMANZI regulated the transcription of the other genes in this genomic neighbourhood, AMANZI was depleted using LNAs delivered into THP-1 monocytes 24 hours prior to LPS stimulation (Figure 3.6C). RT-qPCR was used to measure the transcription of the genes within the *IL-1β* TAD after 24 hours of LPS stimulation. *CKAP2L*, the only non-immune gene in this TAD, was unaffected by the loss of AMANZI when compared to the LNA control condition. However, a 2 fold over expression of *IL-1α* was observed as a result of AMANZI knockdown, producing a trend reminiscent of its pro-inflammatory counterpart *IL-1β* (Figure 3.5B and 3.6C). A similar increase was observed for the previously characterised *IL-1β eRNA*, which was shown to activate *IL-1β* transcription in response to LPS treatment (Ilott et al., 2014). Strikingly, *IL-37* transcription was abrogated (5 fold decrease) upon AMANZI depletion (Figure 3.6C). This revealed that AMANZI was necessary for the transcriptional activation of *IL-37*, suggesting that AMANZI potentially served as an eRNA for *IL-*37, rather than *IL-1β* as previously thought (Figure 3.6D). The over expression of the pro-inflammatory genes and their positive regulators (*IL-1α*, *IL-1β* and *IL-1β eRNA*) was likely to be an indirect effect of AMANZI depletion, as the resultant loss of the broad anti-inflammatory feedback of *IL-37* allowed for their transcription to go unregulated. Thus, these data revealed a biphasic feedback circuit between *IL-1β* and *IL-37* that regulates the pro- and anti-inflammatory response, respectively (Figure 3.6D).

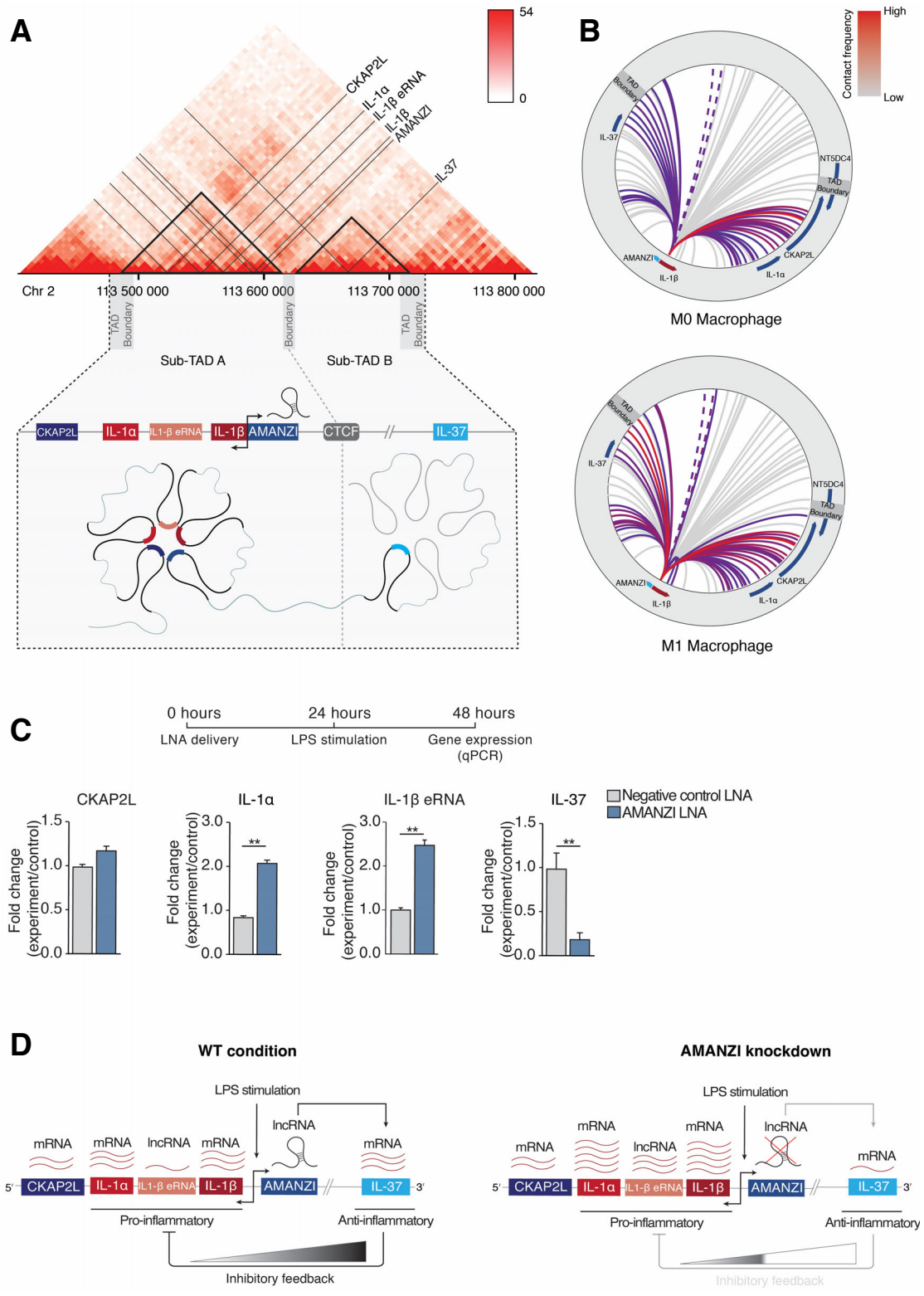

Figure 3.6: *IL-1β* and *IL-37* transcription is regulated by a biphasic circuit that is wired by AMANZI

(A) Hi-C analysis of the *IL-1β* TAD revealed that other members of the IL-1 family of cytokines (*IL-1α* and *IL-37*) co-occupied this TAD with *IL-1β* and AMANZI. The TAD was functionally bisected such that the pro-inflammatory cytokines (*IL-1α* and *IL-1β*) were segregated from the anti-inflammatory *IL-37* by an intervening CTCF demarcated boundary.

(B) Promoter Capture Hi-C analysis of the *IL-1β* TAD showed specific chromatin contacts between *IL-1β* and *IL-37* in naïve macrophages. These contacts were enriched in M1 polarised macrophages.

(C) Knockdown of AMANZI affected the transcription of the immune genes in the *IL-1β* TAD, compared to the negative LNA control (n=3).

(D) A schematic of the biphasic genetic circuit derived from these knockdown experiments. LPS activation of the *IL-1β* promoter results in the activation of *IL-1β* transcription. Accompanying this is the transcription of AMANZI, which is required for the transcriptional activation of *IL-37*. Functionally, the anti-inflammatory IL-37 introduces negative feedback into the system by inhibiting pro-inflammatory gene transcription. The depletion of AMANZI results in loss of IL-37 and its anti-inflammatory effects, thus resulting in pro-inflammatory gene expression to progress uninhibited.

Data are represented as mean±SEM. n=number of independent experiments. p values were calculated using the Student's t-test. *p<0.05, **p<0.01, ***p<0.001.

The *IL-1β*/AMANZI/*IL-37* circuitry is dependent on *IL-1β eRNA*

The *IL-1β eRNA* had been previously described by Ilott et al. 2014, to regulate the activation of the *IL-1β* promoter in response to LPS in human monocytes (Figure 3.7A). The LNA knockdown experiments presented here show that *IL-1β eRNA* was over expressed in response to AMANZI knockdown (Figure 3.6C), implicating a feedback mechanism between the two lncRNAs. In order to understand the role of the *IL-1β eRNA* in the regulation of the genes within this TAD, (in particular the *IL-1β*/AMANZI/*IL-37* circuitry) previously published LNAs were used to deplete *IL-1β eRNA* in THP-1 monocytes, 24 hours prior to LPS stimulation. RT-qPCR measurements showed that the LNA was highly effective at reducing the levels of *IL-1β eRNA* (82% knockdown efficiency) compared to the LNA control (Figure 3.7A). *CKAP2L* remained unaffected by this reduction of *IL-1β eRNA*, however, *IL-1α* was observed to be over expressed by 3.5 fold. Remarkably, *IL-1β eRNA* knockdown abrogated *IL-1β* transcription (as previously shown by Ilott et al. 2014), but also AMANZI and *IL-37*. This indicated that the activity of *IL-1β eRNA* was directed towards the activation of the *IL-1β*/AMANZI promoter unit and indirectly of *IL-37* (through AMANZI), while *IL-1α* was activated independently.

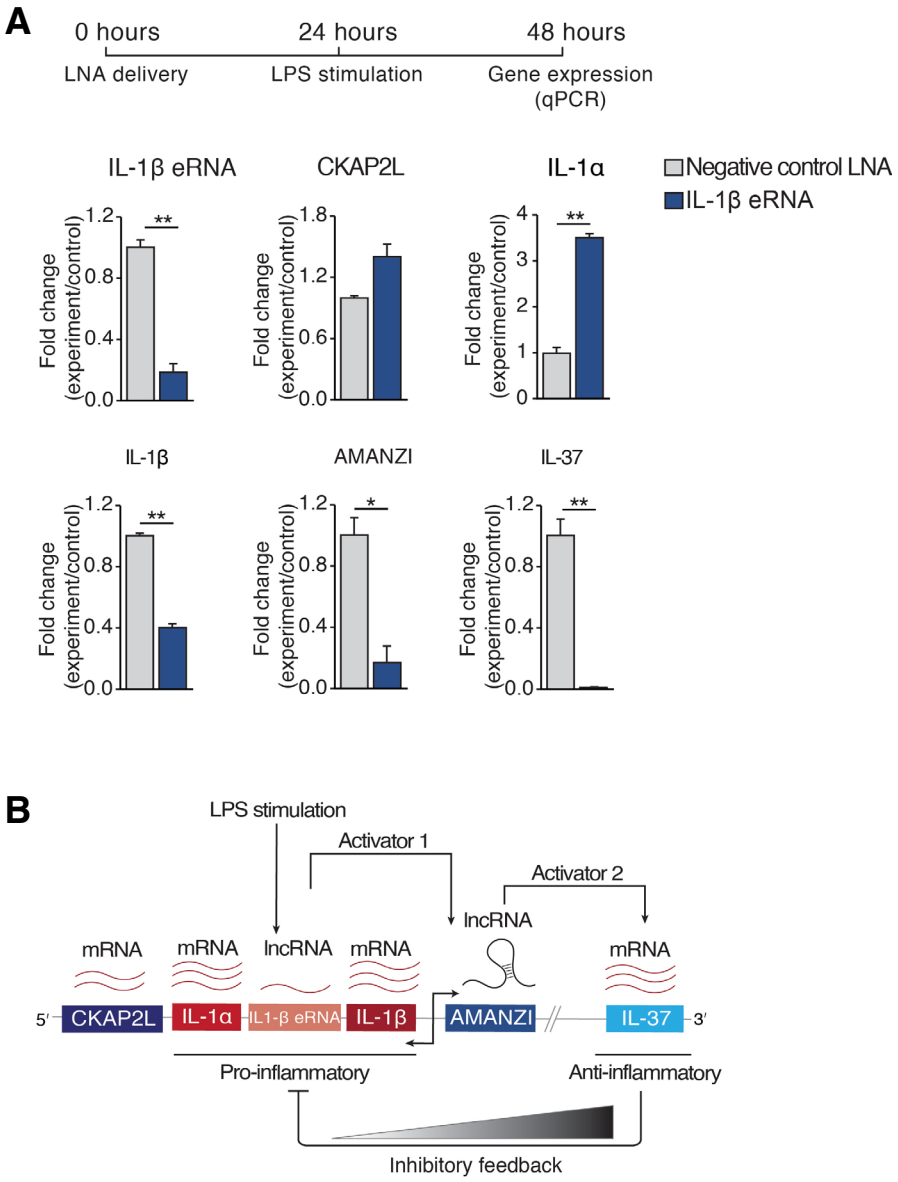

Figure 3.7: *IL-1β eRNA* is the master regulator of the *IL-1β*/AMANZI/*IL-37* biphasic circuit

(A) Depletion of *IL-1β eRNA* strongly abrogated the transcription of *IL-1β*, AMANZI and *IL37* compared to the negative control. *IL-1α* was over expressed, indicating that its activation was independent of *IL-1β eRNA*. (n=3)

(B) A schematic showing a two-tiered lncRNA regulatory system controlling *IL-1β* and *IL-37* transcription. *IL-1β eRNA* (activator 1) is sensitive to LPS and serves as an upstream regulator that activates the *IL-1β*/AMANZI promoter for transcription. Activation of *IL-1β* results in the co-transcription of AMANZI (activator 2), on which the transcription of *IL-37* relies. Expression of IL-37 inhibits *IL-1β* transcription in a negative feedback loop.

Data are represented as mean±SEM. n=number of independent experiments. p values were calculated using the Student's t-test. *p<0.05, **p<0.01, ***p<0.001.

In summary, these data revealed a two-tiered lncRNA regulatory system. At the apex of the regulatory hierarchy, *IL-1β eRNA* (activator 1) is sensitive to LPS stimulation and serves to activate the *IL-1β*/AMANZI promoter. This triggers the transcription of *IL-1β*, which marks the beginning of pro-inflammation. Accompany *IL-1β* is the co-transcription of AMANZI (activator 2), which is essential for the transcriptional activation of *IL-37*. Due to the broad anti-inflammatory function of IL-37, it is able to negatively feed back in the system to reduce the expression of the pro-inflammatory genes. Thus *IL-1β eRNA* serves as the master activator of this biphasic circuit, while AMANZI acts as the central toggle switch between the pro- and anti-inflammatory states mediated by the functionally opposed *IL-1β* and *IL-37*, respectively (Figure 3.7B).

CRISPR/Cas9 can be directed to genomic regions that safely delete AMANZI

In order to validate the observations made by LNA-mediated knockdown of AMANZI, CRISPR gRNAs were designed to delete the AMANZI genomic locus. Previous analysis of transcription factor ChIP-Seq revealed that the 5′ terminal end of AMANZI was enriched for transcription factor binding sites (Figure 3.8A). In particular, this region contained SPI1 and CEBPB binding sites, which are essential for the transcriptional activation of *IL-1β* (Toda et al., 2002). Therefore, CRISPR gRNAs were designed to delete a “safe” region of AMANZI that would preserve the transcriptional activity of *IL-1β* but remove a significant portion of the AMANZI genomic sequence. Six gRNA candidates were chosen to target this region, of which 3 produced cuts in the 5′ end (5′ cuts) and 3 produced cuts in the 3′ end (3′ cuts). The cutting efficiency of each guide was tested in HeLa cells using the T7E1 assay (Figure 3.8B). Cutting efficiency ranged from approximately 11-20%. Mock control conditions made use of an empty gRNA expression cassette, which resulted in no observable cuts in the genomic regions of interest. Functional clones for each gRNA candidate were obtained and used in subsequent experiments.

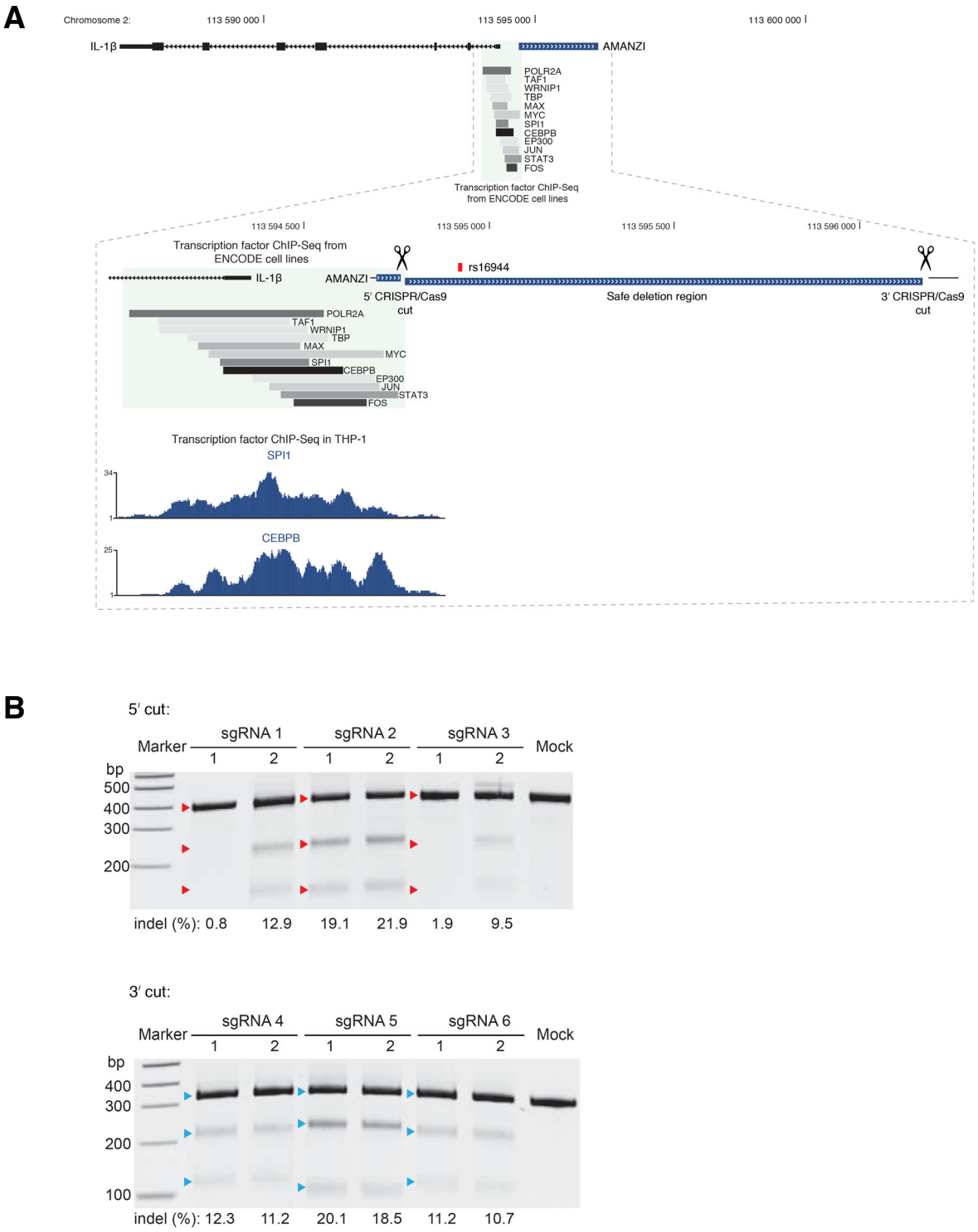

Figure 3.8: Design and validation of CRISPR gRNAs to delete the AMANZI locus

(A) Transcription factor ChIP-Seq analysis of the AMANZI region. CRISPR gRNAs were designed to delete most of the AMANZI sequence and preserve an area rich in transcription factor binding sites, some of which have been shown to be essential for *IL-1β* transcription (SPI1 and CEBPB).

(B) T7EI assay of the 5′ and 3′ targeting gRNAs. gRNA candidates were cloned into pX330 and assessed for cutting efficiency (indel %) in HeLas. Two clones of each guide were screened for cleavage activity.

Deletion of the AMANZI genomic locus recapitulates the gene expression trends observed from AMANZI knockdown

Adeno-associated viral (AAV) vectors (AAV6 serotype) were constructed to effectively deliver the CRISPR/Cas9 payloads into PMA differentiated THP-1 macrophages (Figure 3.9A). In order to improve the efficiency of AMANZI deletion, all the validated gRNAs (6 in total) targeting the 5′ and 3′ ends were delivered in triplex via two sets of viral vectors. Within each viral expression cassette, three gRNAs were expressed in *cis* from independent Pol III promoters. Accompany the two gRNA expression vectors, a third viral vector encoding Cas9 was included. An equimolar ratio of these three AAVs were used to transduce PMA differentiated THP-1 macrophages. A GFP expressing AAV was used to monitor the progression of infection.

14 days post-transduction, PCR was performed on the gDNA extracted from an unselected heterogeneous population of cells (Figure 3.9B). Using primers that flanked the outside of the cut sites (deletion primer F and R), the deletion of AMANZI gDNA (1 927 bp) could be detected as a smaller amplicon (328 bp) compared to the larger wild type amplicon (2 255 bp). Banding patterns were compared to a Cas9 only and water control, which showed wild type amplicons only or no amplicons, respectively. Using primers that bound to the deleted region of AMANZI (internal deletion primer F and R), qPCR was used to quantify the relative loss of AMANZI gDNA relative to an unaffected region nearby (Figure 3.9C). A modest, but significant, 28% reduction in AMANZI gDNA was detected compared to the Cas9 only control. These measurements confirmed that the AMANZI genomic region was deleted by AAV-delivered CRISPR/Cas9 in a proportion of the cell population.

In order to study the effects of this genomic deletion on gene expression, RT-qPCR was performed on this heterogenous population (Figure 3.9D). AMANZI

deletion resulted in the insignificant loss of AMANZI transcripts, but this was sufficient to cause the significant 2 fold over expression of *IL-1β* compared to the Cas9 only control. Further following the trend of the previous knock down experiments, *IL-1α* and *IL-1β eRNA* seemed to be over expressed, while *IL-37* expression was observed to be lower. These changes were however statistically insignificant. Despite this, the results from this mixed population of cells closely recapitulated the gene expression trends observed with the knockdown of AMANZI.

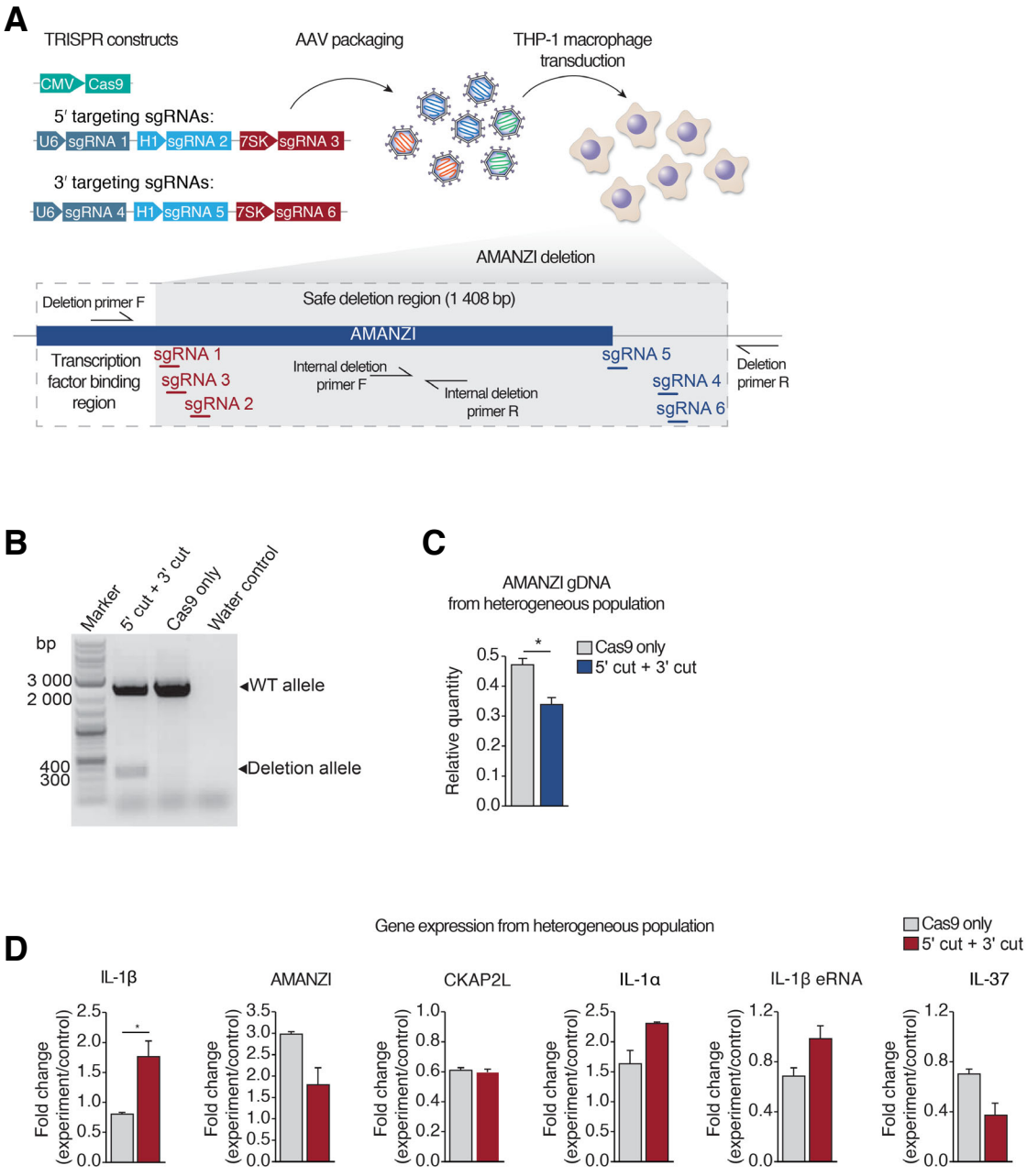

Figure 3.9: Deletion of the AMANZI genomic locus by AAV delivery of triplex gRNA CRISPR/Cas9

(A) AMANZI deletion strategy using AAV vectors to deliver CRISPR/Cas9 payloads into THP-1 macrophages. Validated gRNAs were packaged in AAVs and expressed in triplex by independent Pol III promoters (TRISPR). gRNA expression AAVs were accompanied by a Cas9 expressing AAV vector.

(B) AMANZI deletion was detected by PCR in a heterogenous cell population using primers that bound to regions outside of the cut sites (deletion primer F and R). The detection of the smaller amplicon, compared to the larger wild-type amplicon, was indicative of AMANZI deletion in a proportion of the cell population.

(C) The loss of AMANZI gDNA was quantified using qPCR and primers that targeted the deleted region of AMANZI (internal deletion F and R). (n=2)

(D) RT-qPCR was used to measure the expression of the genes in the *IL-1β* TAD in a heterogenous population of edited cells. The observed trends were concordant with the results of the AMANZI knockdown experiments, but were generally statistically insignificant. (n=2)

Data are represented as mean±SEM. n=number of independent experiments. p values were calculated using the Student's t-test. *p<0.05, **p<0.01, ***p<0.001.

AMANZI mediates a long-range chromatin loop with *IL-37* to activate its transcription

Our analysis indicated that *IL-37* occupied a distinct sub-TAD that was segregated from the *IL-1β*/AMANZI hub by an intervening CTCF boundary (Figure 3.6A). Furthermore, *IL-37* was also located 76 kb downstream of AMANZI. In order for AMANZI to regulate *IL-37*, AMANZI would need to either traverse or collapse this linear distance. It was hypothesised that *IL-37* was being recruited into the active sub-TAD A, containing *IL-1β*, through the formation of a dynamic chromatin loop during LPS stimulation. To map the specific chromosomal interactions within this region, 3C was performed across the boundary of these two sub-TADs in THP-1 monocytes before and after LPS stimulation. The *IL-1β*/AMANZI promoter region was set as the anchor point for this assay. In unstimulated cells, there was no observable chromosomal contact between the *IL-1β* and *IL-37* promoter regions (Figure 3.10A). Remarkably, the formation of dynamic chromosomal contact between the promoters of *IL-1β* and *IL-37* was observed after 60 minutes of LPS stimulation, and this was further consolidated after 12 hours (Figure 3.10A). This indicated that *IL-37* was able to traverse the sub-TAD boundary and enter the transcriptionally active *IL-1β*/AMANZI genomic neighbourhood after LPS stimulation. LNA depletion of AMANZI, prior to stimulation with LPS, resulted in the loss of this contact compared to the LNA control, even after 12 hours of LPS stimulation (Figure 3.10B). This revealed that AMANZI was essential for the formation of this dynamic contact.

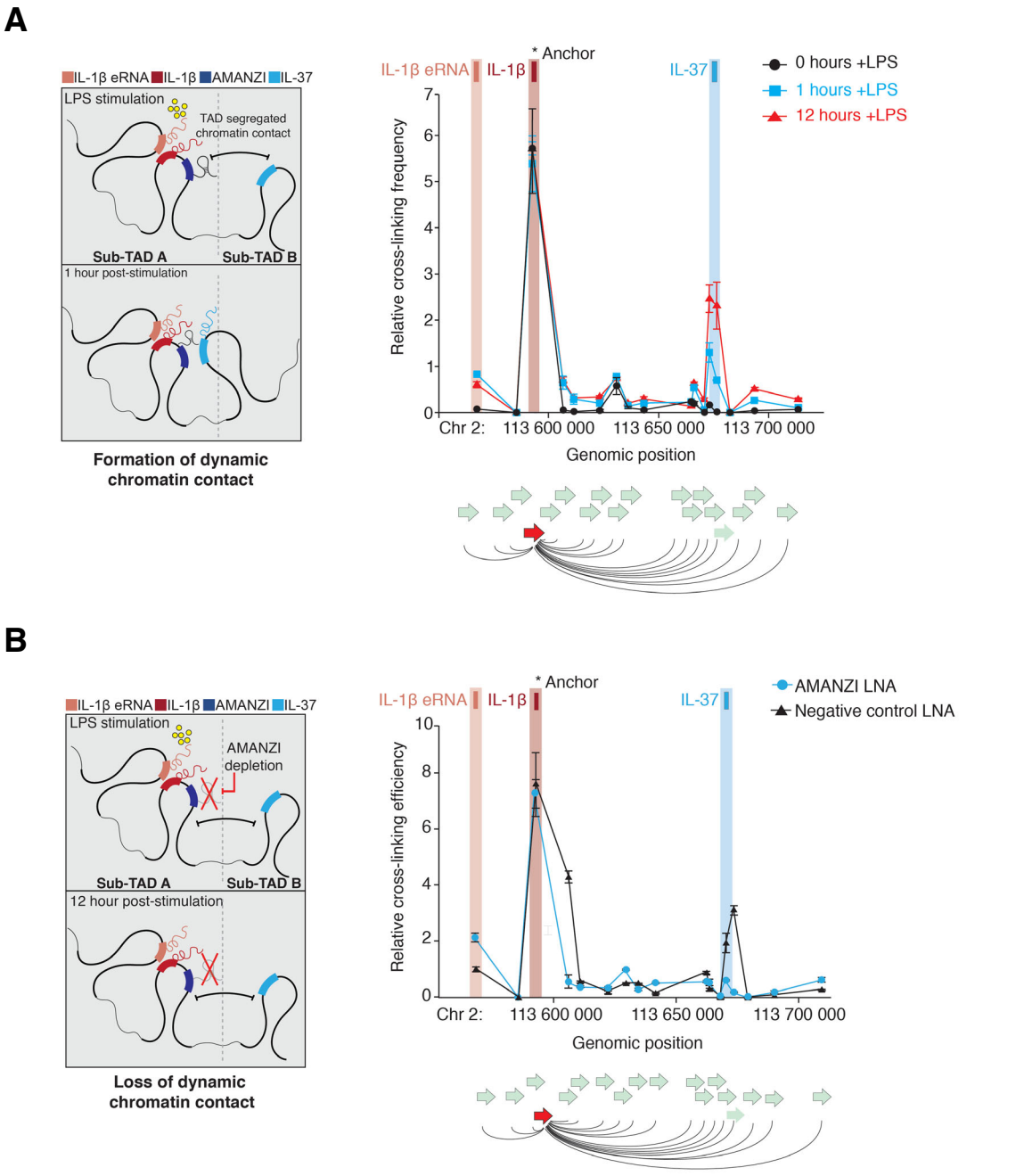

Figure 3.10: AMANZI mediates a long-range chromosomal loop with *IL-37* to activate its transcription

(A) 3C across the sub-TAD boundary revealed that a dynamic contact between the promoter of *IL-1β* and *IL-37* forms after LPS stimulation. The promoter region of *IL-1β* (red primer) was used as an anchor point. (n=2)

(B) Depletion of AMANZI prior to LPS stimulation resulted in the loss of this dynamic contact. (n=2)

(C) Time course measurements by RT-qPCR showed that *IL-37* transcription was delayed by 1 hour, following *IL-1β* and AMANZI transcription. The timing of this transcriptional activation coincided with the timing of the formation of the chromosomal contact between *IL-1β* and *IL-37*. (n=3)

Data are represented as mean±SEM. n=number of independent experiments.

Time course RT-qPCR was used to correlate the transcription kinetics of *IL-1β*, AMANZI and *IL-37* to the timing of this chromosomal reorganisation. This revealed that the establishment of the chromosomal contact between *IL-1β* and *IL-37* coincided with the transcriptional activation of *IL-37*. It was observed that *IL-37* transcription was delayed by an hour after *IL-1β* and AMANZI transcription had initiated (Figure 3.10C). This provided correlative evidence linking the timing of *IL-37* repositioning to its transcriptional activation.

Intuitively, such dynamic chromosomal looping events introduce a temporal delay in the transcriptional activation of genes. In this case, this may be responsible for coordinating IL-37 expression to ensure that its anti-inflammatory effects always follow IL-1β pro-inflammation. This suggests that dynamic chromosomal looping may be coordinating the progression of inflammation.

AMANZI is essential for the recruitment of MED12, Pol II and H3K4me3 deposition at the *IL-37* promoter

eRNAs are known to mediate long-range chromosomal loops in order to facilitate precise stimulus-dependent spatio-temporal regulation of transcription (see section entitled *Enhancer RNAs*). From the previously presented data, it was shown that the AMANZI locus had the epigenetic histone signature of an active enhancer region and produced a transcript that

was essential for the genomic repositioning of *IL-37* and its transcriptional activation. It was hypothesised that AMANZI functioned as an eRNA that regulated *IL-37* transcription and would facilitate the recruitment of transcription factors to the *IL-37* promoter. For example, the Mediator complex has been shown to collaborate with eRNAs to mediate chromosomal looping events which bring the enhancer regions into close spatial proximity to their cognate promoters (Lai et al., 2013). As a result, these promoters can then gain access to enhancer-associated transcription factors and transcriptional machinery, such as Pol II, which are causal to active transcription.

In order to determine whether AMANZI was associated with the recruitment of Mediator and other transcriptional activators, ChIP-qPCR was performed on THP-1 monocytes after AMANZI was depleted. The promoter region of *IL-37* was interrogated for MED12 (a subunit of Mediator), active Pol II (Ser5) and H3K4me3 occupancy after 24 hours of LPS stimulation (Figure 3.11A). An IgG antibody was used to create libraries that controlled for the random recovery of gDNA. When examining the results of the LNA control condition, it was observed that LPS stimulation resulted in the accumulation of MED12, Pol II Ser5 and H3K4me3 at the promoter of *IL-37*. Strikingly, the knockdown of AMANZI resulted in the significant loss of the accumulation these transcriptional activators. This indicated that AMANZI was mediating the establishment of chromosomal contact between *IL-1β* and *IL-37* via the recruitment of the Mediator complex (Figure 3.11B). Furthermore, AMANZI was needed for the accumulation of Pol II and H3K4me3 at the *IL-37* promoter, which are both essential for transcription.

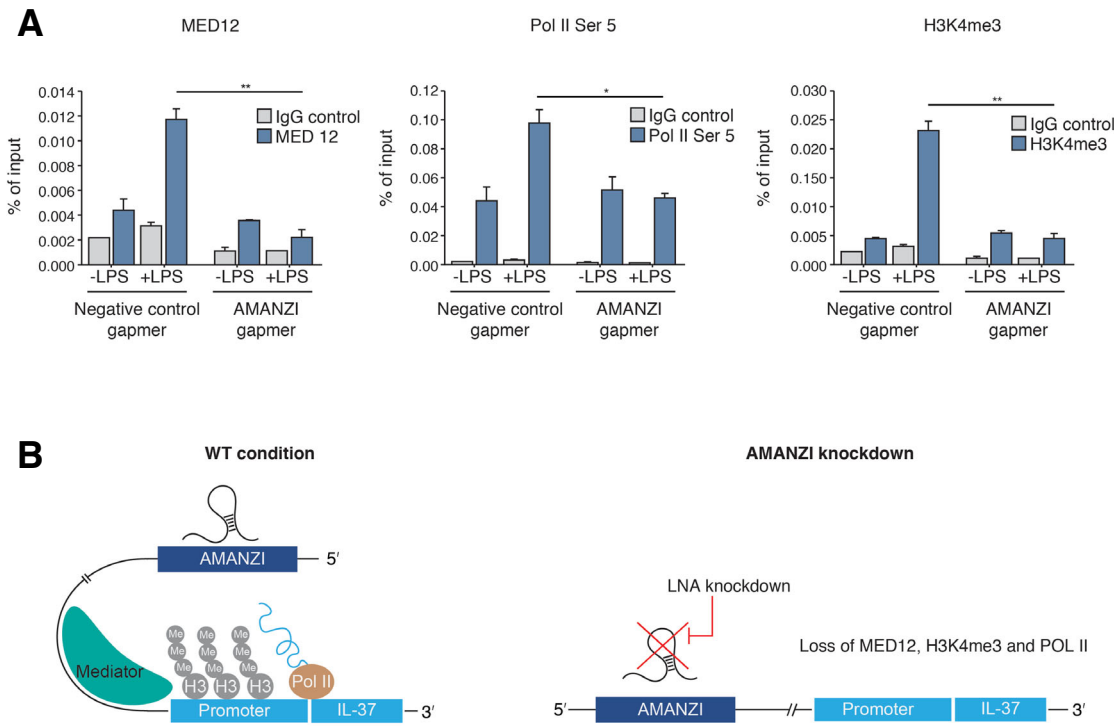

Figure 3.11: AMANZI is required for the recruitment of MED12, Pol II and H3K4me3 at the *IL-37* promoter

(A) ChIP-qPCR in THP-1 monocytes showed that LPS stimulation induced the recruitment of MED12, Pol II and H3K4me3 to the promoter of *IL-37*. Depletion of AMANZI resulted in the loss of these factors, which was likely to be causal to the loss of *IL-37* chromosomal contacts and transcription (n=3)

(B) Schematic showing the dependency on AMANZI for the recruitment of MED12, Pol II and H3K4me3 to the promoter of *IL-37*.

Data are represented as mean±SEM. n=number of independent experiments. p values were calculated using the Student's t-test. *p<0.05, **p<0.01, ***p<0.001.

Discussion

The biphasic nature of inflammation is regulated by the coordinated transcription of pro- and anti-inflammatory cytokines (Figure 1.1) (Medzhitov, 2008, Rogatsky and Adelman, 2014). This coordination ensures that pro-inflammation and anti-inflammation are temporally out of phase, such that the former always precedes the latter. This allows for an effective yet controlled inflammatory response to be mounted.

In this chapter, the data presented reveals that the two functionally opposed states of the innate immune system, pro- and anti-inflammation, are coordinated by a biphasic circuit housed within a single TAD (Figure 3.11). Through a series of knockdown experiments, a two-step lncRNA activation system that regulated the transcription of *IL-1β* and *IL-37* was observed. At the apex of the inflammatory response, *IL-1β* was transcriptionally activated by the previously characterised LPS-sensitive *IL-1β eRNA*, marking the initiation of the pro-inflammatory phase (Ilott et al., 2014). Accompanying this activation was the co-production of a novel unannotated lncRNA, called AMANZI, which emerged from the *IL-1β* promoter in the opposite (forward) direction to *IL-1β* transcription. The concomitant production of AMANZI led to the transcriptional activation of the broadly anti-inflammatory *IL-37*, which negatively fed back into the system to attenuate pro-inflammatory processes and suppress the function of IL-1β (Nold et al., 2010). Indeed, depletion of AMANZI led to the loss of *IL-37* transcription, which caused the over expression of the pro-inflammatory *IL-1α* and *IL-1β*. The over expression of these pro-inflammatory cytokines was the indirect result of the loss of *IL-37*. This was concordant with observations made by previous studies that attenuated the anti-inflammatory response by direct siRNA knockdown of *IL-37* (Nold et al., 2010). The work presented here essentially revealed that the functionally opposed *IL-1β* and *IL-37* are co-regulated by a biphasic circuit that is wired by AMANZI and triggered by *IL-1β eRNA* (Figure 3.12).

Central to the biphasic function of this genetic circuit is the ability of AMANZI to serve as a toggle switch that controls the two states of inflammation. This highlighted the importance of non-coding elements hidden in the genome that regulate complex biological processes. Currently, there are no reliable methods to identify regulatory elements genome-wide experimentally or computationally. However, phenotypic variations associated with SNPs occurring in the non-coding genome can direct investigators to regions that may encode for important regulatory function.

In this work, the discovery of AMANZI, and the biphasic genetic circuit that it regulates, was guided by the pathology-associated rs16944 SNP. The position of this polymorphism led to the finding of an underlying regulatory feature that encoded for AMANZI, which functionally coupled *IL-1β* and *IL-37* transcription. Importantly, homozygous rs16944 genotypes are associated with divergent inflammatory phenotypes, each of which can be associated with the function of IL-1β (pro-inflammation) and IL-37 (anti-inflammation) (Figure 3.1B). While the precise mechanism of the SNP currently remains unknown, it is possible that rs16944 alters the function of AMANZI to perturb the natural balance of this biphasic circuit, causing shifts that tilt the circuit to favour one state over the other. Future work that includes measurements of the transcriptional state of the genetic circuit in genotyped individuals may prove to be very insightful in this matter (see Chapter 4).

Functional characterisation of AMANZI showed that it mediates a dynamic chromosomal looping event across a CTCF sub-TAD boundary, to bring *IL-37* into close proximity to the active *IL-1β*/AMANZI transcriptional hub. Previous studies have corroborated this dynamic long-range contact between *IL-37* and *IL-1β* in LPS stimulated human monocytes (Sharaf et al., 2014). Coinciding with the establishment of this contact was the transcriptional activation of *IL-37*, suggesting that this chromatin reorganisation was linked to *IL-37* activation. Indeed, the loss of AMANZI resulted in the loss of transcriptional activators (Mediator, Pol II and H3K4me3) accumulating at the *IL-37* promoter. These data evoke a model whereby AMANZI functions like an eRNA to reposition the transcriptionally inactive *IL-37* to the active *IL-1β*/AMANZI transcriptional hub. At this position, *IL-37* can access transcription factors and histone modifiers (such as the *IL-1β IPL*) that can help activate its transcription. However, it remains unclear how *IL-37* physically traverses a clearly demarcated CTCF sub-TAD boundary to facilitate contact with *IL-1β*.

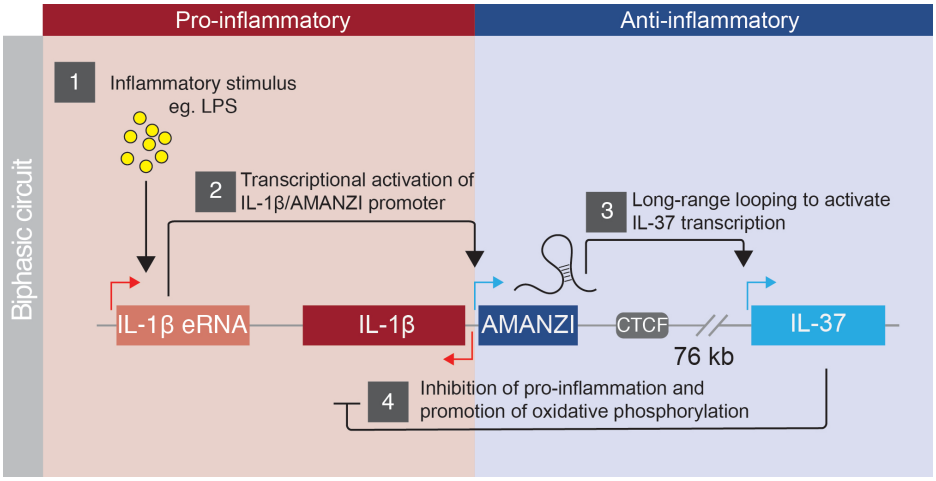

Figure 3.12: A schematic of the biphasic circuit regulating *IL-1β* and *IL-37* transcription
Inflammatory stimulation activates the LPS-sensitive *IL-1β eRNA*, which in turn can induce transcriptional activity at the *IL-1β*/AMANZI promoter unit. The transcription of *IL-1β* initiates the pro-inflammatory phase of inflammation. Accompanying *IL-1β* transcription is the production of AMANZI, which mediates long-range chromosomal rearrangements that are essential to the activation of *IL-37* transcription. The expression of the anti-inflammatory IL-37 negatively feeds back into the system to broadly inhibit pro-inflammation.

Chromosomal loops are formed by the extrusion of chromatin (see section entitled *Nuclear architecture*). It is possible that dynamic changes in CTCF boundary demarcation and cohesin recruitment at this locus, results in the extrusion of *IL-37* from sub-TAD B into the *IL-1β*/AMANZI sub-TAD A during inflammation. This dynamic physical remodelling of the sub-TAD structures could be causal to the distinct functional states of inflammation. Future experiments using sophisticated genetic manipulations, such as the deletion of the intervening CTCF site or the forced looping of chromosomal loci, will be useful in validating this model.

Chromosomal contacts can also be mediated by homotypic chromatin interactions across compartments (Monahan et al., 2019). Recent analyses of Hi-C data have suggested that nuclear A/B compartments are significantly smaller than previously thought (Rowley and Corces, 2018). Classically, compartments were defined to comprise multiple TADs that associated according to their chromatin state. The new model indicates that compartments are smaller than the size of TADs. This suggests that within the

boundaries of a single TAD, regions of the chromatin fibre as small as an individual active or inactive locus can be assigned to the A or B compartment, respectively (Rowley and Corces, 2018). As compartments are defined by their chromatin state, loci with homotypic chromatin are likely to engage in LLPS-mediated interactions. These can direct the formation of chromosomal contacts and be causal to transcription (see section entitled *Nuclear architecture*).

Perhaps one of the most exquisite examples of this type of regulation is how a singular olfactory receptor gene is expressed in individual olfactory sensory neurons. Over a thousand olfactory receptors genes are confined within a transcriptionally heterochromatic phase separated compartment. Their regulatory enhancers and transcriptional activators are located in an adjacent euchromatic compartment (Monahan et al., 2019). While the two adjacent regions are incompatible, changes in the chromatin state by transcription factors and histone modifiers to a single olfactory receptor gene, allows it to switch compartments and penetrate into its active neighbour. This compartment switching allows for the stable transcription of a single olfactory receptor in each olfactory sensory neuron (Rodriguez, 2013, Monahan et al., 2019). Such discrete compartment switching provides extremely fine control of chromosomal interactions and transcription. In the *IL-37* sub-TAD, such locus specific compartment switching could be the driving mechanism of the chromosomal interactions between the active *IL-1β* and the inactive *IL-37*, providing highly precise regulation of the pro- and anti-inflammatory response.

Despite certain aspects of the *IL-1β/*AMANZI/*IL-37* genetic circuit being incompletely described, our current understanding is sufficient to realise that the architecture of this genetic circuit can provide features that are fundamental for the regulation and coordination of the inflammatory response. Firstly, *IL-1β* and *IL-37* transcription are coupled by the function of AMANZI in this biphasic circuit. The production of AMANZI is hardwired into the transcription of *IL-1β*, as they both emerge from a common promoter. Therefore, the activation of *IL-37* is essentially dependent on the activity of the

IL-1β/AMANZI promoter unit. This coupling of *IL-1β* and *IL-37* transcription ensures that the *IL-37* anti-inflammatory response is always calibrated to the amplitude of the *IL-1β* pro-inflammatory response, in a dose-dependent manner. This suggests that the primary function of *IL-37* is to regulate the *IL-1β* pro-inflammatory response by serving as a direct counterbalance.

Secondly, dynamic spatial reorganisation of the genome inherently introduces a temporal delay in the transcriptional activation of the genes that are dependent on the formation of *de novo* chromosomal contacts. Indeed, the contact between *IL-1β* and *IL-37* only emerges after an hour of LPS stimulation and this timing coincides with the transcriptional activation of *IL-37*. While *IL-1β* is transcribed immediately after stimulation to initiate pro-inflammation, *IL-37* transcription is dependent on the production of AMANZI and the reorganisation of chromosomal loops, introducing a temporal delay that ensures anti-inflammation always follows pro-inflammation. Thus, by serving as a kinetic barrier to *IL-37* transcription, this dynamic reorganisation of the locus allows for *IL-1β* (pro-inflammatory) and *IL-37* (anti-inflammatory) processes to be temporally coordinated during inflammation.

Thirdly, characterisation of this circuit revealed that its behaviour is reminiscent of bistable switches that oscillate between different transcriptional states, such as the synthetic mammalian oscillator and the repressilator (Elowitz and Leibler, 2000, Tigges et al., 2009). This is unsurprising as cyclical expression patterns of immune genes, characterised by successive waves of immune gene activation and attenuation, have been previously reported (Amit et al., 2009). mRNA stability plays an integral role in shaping the kinetics of these oscillatory gene expression patterns (Hao and Baltimore, 2009). Fast mRNA turnover ensures that the dynamics of the transcriptional control elements are not overridden by long-lived mRNA species (Hao and Baltimore, 2009). In this body of work, time course measurements exhibit out of phase oscillations between *IL-1β* and *IL-37*, with approximately 12 hour periods (Figure 3.10C). Previous studies have shown that *IL-1β* and *IL-37* mRNAs are unstable and exhibit a faster turnover rate, which can be as short as 4 hours

(Bufler et al., 2004, Hadadi et al., 2016). This discrepancy can be explained by the 6 hour measurement intervals made in this study, which would mask any oscillations occurring at smaller timescales. Importantly, faster turnover rates of *IL-1β* and *IL-37* would allow for higher frequency oscillations in their cellular mRNA abundance under stimulation (Bufler et al., 2004, Adelman et al., 2009). Intuitively, more dynamic levels of *IL-1β* and *IL-37* afford greater regulatory resolution, allowing for the more precise and fine tuned control of pro- and anti-inflammation, compared to oscillations with larger periods (Figure 3.13). By encoding these different inflammatory states within a single bistable control unit, *IL-1β* and *IL-37* transcription can be dynamically regulated to produce a coordinated and well calibrated immune response to a constantly changing environment during infection.

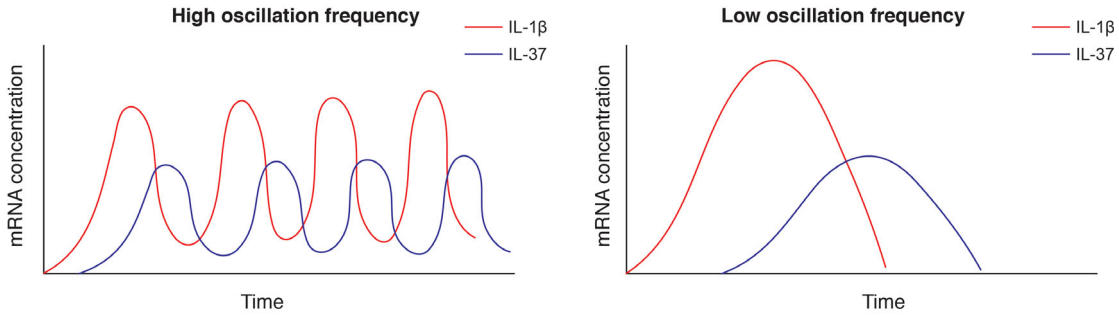

Figure 3.13: A schematic showing high frequency and low frequency oscillations in *IL-1β* and *IL-37* mRNA concentration

The fast turnover rate of *IL-1β* and *IL-37* mRNA along with the bistable nature of this genetic circuit allows for high frequency oscillations in the cellular mRNA abundance of *IL-1β* and *IL-37*. Compared to low frequency oscillations, this provides for more precise and highly dynamic regulation of inflammation.

In summary, the elucidation of this biphasic circuit reveals an exquisite mechanism that balances the two states of inflammation. The chromatin-regulated coordination of *IL-1β* and *IL-37* transcription from a single TAD, through the function of the lncRNA AMANZI, introduces a novel paradigm for immune gene regulation and inflammation. Furthermore, considering that this genetic circuit coordinates and regulates the expression of two integral mediators of inflammation, this study has potentially uncovered the workings

of a “master TAD” of inflammation. This has important implications in health and disease, as many aspects of cellular homeostasis and inflammatory function rely on IL-1β and IL-37 expression. Manipulation of this genetic circuit could possibly yield favourable outcomes in the modulation of inflammatory conditions, infection and vaccination. It is also possible that such biphasic circuits exist to regulate other immune genes or functionally opposed genes elsewhere. Essentially, this work illuminates a framework that involves numerous layers of transcriptional regulation, which function together to direct the progression of contradictory cellular processes.

Chapter 4

THE *IL-1β*/AMANZI/*IL-37* BIPHASIC CIRCUIT REGULATES TRAINED IMMUNITY

Introduction

Immunological memory refers to the ability of the immune system to recognise pathogens from prior exposures in order to elicit a more rapid and effective secondary immune response upon re-exposure. The ability to form these memories have traditionally been ascribed to the adaptive arms of the immune system. Here, adaptive immunological memory is preserved as a collection of epitopes in T- and B cells. Re-exposure to the pathogen will lead to the activation and expansion of these memory cell reservoirs to potentiate a subsequent immune response and the production of antigen-specific antibodies (O'Leary et al., 2006, Ratajczak et al., 2018). However, many plants and invertebrates lacking adaptive immune systems have displayed long-term protection against secondary infections, suggesting that the innate immune system is also capable of forming immunological memories. (Kurtz and Franz, 2003, Kurtz, 2005, Gourbal et al., 2018, Ramirez-Prado et al., 2018). Indeed, recent studies have demonstrated that human innate immune cells, particularly those of the myeloid lineage, such as monocytes and macrophages, are able to elicit immune responses that are shaped by past engagements with pathogens and vaccines (Quintin et al., 2012, Sun et al., 2012, Saeed et al., 2014).

The earliest observations of innate immune memory in mammals came from athymic mice which were vaccinated with the attenuated yeast strain *Candida albicans* (*C. albicans*). Subsequent infection of these immunocompromised mice with a virulent strain of *C. albicans* or the pathogenic bacteria *Staphylococcus aureus* (*S. aureus*) showed improved immunological

protection as a result of the vaccination independently of T-cells (Bistoni et al., 1986, Bistoni et al., 1988). Importantly, the acquisition of this protection was associated with the activation of macrophages and the strong induction of pro-inflammatory cytokines, which are both components of the innate immune system (Bistoni et al., 1986, Vecchiarelli et al., 1989). In humans, vaccination with BCG (Bacille Calmette-Guérin) improved non-specific immunological protection and survival against infection in West African children (Garly et al., 2003). This broad immunological protection was attributed to the enhanced production of cytokines in myeloid cells and persisted for over a month (Arts et al., 2018b). This revealed a long-lived form of innate immune memory associated with vaccination that is now called trained immunity.

Trained immunity can be induced in myeloid cells by a variety of stimuli, including cytokines, fungal, bacterial and metazoan antigens (Rizzetto et al., 2016, Arts et al., 2018b, Rusek et al., 2018, Schrum et al., 2018). However, the standard model used to induce and study trained immunity in the laboratory setting is through the pre-exposure of monocytes to β-glucan (BG), which is a major component of the cell wall from *C. albicans* (Quintin et al., 2012). Irrespective of the induction method, trained immunity culminates in the significantly increased transcription of pro-inflammatory cytokines upon re-stimulation, providing enhanced broad immunological protection in response to heterologous infections (Figure 4.1A) (Quintin et al., 2012, Saeed et al., 2014).

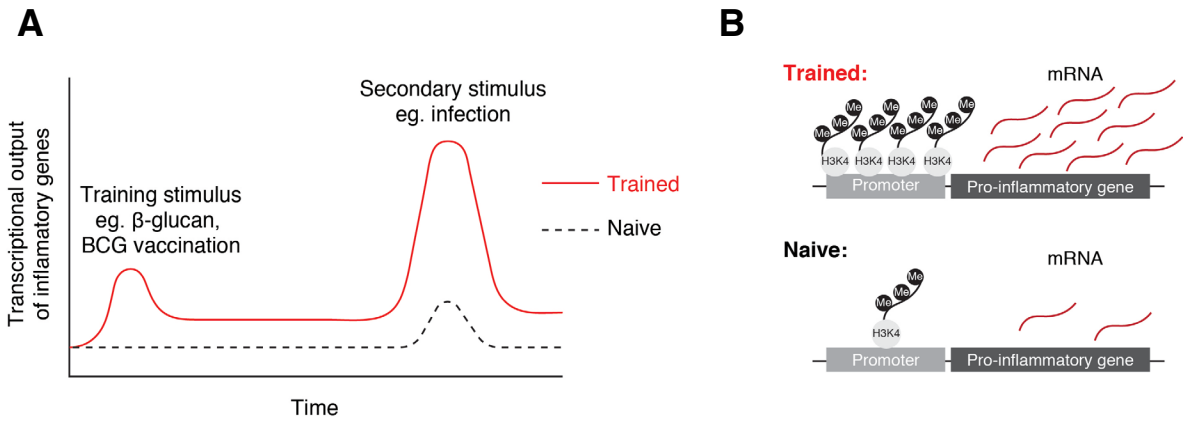

Figure 4.1: A schematic showing the transcriptional basis of trained immunity

(A) Trained immunity is induced through the pre-exposure of innate immune cells (such as monocytes) to training stimuli, which include BG or BCG vaccination. This training exposure is embedded as a long-lived immunological memory. Re-exposure of these trained cells to heterologous stimuli induces a significantly more power inflammatory response, compared to naive cells. Underlying this enhanced inflammatory response is the increased transcriptional output of inflammatory genes. As a result, trained immunity provides enhanced broad orthologous immunological protection.

(B) The immunological memory of trained immunity is embedded as epigenetic changes on the promoters of innate immune genes. After the induction of trained immunity (i.e the exposure to the training stimulus), increased H3K4me3 accumulation is observed at the promoters of the pro-inflammatory genes. This allows for the more rapid and robust transcription of these genes, allowing for the enhanced inflammatory response provided by trained immunity.

Hallmark characteristics of trained immunity include the metabolic reprogramming of cells towards aerobic glycolysis (Warburg effect) and genome-wide changes in epigenetic histone modifications, both of which are causal to trained immunity (Quintin et al., 2012, Cheng et al., 2014, Saeed et al., 2014, Arts et al., 2016). In particular, trained immunity is encoded as the discrete accumulation of H3K4me3 on the promoters of the immune genes, allowing for their transcriptional priming and rapid and robust activation upon re-stimulation (Figure 4.1B) (Quintin et al., 2012, Saeed et al., 2014). Recent work has implicated the IPLs in facilitating the discrete deposition of H3K4me3 at specific immune gene promoters during training, firmly establishing the role of lncRNAs and nuclear architecture in trained immunity (Fanucchi et al., 2019). Importantly, this epigenetic storage of innate

immunological memory is supported by the cellular switch towards glycolytic metabolism, which redistributes energy and metabolite stores to support this phenotype (Arts et al., 2016, Fok et al., 2018). The metabolic reprogramming during trained immunity is driven by hypoxia inducible factor-1α (HIF-1α) signalling (Cheng et al., 2014). Changes in cellular metabolism during trained immunity allow for the accumulation of key metabolites, such as succinate and fumarate, which serve as substrates and cofactors for chromatin writers and erasers (Cheng et al., 2014, Arts et al., 2016, Fok et al., 2018). These consolidate H3K4me3 deposition during training, highlighting a strong link between cellular metabolism and the epigenetic regulation of transcription.

IL-1β is an important endogenous mediator of trained immunity that can induce trained immunity itself (Arts et al., 2018b). Metabolically, IL-1β can up regulate HIF-1α expression to reinforce the essential glycolytic metabolism of trained immunity (Jung et al., 2003, Cheng et al., 2014). Furthermore, the elevated levels of IL-1β during trained immunity, drive the pro-inflammatory responses that are associated with improved immunological protection. This has been observed in cases of BCG vaccination, in which the resultant broad orthogonal immune protection is directed by elevated levels of IL-1β production (Garly et al., 2003, Kleinnijenhuis et al., 2012, Arts et al., 2018b). When IL-1β signalling was blocked, the loss of these functions hindered trained immunity (Kaufmann et al., 2018, Mitroulis et al., 2018). Thus, IL-1β is causal to the establishment and consolidation of trained immunity and provides the immunological protection associated with enhanced pro-inflammation. It is therefore evident that IL-1β plays a central role in trained immunity, suggesting that its regulation shapes the phenotype.

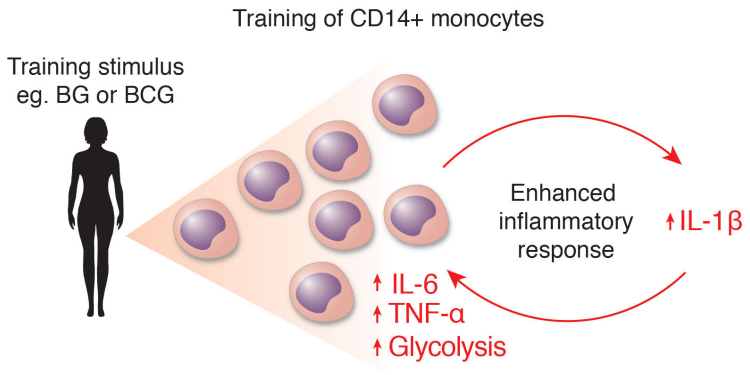

Figure 4.2: Trained immunity is directed by IL-1β

Pre-exposure of monocytes to BG or BCG results in the induction of trained immunity. This response is primarily mediated by the increased expression of IL-1β. Functionally, IL-1β is able to mediate the progression of pro-inflammation by inducing the expression of other pro-inflammatory immune genes such as *IL-6* and *TNF-α*. This enhanced pro-inflammatory response provides the enhanced immunological protection associated with trained immunity. IL-1β is also able to help establish and consolidate trained immunity by metabolically reprogramming the cells towards glycolytic metabolism. This shift in cellular metabolism redistributes energy and metabolites which are essential for the establishment and maintenance of the epigenetic changes that underly trained immunity.

The previously described rs16944 polymorphism, occurring in the promoter region of *IL-1β* (see Chapter 3), has been shown to modulate trained immunity (Arts et al., 2018b). BCG vaccination consistently elicited a more powerful pro-inflammatory (protective) response in rs16944 GG individuals compared to rs16944 AA individuals (Arts et al., 2018b). This observation has particular importance for vaccinations that rely on trained immunity (such as BCG), as it implies that the efficacy of trained immunity (and vaccination) depends on modulators of *IL-1β* transcription. Furthermore, while it is clear that the regulation of *IL-1β* plays an important role in driving the pro-inflammatory components of trained immunity, compensatory molecules which are able to modulate and promote anti-inflammatory responses that antagonise IL-1β during trained immunity, have remained unidentified.

The elucidation of the *IL-1β*/AMANZI/*IL-37* biphasic circuit (see Chapter 3) revealed how *IL-1β* was transcriptionally regulated. Importantly, through the function of AMANZI, the genetic circuit coupled *IL-1β* transcription to *IL-37*.

Functionally, IL-37 has broad anti-inflammatory capabilities that include the inhibition of IL-1β expression in peripheral blood mononuclear cells (PBMCs) (Nold et al., 2010). Furthermore, IL-37 can activate AMPK to reverse glycolytic metabolism (Cavalli et al., 2017). These functions of IL-37 diametrically oppose those of IL-1β and are able to modulate many of the processes which are essential for trained immunity. This suggests that IL-37 could function as a key modulator of this cellular response. As the previous work in this thesis demonstrated the genetic circuitry that regulates *IL-1β* and *IL-37* transcription, it was hypothesised that the *IL-1β*/AMANZI/*IL-37* biphasic circuit plays an important role in regulating the establishment of innate immunological memory.

In this chapter, trained immunity was induced in rs16944 genotyped human-derived monocytes. The state of the genetic circuit was measured in these samples to reveal a divergent tilt between rs16944 GG and AA individuals, who either favoured elevated *IL-1β* or AMANZI/*IL-37* transcription, respectively. These reciprocal transcription patterns suggested that changes in the balance of the *IL-1β*/AMANZI/*IL-37* genetic circuit modulated the efficacy of trained immunity between individuals of different rs16944 genotypes. In order to prove causality, suppression of AMANZI (and *IL-37*) in the THP-1 cell line recapitulated the transcription pattern as well as the enhanced trained immunity observed in rs16944 GG individuals. These results implicated the *IL-1β*/AMANZI/*IL-37* genetic circuit in regulating trained immunity.

Materials and Methods

200 Functional Genomics (200FG) cohort and ethics statement

Individuals in this study were healthy volunteers from the 200FG cohort. Volunteers were between 23 and 73 years of age, and consisted of 23% females and 77% males. Venous blood was drawn after healthy volunteers had given informed consent. The study was approved by the Ethical Committee of Radboud University Nijmegen, the Netherlands (2011/399). Experiments were conducted according to the principles expressed in the Declaration of Helsinki. All experiments on these human samples was performed by Simone Moorlag from Radboud University Nijmegen, Netherlands.

Human-derived monocyte isolation and culture

Venous blood was drawn from volunteers into 10 ml ethylenediaminetetraacetic acid (EDTA) tubes (Monoject). PBMCs were isolated by density centrifugation of 1:1 diluted blood in PBS over Ficoll-Paque (GE Healthcare). Recovered cells were washed twice in PBS and cultured in RPMI (Invitrogen) supplemented with 50 μg/ml gentamicin (Centrafarm), 2 mM GlutaMAX (Gibco) and 1 mM pyruvate (Gibco).

Training of human-derived monocytes

$5x10^5$ PBMCs were seeded in 96-well flat bottom plates in 100 μl of culture medium and were allowed to adhere at 37˚C for 1 hour. Non-adherent cells were washed off with PBS. Adherent cells were treated with 2 μg/ml of BG for 24 hours in the presence of 10% pooled human serum. Cells were then washed with 200 μl of PBS and incubated for 5 days in culture medium containing 10% human pooled serum. Medium was changed on day 3. On day 6, the cells were re-stimulated with 10 ng/ml of LPS for 24 hours before

analysis by ELISA or RT-qPCR (as described previously). Primer sequences are presented in Table 2.4.

Cytokine ELISA

Excreted cytokines in the supernatant were quantified using ELISA kits for human IL-6 (Sanquin) and TNF-α (R&D Systems) according to the manufacturer's instructions.

AMANZI knockdown and training of THP-1 monocytes

24 hours prior to BG training, LNA gapmeRs were electroporated into THP-1 monocytes as described in the section *Locked nucleic acid (LNA) delivery in THP-1 monocytes* from Chapter 3. LNA sequences are provided in Table 2.3. 10 μg/ml of BG was then used to train these electroplated cells for 24 hours, after which the BG was washed off by collecting the cells via centrifugation at 300 g for 3 mins and resuspending the pellet in 5 ml of PBS. This was repeated twice. Washed cell pellets were then resuspended in 0.5 ml THP-1 culture medium and allowed to rest for 5 days. The culture medium was replaced after 3 days. On day 7, the cells were stimulated with 10 ng/ml LPS for 24 hours prior to RNA extraction and RT-qPCR using the primers presented in Table 2.4 as described previously.

Results

rs16944 SNP alters the induction of trained immunity *in vitro*

Trained immunity can be recapitulated in the laboratory by pre-exposing human-derived monocytes to BG (Figure 4.3A). After 24 hours of exposure to this training stimulus, BG is washed off and the cells are allowed to rest for 5 days. LPS is then administered to challenge the cells for 24 hours, after which the immune response is assayed for the enhanced expression of pro-inflammatory cytokines (commonly IL-6 and TNF-α) associated with successful training. To validate this *in vitro* model, trained immunity was induced in monocytes derived from 36 healthy individuals from the 200FG cohort (Li et al., 2016). Using enzyme-linked immunosorbent assay (ELISA) to measure secreted IL-6 and TNF-α, significantly elevated levels of these cytokines were detected in the supernatant of BG trained monocytes, compared to the untrained (RPMI) controls (Figure 4.3B). Unfortunately, IL-1β production from these cells could not be measured due to the inability of monocytes to secrete this cytokine after a week in *ex vivo* culture. These results indicated that the primary monocytes from this cohort could be successfully trained *in vitro*.

A previous study by Arts *et al*. demonstrated that the rs16944 polymorphism affected the efficacy of trained immunity provided by BCG vaccination (Arts et al., 2018b). In order to determine whether this polymorphism had similar affects on BG induced trained immunity, the ELISA measurements for IL-6 and TNF-α were stratified according to the rs16944 genotype of the individuals in this study group (Figure 4.3C). Although this analysis did not yield statistically significant differences, the trend of the data was concordant with observations made in previous studies using BCG, where rs16944 GG individuals were consistently better trained than rs16944 AA individuals. This was evident by the enhanced production of IL-6 and TNF-α by the rs16944 GG individuals compared to the rs16944 AA individuals, after training.

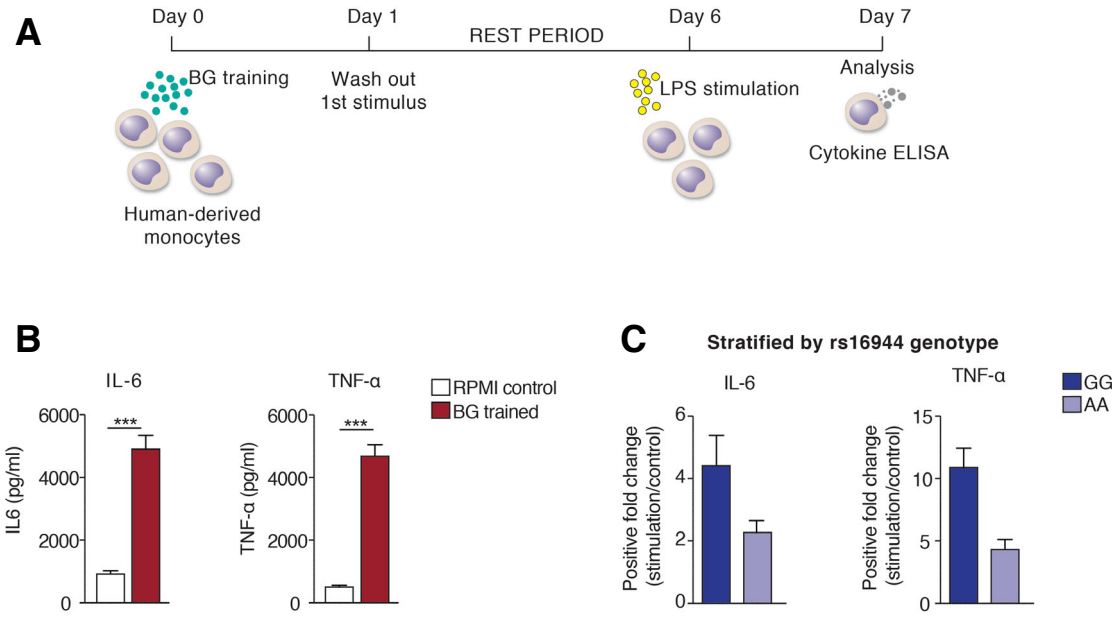

Figure 4.3: rs16944 SNP alters trained immunity *in vitro*

(A) A schematic showing the *in vitro* protocol for BG training of human-derived monocytes.

(B) BG training of human-derived monocytes harvested from healthy individuals of the 200FG cohort. Immune responses were assessed by measuring secreted IL-6 and TNF-α by ELISA (n=36).

(C) Trained immune responses (as determined by IL-6 and TNF-α ELISA) were stratified according to the rs16944 polymorphism. rs16944 GG individuals (n=22) showed patterns of enhanced trained immunity compared to rs16944 AA individuals (n=14)

Data are represented as mean±SEM. n=number of independent experiments. p values were calculated using the Student's t-test. *p<0.05, **p<0.01, ***p<0.001.

rs16944 SNP alters the expression of *IL-1β*, AMANZI and *IL-37* in response to BG

The enhanced inflammatory capacity associated with trained immunity is heavily reliant on IL-1β, suggesting that its regulation is paramount in shaping the trained immune response. With the elucidation of the *IL-1β*/AMANZI/*IL-37* genetic circuit, it became apparent that the regulation of *IL-1β* was coupled to the transcription of AMANZI and *IL-37*. It was hypothesised that the rs16944 SNP could potentially alter *IL-1β* or AMANZI (and indirectly *IL-37*) transcription due to its genomic position. This could potentially tilt the genetic circuit to favour the differences observed between the rs16944 genotypes in

trained immunity. In order to test this, the transcriptional state of the genetic circuit was measured by RT-qPCR and the results were stratified according to the rs16944 genotype of the volunteers in this study group. Previously, it was demonstrated that BG treatment induced trained immunity within 24 hours of exposure (Saeed et al., 2014). Thus *IL-1β*, AMANZI and *IL-37* levels were measured immediately after this 24 hour training period (Figure 4.4A).

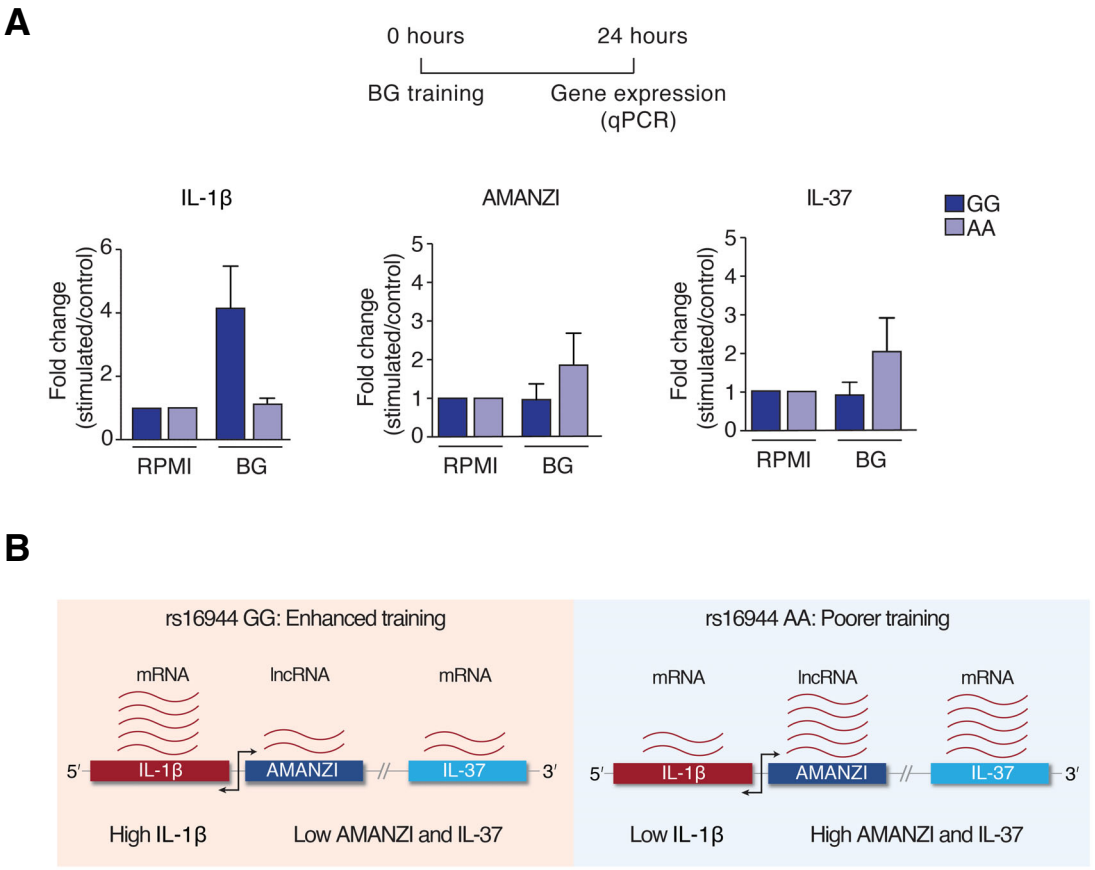

Figure 4.4: Transcriptional analysis of the *IL-1β*/AMANZI/*IL-37* genetic circuit according to the rs16944 genotype

(A) RT-qPCR of *IL-1β*, AMANZI and *IL-37* in human derived monocytes stratified by the rs16944 genotype after 24 hours of BG training. (n=36)

(B) Schematic showing that rs16944 GG individuals who are associated with enhanced trained immunity express higher levels of *IL-1β* and lower levels of AMANZI and *IL-37*, compared to rs16944 AA individuals who show the reciprocal transcription pattern and are more poorly trained.

Data are represented as mean±SEM. n=number of independent experiments. p values were calculated using the Student's t-test. *p<0.05, **p<0.01, ***p<0.001.

RT-qPCR measurements revealed that rs16944 GG individuals transcribed more of the pro-inflammatory *IL-1β* compared to AA individuals, whereas rs16944 AA individuals expressed higher levels the anti-inflammatory AMANZI and *IL-37*. While these differences were statistically insignificant, the trends suggested that the rs16944 SNP was associated with differences in the transcriptional response of *IL-1β*, AMANZI and *IL-37*. Furthermore, these transcription patterns were correlated with the differences in trained immunity that were previously observed amongst rs16944 individuals (Figure 4.4B). More specifically, rs16944 GG individuals expressed lower levels of AMANZI and *IL-37*, which would allow for the unencumbered expression of *IL-1β* and enhanced trained immunity. rs16944 AA individuals exhibited the reciprocal profile, expressing higher levels of AMANZI and *IL-37*. This stunted *IL-1β* transcription, resulting in poorer trained responses. This data suggested that the rs16944 SNP could be altering trained immunity by tilting the biphasic genetic circuit to affect the relative levels of *IL-1β* and AMANZI (and *IL-37*) to predispose individuals for enhanced or attenuated trained immunity.

AMANZI modulates trained immunity by regulating *IL-37* transcription

rs16944 GG individuals showed skewed transcription favouring elevated *IL-1β* levels during the 24 hour BG training period (Figure 4.4A). In order to determine if this was causal to enhanced trained immunity, AMANZI was depleted in THP-1 monocytes, prior to BG training, to recapitulate the relative levels of high *IL-1β* and low *IL-37* observed in these individuals (see *Results* section of Chapter 3). It was hypothesised that the role of *IL-37* featured prominently to regulate *IL-1β* and the induction of trained immunity.

Using the same LNAs that were previously validated in Chapter 3, AMANZI was depleted in THP-1 monocytes prior to BG training (Figure 4.5A). 5 days after the removal of the BG, the cells were challenged with LPS for 24 hours and *IL-1β* and *IL-37* transcript levels were measured by RT-qPCR (Figure 4.5B). When examining *IL-1β* transcript levels between untrained and BG trained cells in the negative control LNA condition, a 2.5 fold increase in *IL-1β*

transcription was observed as a result of BG training. This indicated that trained immunity was successfully induced in THP-1 monocytes. Strikingly, a significant 4.5 fold increase in *IL-1β* transcription was observed in trained THP-1 monocytes that had AMANZI depleted prior to BG training. This indicated that trained immunity was significantly enhanced as a result of AMANZI depletion, compared to the negative control LNA. This suggested that AMANZI is capable of modulating trained immunity by regulating the transcriptional activation of *IL-37* during the initial BG exposure time period.

When comparing the levels of *IL-37* between the AMANZI LNA and negative control LNA conditions, it would appear that *IL-37* transcript levels had returned to normal at the time of measurement. This suggested that the inhibitory effects of the AMANZI LNA was no longer active 8 days after the introduction of the LNAs. This indicated that the modulatory effects of IL-37 on trained immunity occurred within the 24 hours of BG exposure, when trained immunity was being established.

In summary, these data revealed that AMANZI is a modulator of trained immunity by regulating *IL-37* transcription. They also prove that shifts in the *IL-1β*/AMANZI/*IL-37* circuit can induce different outcomes of trained immunity. Specifically, rs16944 can seemingly tilt this circuit to enhance or reduce trained immunity. Indeed, by mimicking the shifts observed in rs16944 GG individuals through the depletion of AMANZI, significantly enhanced trained immunity was acquired via the indirect loss of *IL-37* and the gain of *IL-1β* transcription. This suggests that the balance of this biphasic circuit is central in the regulation of trained immunity, with AMANZI and *IL-37* being important modulators of this response.

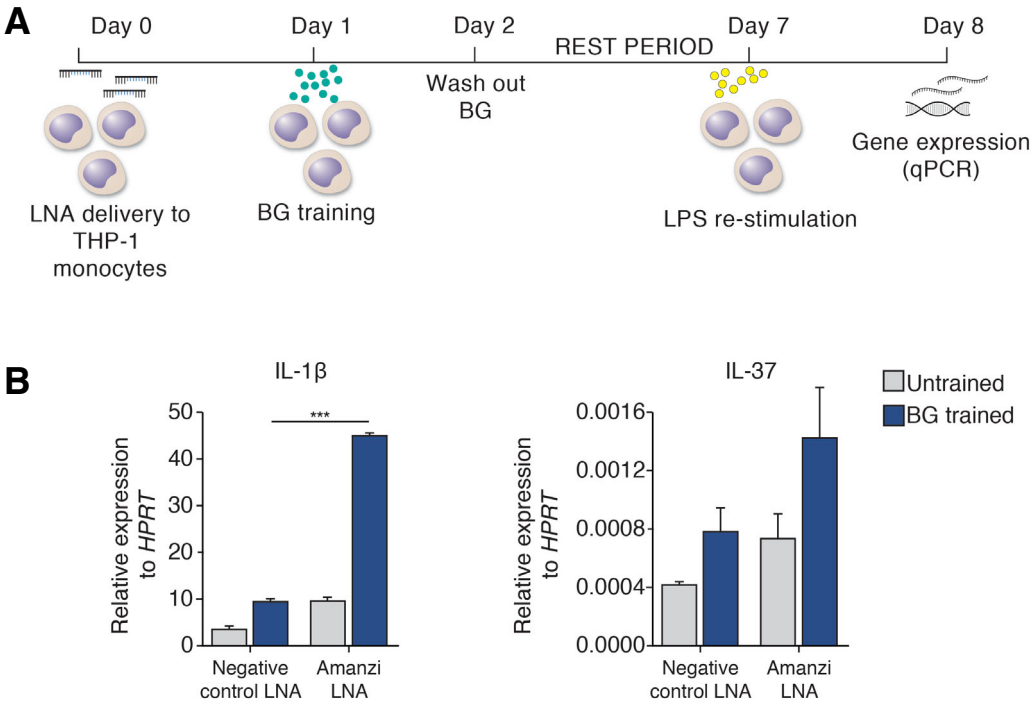

Figure 4.5: Depletion of AMANZI enhances trained immunity

(A) A schematic showing the protocol for the knock down of AMANZI prior to the induction of BG trained immunity.

(B) RT-qPCR of *IL-1β* and *IL-37* in cells that had AMANZI depleted prior to BG training. An enhanced trained response, detected as elevated *IL-1β* transcription, was elicited when AMANZI was depleted during BG training (Day 1) in THP-1 monocytes. The low concentrations of AMANZI and *IL-37* during this period (Day 1) mimicked the state of the genetic circuit in rs16944 GG individuals, resulting in an enhanced trained phenotype when re-stimulated with LPS 7 days later. (n=3)

Data are represented as mean±SEM. n=number of independent experiments. p values were calculated using the Student's t-test. *p<0.05, **p<0.01, ***p<0.001.

Discussion

Trained immunity is a fundamental feature of the innate immune system which provides enhanced pro-inflammatory responses and improved immunological protection against reoccurring pathogenic attacks (Garly et al., 2003, Kleinnijenhuis et al., 2012, Quintin et al., 2012, Saeed et al., 2014, Arts et al., 2018b). Due to the central role of IL-1β in pro-inflammatory processes, the regulation of *IL-1β* plays an important part in the induction of trained immunity (Garly et al., 2003, Kleinnijenhuis et al., 2012, Arts et al., 2018b, Kaufmann et

al., 2018, Mitroulis et al., 2018). Indeed, the data presented here corroborates previous observations which showed that the rs16944 polymorphism, located in the promoter of *IL-1β*, can modulate the inflammatory capacity of trained immunity (Arts et al., 2018b). Furthermore, SNPs in the downstream participants of IL-1β signalling have also been shown to affect the induction of trained immunity (Arts et al., 2018b). Together, this highlights the importance of IL-1β signalling in trained immunity and implicates the newly discovered *IL-1β*/AMANZI/*IL-37* genetic circuit in the regulation of trained immunity, where IL-37 could play a counter-modulatory role in the process.

In order to contextualise the identity of the rs16944 SNP with the function of the biphasic genetic circuit, transcriptional measurements revealed that the polymorphism affected the relative levels of *IL-1β*, AMANZI and *IL-37*. More specifically, rs16944 GG individuals produced more pro-inflammatory *IL-1β*, while rs16944 AA individuals transcribed more anti-inflammatory *IL-37*. Elevated levels of *IL-1β* are likely to underly the enhanced trained immunity observed in the rs16944 GG individuals. Conversely, the higher levels of *IL-37*, through its broad anti-inflammatory capabilities, can counter *IL-1β* and lead to the attenuation of trained immunity in rs16944 AA individuals. Such differences would explain why homozygous rs16944 individuals are so divergent in their inflammatory capabilities, with GG individuals being at risk of hyper-inflammatory conditions and AA individuals predisposed to immunosuppression (see Chapter 3).

The data presented here suggests that the rs16944 SNP is able to shift the balance of the *IL-1β*/AMANZI/*IL-37* biphasic circuit to favour pro- or anti-inflammation and enhance or attenuate trained immunity, respectively. Indeed, when the genetic circuit was forcefully shifted to favour *IL-1β* transcription (through the knockdown of AMANZI and the loss of *IL-37),* the enhanced trained immunity observed in rs16944 GG individuals was recapitulated. This proved that the *IL-1β*/AMANZI/*IL-37* circuit was important for regulating trained immunity, by controlling the relative levels of *IL-1β*, AMANZI and *IL-37*.

In addition to the inflammatory processes regulated by this biphasic circuit, it is also involved in regulating cellular metabolism. Studies have shown that a shift towards aerobic glycolysis is imperative for the induction of trained immunity (Cheng et al., 2014). This is mediated by HIF-1α signalling, which is consolidated by IL-1β (Jung et al., 2003, Cheng et al., 2014). Intriguingly, IL-37 can reverse glycolysis and promote oxidative phosphorylation via the activation of AMPK (Hardie et al., 2012, Cavalli et al., 2017). Thus, in addition to the pro- and anti-inflammatory function of this genetic circuit, it is likely to regulate the cellular metabolic state during trained immunity (Figure 4.6).

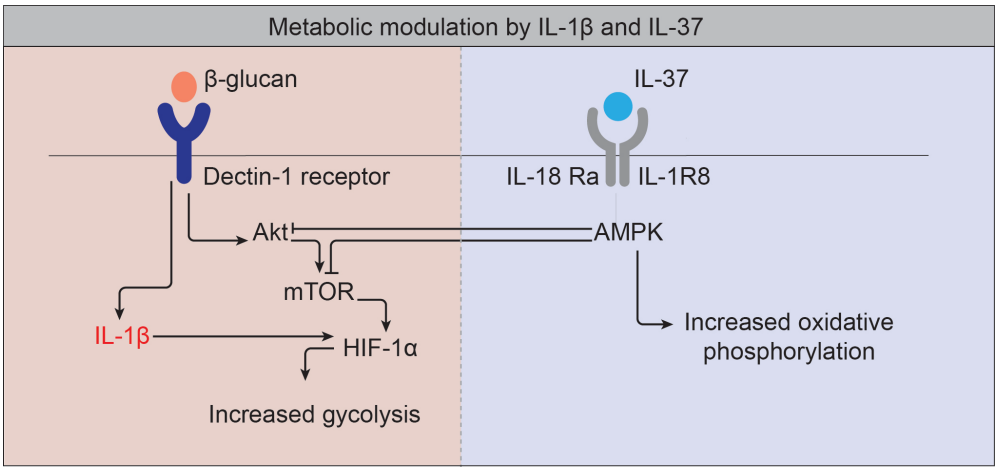

Figure 4.6: Metabolic modulation by IL-1β and IL-37

During BG training, activation of the Dectin-1 receptor induces trained immunity, resulting in the increased expression of IL-1β. Accompanying this is a shift towards glycolytic metabolism that is mediated by HIF-1α signalling. IL-1β is able to upregulate HIF-1α expression, consolidating the glycolytic metabolism that is essential for trained immunity. IL-37 signalling functionally opposes this through the activation of AMPK. This results in the reversal of glycolysis and the restoration of oxidative phosphorylation.

While the clinical data presented in this chapter revealed trends that fitted well with a model where rs16944 skews the genetic circuit to favour IL-1β pro-inflammation or IL-37 anti-inflammation, the comparisons between the genotypes were mostly statistically insignificant. This was the result of large variations in the inflammatory response between individuals. Such variations have previously been well documented, highlighting the pervasive and compounding roles of SNPs in shaping inflammation and immunity (Li et al.,

2016). Furthermore, the majority of these variations occur in the non-coding genome, suggesting that they affect the function of transcriptional regulatory elements (Nishizaki and Boyle, 2017). Phenotypic variations associated with these polymorphisms can be used to pinpoint genomic regions that encode for regulatory function. However, how these variations exactly affect the function of these regulatory elements to shape biological responses, such as inflammation, remains a long standing question.

Intriguingly, the rs16944 SNP was seemingly able regulate *IL-1β* and *AMANZI* in a divergent manner (i.e high *IL-1β* and low AMANZI versus low *IL-1β* and high AMANZI), even though they both emanate from a common promoter region. Usually, SNPs in the promoter region of genes modify transcription factor binding sites to alter their transcriptional activity. However, transcription factor ChIP-Seq analysis (see Chapter 3) has shown that the SNP does not fall within any transcription factor binding sites. Specifically, it has been demonstrated that *IL-1β* transcription is highly dependent on the PU.1 and CEBPB transcription factors, both of which were mapped to bind upstream of the SNP. However, changes in the 3D DNA shape proximal to transcription factor binding sites have been shown to affect DNA accessibility and alter transcription factor binding (Zhou et al., 2013, Abe et al., 2015). Predictive analysis of the local 3D DNA shape revealed that rs16944 variants did in fact alter key characteristics of the DNA structure, particularly the minor groove width, propeller twist and the helix twist of the DNA (Figure 4.7). Such changes in the DNA shape may alter the nearby chromatin accessibility and divergently affect *IL-1β* and AMANZI transcription. Alternatively, since the position of the SNP falls within the AMANZI sequence, variants of the SNP could be affecting the function of the AMANZI transcript, by altering its stability or its interactions with other biomolecules. It is possible that in rs16944 AA, AMANZI is stabilised to induce higher levels of *IL-37*, whereas in rs16944 GG, AMANZI is more readily degraded, allowing for the higher levels of *IL-1β*. Such a hypothesis will have to be experimentally tested in future work and is outside the scope of this current thesis.

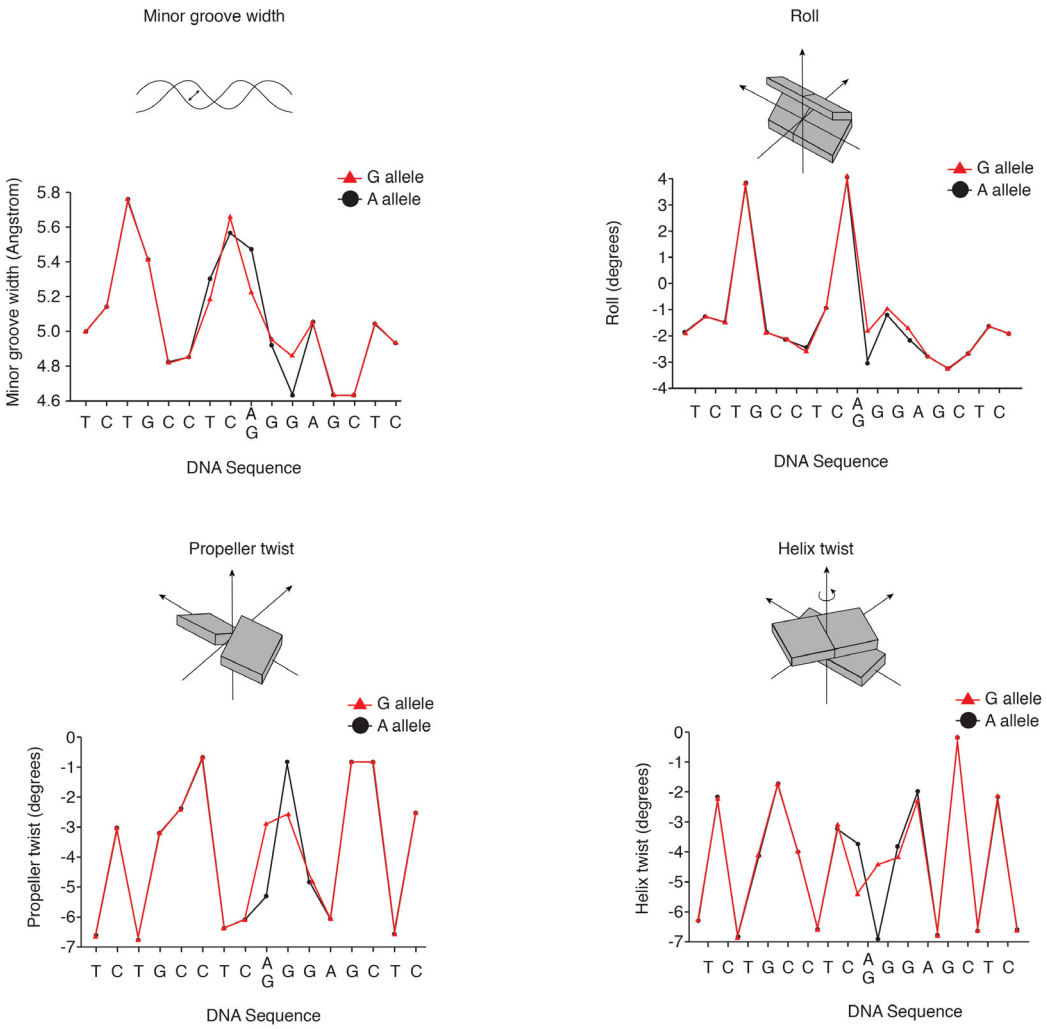

Figure 4.7: DNA shape analysis of the genomic region around the rs16944 SNP (A/G)
Predictive analysis showed significant changes in the minor grove width, propeller twist and the helix twist of the DNA shape between the rs16944 genotypes. These changes could affect the local DNA accessibility and proximal transcription factor binding to alter gene expression. Changes to the DNA roll were insignificant.

While the precise mechanism by which this SNP coordinates this divergent bidirectional transcription currently remains unclear, its role in the regulation of trained immunity has important implications. For example, the BCG vaccine relies heavily on the induction on trained immunity for protection against the pervasive and lethal Mycobacterium tuberculosis. However its efficacy is highly variable (0-80%) amongst vaccinated individuals (Andersen and Doherty, 2005). The rs16944 SNP could serve as a predictive marker to gauge trained immunity and BCG vaccination efficacy, allowing for adjuvant measures to be implemented to enhance trained immunity in rs16944 AA

individuals. This could include the use of more virulent BCG strains, which have been shown to provide more effective protection (Zhang et al., 2016). Alternatively, modulation of the *IL-1β*/AMANZI/*IL-37* circuit could also be helpful. Depletion of AMANZI prior to vaccination would augment the *IL-1β*/AMANZI/*IL-37* genetic circuit to favour pro-inflammation and yield improved trained immunity and vaccination efficacy.

Trained immunity clearly provides immunological protection, but it is also thought to be the basis of many diseases brought about by excessive inflammation (Arts et al., 2018a). In many of these diseases, the hallmarks of trained immunity, including epigenetic changes, cellular metabolic shifts and excessive pro-inflammatory gene expression have been observed (Arts et al., 2018a). Conversely, conditions afflicted by severe immunosuppression may benefit from the enhanced pro-inflammation associated with trained immunity. Indeed, the use of BG to reverse the immunosuppressive state of tumour-associated macrophages in cancer has already demonstrated success in a few studies (Tian et al., 2013, Liu et al., 2015). Thus, the ability to curb or enhance the effects of trained immunity could be highly effective in treating disease. By implicating the *IL-1β*/AMANZI/*IL-37* circuit in the regulation of trained immunity, it has provided novel ways to modulate this heightened pro-inflammatory response. Therapeutic augmentation of this genetic circuit could alter trained immunity to favour enhanced or attenuated inflammation and reverse or mitigate pathological inflammatory states.

Chapter 5

GENERAL DISCUSSION AND CONCLUSION

In the eukaryotic nucleus, functional complexity is embedded within the non-coding portion of the genome. Here, numerous layers of transcriptional regulation serve to control the expression of the protein-coding genome in space and time. Each of these layers function at different size scales within the nucleus, allowing for the increasingly finer control of transcription. Many of these regulatory mechanisms function cooperatively and combinatorially to give rise to higher-order biological processes.

Inflammation is an important and complex cellular response that is required for immunological protection against pathogens (Rogatsky and Adelman, 2014). During the initial acute pro-inflammatory phase of this response, cytokine transcription needs to be rapid and robust in order to effectively initiate host defence mechanisms. The subsequent anti-inflammatory phase needs to be temporally delayed to follow pro-inflammation. This requires the precise coordination of pro- and anti-inflammatory cytokine expression. Dysregulation of these key processes during inflammation is a major cause of many diseases (Netea et al., 2017).

The studies presented in this thesis illuminate some of the mechanisms that regulate these phases of the inflammatory response and have been shown here, and elsewhere (Fanucchi et al., 2019), to regulate trained immunity. In particular, the work highlights the role of two novel lncRNAs which provide highly discrete, locus specific regulation of immune gene transcription. UMLILO was shown to exploit the local 3D topology and epigenetically prime the ELR+ CXCL chemokines for their signal-dependent transcription. AMANZI was found to function as a central toggle switch in a biphasic genetic circuit that coordinated pro- and anti-inflammation by dynamically reorganising key

chromosomal contacts. Due to the central role of these lncRNAs in regulating inflammation, they provide novel potential targets for the therapeutic modulation of inflammation. In this chapter, prospects of targeting lncRNAs to therapeutically treat pathological inflammation will be discussed.

Drugging lncRNAs: A novel paradigm for modern medicine

Inflammatory diseases are generally characterised by the deregulated production of cytokines, which contribute to excessive states of pro- or anti-inflammation. In order to restore homeostasis, strategies to block aberrant cytokine signalling or initiate counteracting signalling pathways have been pursued.

Cytokine therapy makes use of exogenous recombinant cytokines to activate or inhibit endogenous signalling pathways that counteract pathological states of inflammation. This has been particularly effective in treating certain cancers, where pro-inflammatory cytokines, such as IL-2 and interferon-α (INF-α) have been approved by the Food and Drug Administration (FDA) for their use in inducing anti-tumour immunity (Lee and Margolin, 2011). Other studies have demonstrated the benefits of using exogenous interferon-ɣ (INF-ɣ) and IL-10 for treating infections and autoimmune diseases, respectively (Delsing et al., 2014, Saxena et al., 2015). However, due to the broad effects of cytokine signalling, the systemic delivery of recombinant cytokines has many adverse side-effects, making this treatment less than ideal (Weber et al., 2015).

In contrast, anti-cytokine therapies block excessive cytokine signalling through the use of monoclonal antibodies or mimetic peptides to ameliorate their inflammatory effects. IL-1β has emerged as a key therapeutic target for many diseases due to its central role as the gatekeeper of pro-inflammation. Three IL-1β targeting modalities, including a receptor antagonist, a decoy receptor and a monoclonal antibody, have already been successfully developed to block IL-1β signalling. These have been shown to effectively reduce the

severity of inflammation associated with many diseases such as rheumatoid arthritis, gout, diabetes and myocardial infarction (Dinarello, 2011, Dinarello et al., 2012). While anti-cytokines for IL-37 have not been therapeutically explored yet, blocking of IL-10, a similarly powerful anti-inflammatory cytokine, has been effective in enhancing the efficacy of certain vaccines and promoting the anti-tumour effects of immunotherapies (Sato et al., 2011, Ni et al., 2015). However, anti-cytokine therapies function at the protein level and serve to titrate cytokines away from their inflammatory action. This is intrinsically an inefficient way of controlling inflammation as the therapeutic effects will be transient and dosages will have to persistently compensate for the continued expression of these cytokines.

With a deeper understanding of the mechanisms that govern cytokine expression, especially at the transcriptional level, new strategies that circumvent some of the shortfalls of conventional protein-based cytokine therapies can be developed. The newly described lncRNAs in this body of work, as well as those described elsewhere (Chen et al., 2017), are potential targets for the modulation of cytokine transcription. This provides a novel modality for regulating cytokine levels during pathological inflammation. Importantly, transcription is at the apex of the gene expression process, placing these lncRNAs in a prime position for modulating cytokines at the source of their expression. Thus, the therapeutic depletion of these lncRNAs may prove to be a highly effective and efficient alternative or adjuvant to protein-based anti-cytokine therapies. Furthermore, due to the cell-type specific transcription of many lncRNAs and their unique nucleotide sequence, lncRNAs can be targeted in a much more precise and discrete manner, potentially mitigating side-effects and therapeutic toxicity associated with broad, systemically delivered cytokine therapies.

The IPLs (such as UMLILO) epigenetically prime the promoters of innate immune genes for transcriptional activity. The loss of the IPLs would render pro-inflammatory gene transcription impotent and effectively ameliorate conditions of hyper-inflammation. Conversely, therapeutically targeting

AMANZI would completely abrogate the IL-37 anti-inflammatory response, allowing for enhanced IL-1β signalling and pro-inflammation. This has been demonstrated in this work to enhance trained immunity, which may be beneficial for vaccination or the reversal of immunosuppression. In both these examples, the loss of the IPLs or AMANZI present significant barriers to the transcriptional activation of their respective innate immune genes, providing novel targets that can essentially shut off pro- or anti-inflammation.

LncRNAs can be modulated transcriptionally, functionally and post-transcriptionally. Drugging lncRNAs at the transcriptional level is probably the most effective method to control lncRNA activity. However, this requires in depth knowledge of the upstream regulatory mechanisms that govern lncRNA transcription. Recently, UMLILO and the IPLs were found to be regulated by calcium-dependent nuclear factor of activated T-cells (NFAT) signalling (Fanucchi et al., 2019). Calcium influx in response to certain stimuli results in the activation of calcineurin and the dephosphorylation of NFAT, which allows for its passage into the nucleus to activate transcription (Goodridge et al., 2007). Inhibition of calcineurin activation using the small molecule inhibitor tacrolimus, blocked IPL transcription and resulted in the loss of immune gene expression (Fanucchi et al., 2019). Clinically, tacrolimus is widely administered to blunt pro-inflammatory responses and prevent organ rejection and treat autoimmune diseases (Larsen et al., 2007, Ge et al., 2015, Hannah et al., 2016, Yu et al., 2017). The effectiveness of this drug is now partly attributed to its role in regulating IPL transcription, highlighting the potency and long track record of drugging lncRNAs (although inadvertently) at the transcriptional level. However, calcineurin signalling is not exclusive to IPL regulation and plays an important role in numerous biological functions, particularly in excitatory cells such as neurons and cardiomyoctes (Parra and Rothermel, 2017). Thus, the use of tacrolimus to manage inflammation is often associated with cellular toxicity and adverse side-effects that results from broad disruptions in calcium signalling (Hoorn et al., 2011, Sikma et al., 2015).

Small molecules that disrupt the assembly of ribonucleoprotein complexes on the lncRNA, can also be effective in modulating lncRNA function. These can include inhibitors that occlude or distort lncRNA structures that are essential for functional interactions with other biomolecules. Such modalities require in depth characterisation of the lncRNA candidates, including the mechanism of lncRNA function and potentially RNA shape. For example, the IPLs are known to interact with the WDR5/MLL1 complex in order to execute their function. The small molecule inhibitor MM102 blocks the WDR5/MLL1 interaction, thereby interfering with the assembly of the complete protein complex on the IPL. As a result, treatment of cells with MM102 causes the decreased expression of pro-inflammatory chemokines (Fanucchi et al., 2019). However, WDR5/MLL1 activity is ubiquitous in the cell and is also important for the function of other lncRNAs (Wang et al., 2011). Thus, broad inhibition of WDR5/MLL1 can have detrimental side-effects. Furthermore, small molecules (such as MM102 and tacrolimus) act indiscriminately on all cell types, disrupting biological functions within the entire organism. In order to implement these small molecules effectively, conjugated molecules or drug carriers that can specify cell targets will greatly mitigate potential adverse side-effects and enhance efficacy.

At the post-transcriptional level, the classical RNA-targeting modalities of RNAi, such as siRNAs or short hairpin RNAs (shRNAs) can be used to deplete cellular concentrations of the lncRNA in a sequence-specific manner (Rinn et al., 2007, Lai et al., 2013, Yang et al., 2013, Fanucchi et al., 2019). Despite numerous examples showing the success of RNAi in targeting lncRNAs, there has been controversy around the activity of RNAi in the nucleus (Zeng and Cullen, 2002). Thus, for the knockdown of nuclear-resident lncRNAs, it may be more prudent to use antisense oligonucleotides (ASOs), such as LNAs, as their mechanism of RNAseH-mediated degradation is specific to the nuclear compartment (Lennox and Behlke, 2016). While the knockdown of lncRNAs is the most discrete and specific method of targeting lncRNA function, the delivery of RNAi or ASOs has remained the biggest challenge for their therapeutic use. It has been particularly difficult to deliver

effective and safe dosages that balance between the poor stability of naked nucleic acids and their associated immunotoxicity. Cationic liposomes have shown great success in the delivery of nucleic acid-based drugs (NABDs) in experimental cell cultures and animal models for quite some time. Only recently have these lipid-based carriers been approved for human use (Barba et al., 2019). Furthermore, significant improvements in NABDs involving the use of functionalised nanoparticles, chemical modifications and cell-type specific ligand conjugates have increased their stability and specificity while reducing immunogenicity (Juliano, 2016, Kaczmarek et al., 2017). In contrast, shRNAs can be delivered much more readily with therapeutic viral expression vectors, such as AAVs. These can be engineered to have particular tropisms for cell-type specific delivery of the shRNA expression payload (Muik et al., 2017, Naso et al., 2017, Hartmann et al., 2018).

The implementation of many of these post-transcriptional strategies have already progressed to clinical trials for the depletion of disease-causing mRNAs, suggesting that their use is transferable to drugging lncRNAs. With the development of novel methods to target lncRNAs and deliver these modulators in a tissue and cell-specific manner, the highly discrete, efficacious and durable therapeutic transcriptional regulation of cytokine expression will be the basis of the next generation of immunotherapies.

Beyond cytokines

Receptors and signalling cascades

While the main focus of the work presented here is around the regulation of cytokines, there are other key components that contribute to shaping the inflammatory response. Cytokines function as integral signalling effectors for inflammation, but their encoded signals must be received by cognate receptors in order for specific functions to be elicited. This suggests that the regulation of receptor expression is equally important as the regulation of cytokine expression in order for a successful inflammatory response to be

mounted. Furthermore, this is not limited to just the receptors, but also the downstream partners that constitute signalling cascades. In a study that examined the variation of BCG-induced trained immunity, strong associations with SNPs occurring in the components of the IL-1 signalling pathway were discovered (Arts et al., 2018b). It was found that polymorphisms occurring in the IL-1 and IL-18 receptors as well as in components of the inflammasome, significantly modulated BCG-induced trained immunity. Importantly, the IL-1 receptor and inflammasome are integral for IL-1β function, which has been implicated as a key driver of trained immunity (Moorlag et al., 2018). Furthermore, the IL-18 receptor is important for IL-37 signalling, which has been shown in this present study to be involved in the modulation of trained immunity (Moorlag et al., 2018). This highlights the importance of receptors and components of signalling cascades for the successful execution of cytokine signalling.

Similar to how the transcription of cytokine genes are locally regulated by lncRNAs, cytokine receptor genes and their signalling partners are likely to be subjected to the same rigorous transcriptional control. This would provide the additional layer of regulation that allows certain subsets of cells to either be responsive or refractory to cytokine signalling at different timepoints of the inflammatory process (Gupta et al., 1998, Belay et al., 2002). However, the lncRNA regulation of cytokine receptors and their signalling partners has mostly been overlooked, with only a few examples of cytokine and chemokine receptors being shown to be regulated by lncRNAs (Hu et al., 2013, Wang and Zheng, 2018). Efforts to discover these lncRNA regulators could reveal additional targets for lncRNA-based therapies that modulate cytokine receptor and signalling pathways to control pathological inflammation.

Cellular metabolism

Conventionally, changes in cellular metabolism are associated with the growth and survival of the cell. However, in the recent years, it has become clear that cellular metabolism is deeply connected to the immune response (O'Neill et

al., 2016). Perhaps the best example that illustrates this is during macrophage polarisation. M1 pro-inflammatory macrophages become highly glycolytic compared to their M2 anti-inflammatory counterparts which predominantly make use of oxidative phosphorylation (O'Neill et al., 2016). A similar glycolytic shift in metabolism has been observed in macrophages during trained immunity (Cheng et al., 2014). These metabolic changes redirect energy sources to power pro-inflammatory activities as well as allow for the accumulation of key metabolites, which serve as substrates and cofactors for the epigenetic regulation of pro-inflammatory gene transcription (Fok et al., 2018). Central to the glycolytic state is the mammalian target of rapamycin (mTOR)-HIF-1α signalling axis, with inhibition of mTOR signalling reducing pro-inflammation and blocking the induction of trained immunity (Cheng et al., 2014, Jiang et al., 2014). This suggests that the metabolic state of the cell is highly important during inflammation, revealing a prime target for modulating inflammation during disease.

During trained immunity, it was observed that the accumulation of H3K4me3 was not exclusive to the immune genes, but also occurred on the metabolic genes (Saeed et al., 2014). This suggests that these metabolic genes are primed for transcriptional activation during training and may make use of a family of lncRNAs with a similar function to the IPLs. By applying the bioinformatic pipeline developed by Fanucchi et al., it may be possible to identify such lncRNA candidates (Fanucchi et al., 2019). These metabolic gene priming lncRNAs (MPLs) could prove to be highly desirable drug targets for manipulating cellular metabolism during inflammation as well as during other metabolic diseases.

Conclusion

In this thesis, the regulatory mechanisms and genetic circuitry underlying the transcription patterns during inflammation were dissected. These include the epigenetic priming of pro-inflammatory genes for their rapid and robust transcription during acute pro-inflammation and the elucidation of a biphasic

genetic circuit that coordinates the functionally opposed phases of inflammation. Importantly, this work implicates a central role of lncRNAs in mediating these processes. By characterising the function of these lncRNAs, this work contributes to (1) the functional annotation of the human genome, (2) deepening our understanding of the molecular mechanisms that regulate inflammation and (3) potentially providing novel targets for therapies that modulate its response.

As the role of the non-coding genome is becoming apparent in almost every cellular process, it is now more important than ever to understand biological function in the context of genome regulation. This perspective provides a more granular understanding of the molecular basis of these processes, allowing them to be manipulated with greater precision. Currently, one of the greatest challenges in this post-genomics era is to decipher the hidden functions within the non-coding genome and uncover the regulatory network that underlies higher-order biological processes. This remains difficult because there are no reliable ways to identify and predict the regulatory function of a genomic region. Our efforts so far, have completely relied on the laborious experimental testing of individual genomic regions. However, these efforts have been greatly aided by genome-wide datasets which can help investigators navigate to the location of potentially functional genomic regions and assist in the development of hypotheses about their activity. With the continuous development of powerful high-throughput assays and technologies, the functional annotation of the genome can only become easier and progress more rapidly. As we continue to decode the genome and catalogue functional regulatory elements, the underlying genetic basis of the organismal complexity that defines our species will be appreciated more than ever before.

Appendices

Appendix 1: Supplemental data

A1.1 UMLILO 3C primer testing

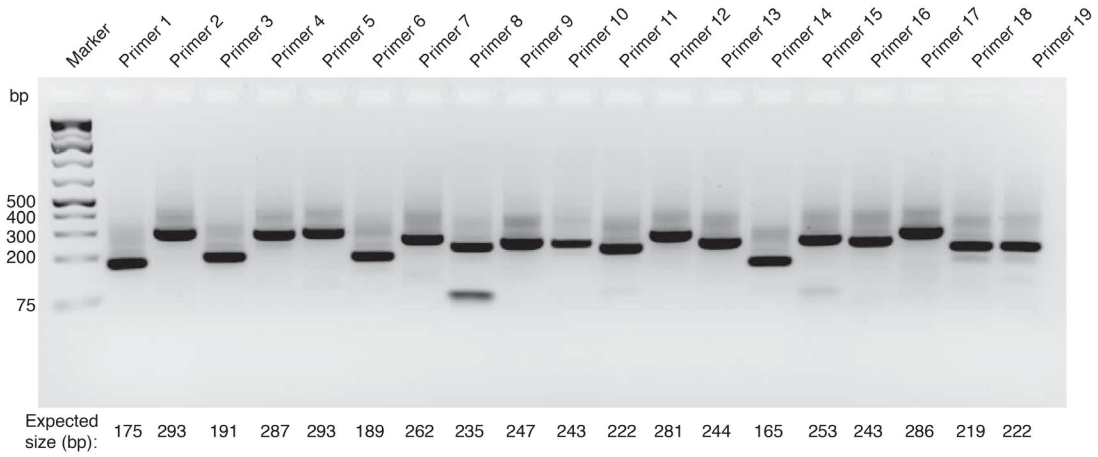

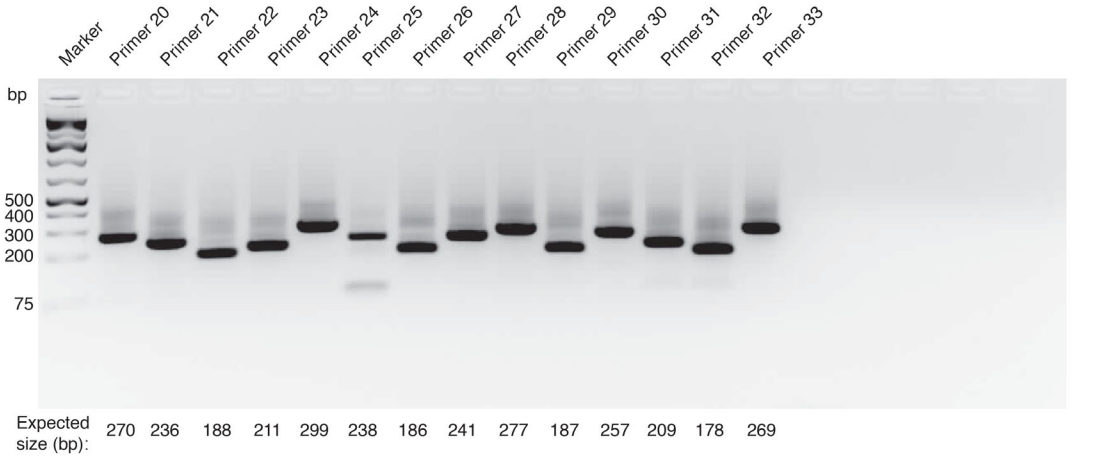

Supplementary Figure 1: UMLILO 3C primers tested by PCR

Primers designed for UMLILO 3C were tested in combination with the anchor primer on a BAC library by PCR. Amplicons were visualised on a 1% TAE agarose gel stained with 1 μg/ml ethidium bromide. Primers that showed the specific amplification of the correct sized product were considered for use in the 3C assay.

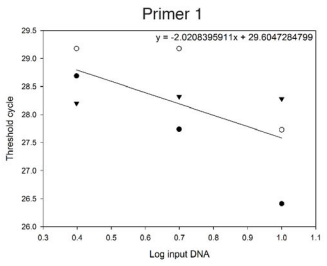
Primer 1
y = -2.0208395911x + 29.6047284799
Threshold cycle
Log input DNA

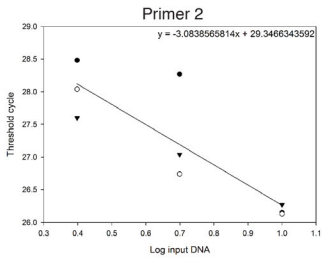
Primer 2
y = -3.0838565814x + 29.3466343592
Threshold cycle
Log input DNA

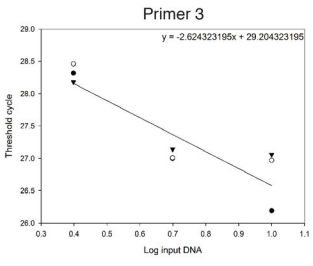
Primer 3
y = -2.624323195x + 29.204323195
Threshold cycle
Log input DNA

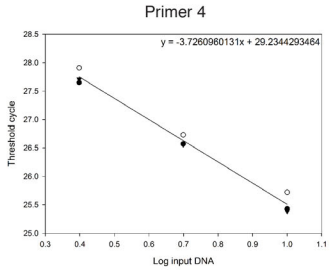
Primer 4
y = -3.7260960131x + 29.2344293464
Threshold cycle
Log input DNA

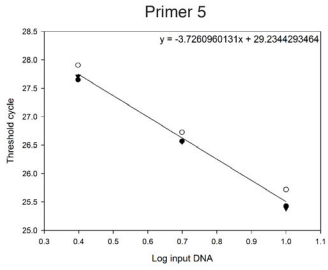
Primer 5
y = -3.7260960131x + 29.2344293464
Threshold cycle
Log input DNA

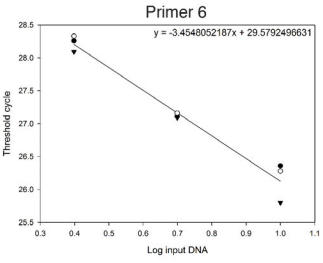
Primer 6
y = -3.4548052187x + 29.5792496631
Threshold cycle
Log input DNA

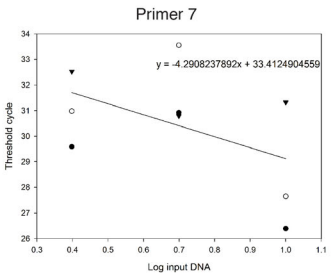
Primer 7
y = -4.2908237892x + 33.4124904559
Threshold cycle
Log input DNA

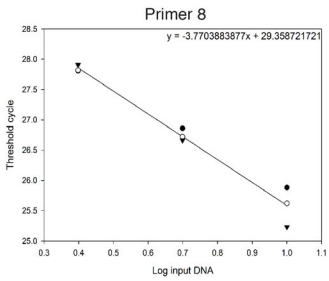
Primer 8
y = -3.7703883877x + 29.358721721
Threshold cycle
Log input DNA

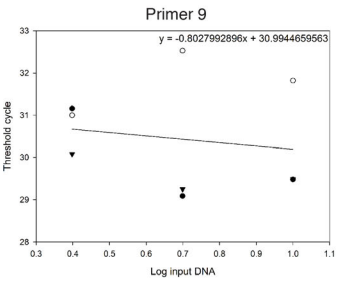
Primer 9
y = -0.8027992896x + 30.9944659563
Threshold cycle
Log input DNA

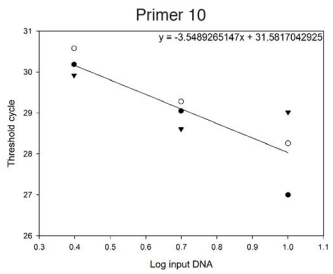
Primer 10
y = -3.5489265147x + 31.5817042925
Threshold cycle
Log input DNA

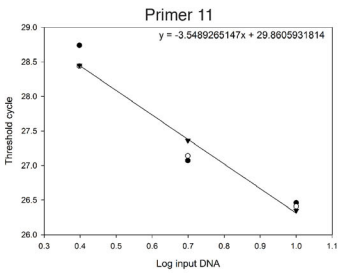
Primer 11
y = -3.5489265147x + 29.8605931814
Threshold cycle
Log input DNA

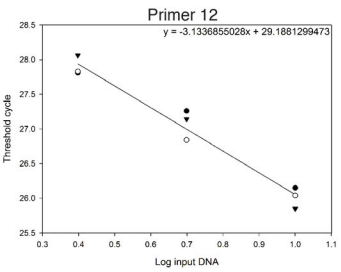
Primer 12
y = -3.1336855028x + 29.1881299473
Threshold cycle
Log input DNA

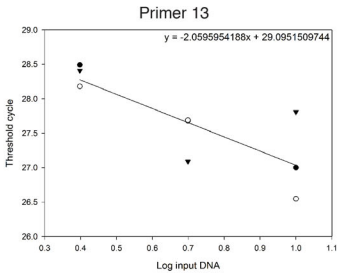
Primer 13
y = -2.0595954188x + 29.0951509744
Threshold cycle
Log input DNA

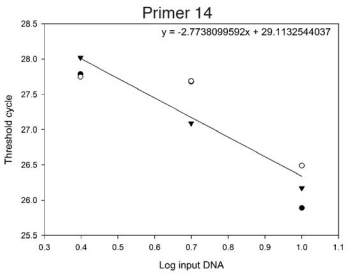
Primer 14
y = -2.7738099592x + 29.1132544037
Threshold cycle
Log input DNA

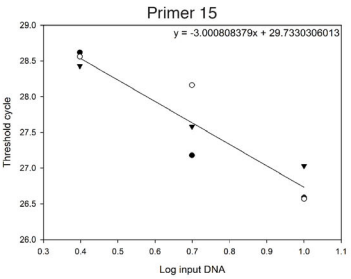
Primer 15
y = -3.000808379x + 29.7330306013
Threshold cycle
Log input DNA

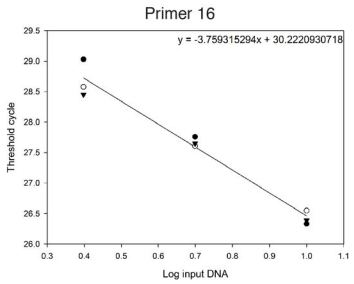
Primer 16
y = -3.759315294x + 30.2220930718
Threshold cycle
Log input DNA

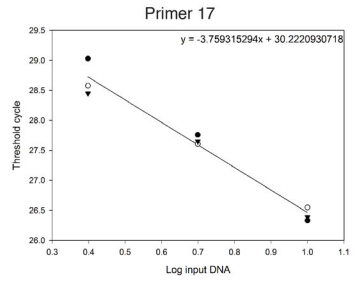
Primer 17
y = -3.759315294x + 30.2220930718
Threshold cycle
Log input DNA

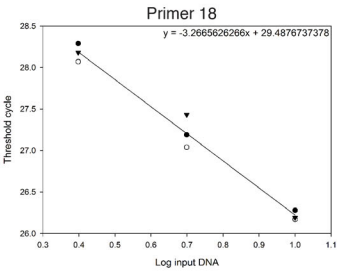
Primer 18
y = -3.2665626266x + 29.4876737378
Threshold cycle
Log input DNA

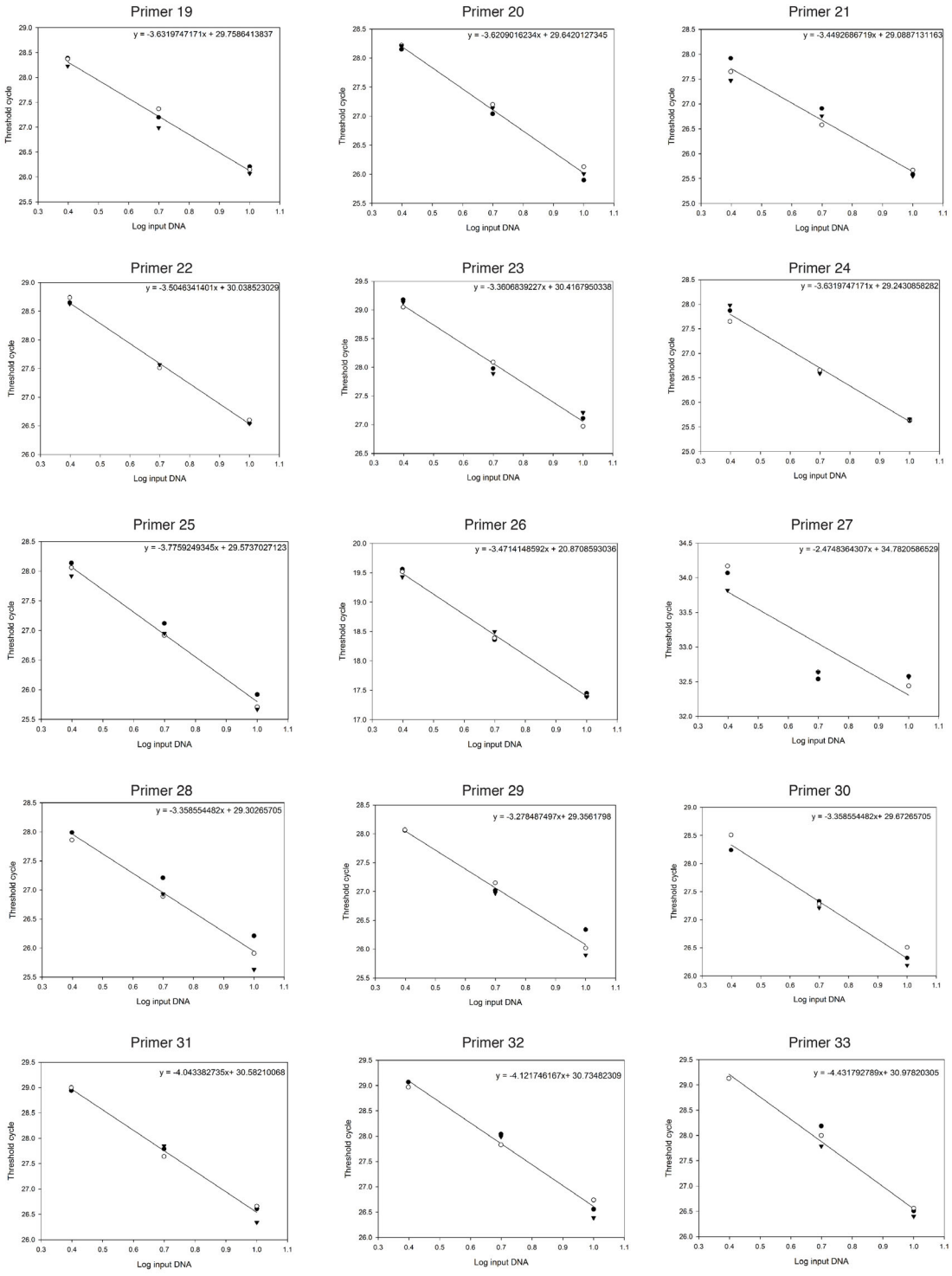

Supplementary Figure 2: UMLILO 3C primers tested by qPCR

Primers designed for UMLILO 3C were tested in combination with the anchor primer on a BAC library by qPCR. A serial dilution of the template BAC library was made and qPCR was performed to ensure that all primers used in the 3C assay were similarly efficient.

A1.2 AMANZI 3C primer testing

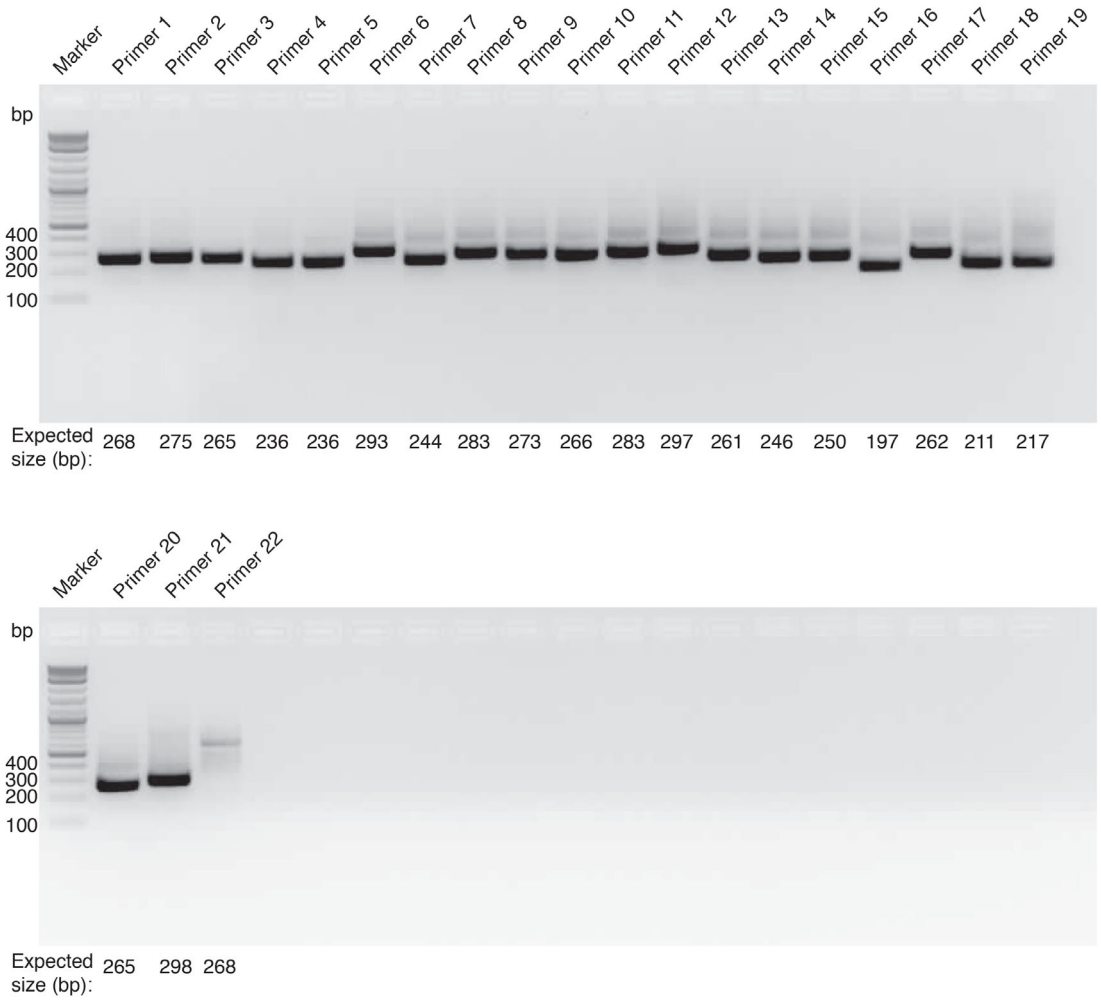

Supplementary Figure 3: AMANZI 3C primers tested by PCR

Primers designed for AMANZI 3C were tested in combination with the anchor primer on a BAC library by PCR. Amplicons were visualised on a 1% TAE agarose gel stained with 1 μg/ml ethidium bromide. Primers that showed the specific amplification of the correct sized product were considered for use in the 3C assay.

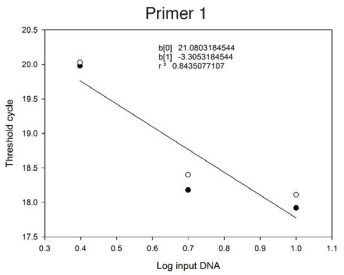
Primer 1
b[0] 21.0803184544
b[1] -3.3053184544
r² 0.8435077107
Threshold cycle
Log input DNA

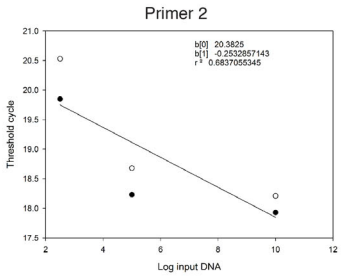
Primer 2
b[0] 20.3825
b[1] -0.2532857143
r² 0.6837055345
Threshold cycle
Log input DNA

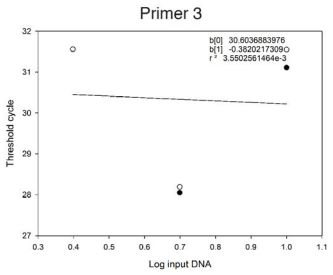
Primer 3
b[0] 30.6036883976
b[1] -0.3620217309
r² 3.5502561464e-3
Threshold cycle
Log input DNA

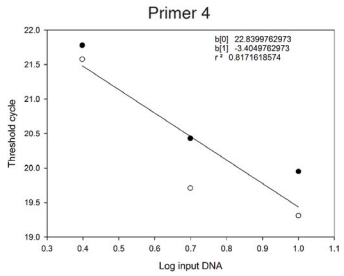
Primer 4
b[0] 22.8399762973
b[1] -3.4049762973
r² 0.8171618574
Threshold cycle
Log input DNA

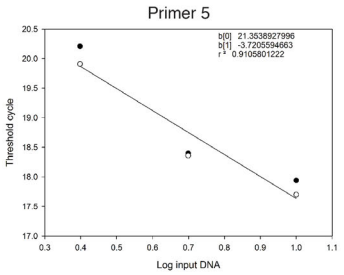
Primer 5
b[0] 21.3538927996
b[1] -3.7205594663
r² 0.9105801222
Threshold cycle
Log input DNA

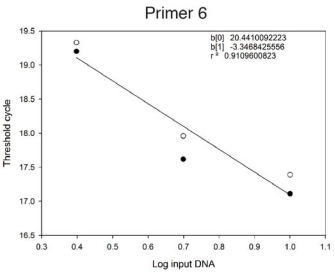
Primer 6
b[0] 20.4410092223
b[1] -3.3488425556
r² 0.9109600823
Threshold cycle
Log input DNA

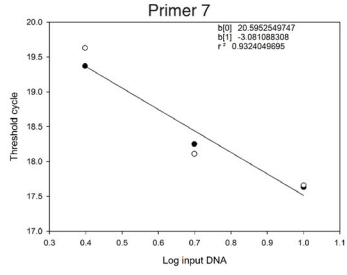
Primer 7
b[0] 20.5952549747
b[1] -3.081088308
r² 0.9324049695
Threshold cycle
Log input DNA

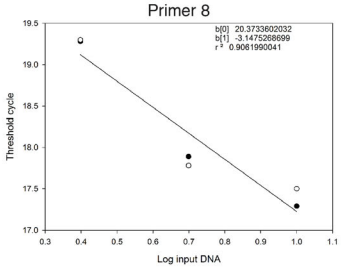
Primer 8
b[0] 20.3733602032
b[1] -3.1475268699
r² 0.9061990041
Threshold cycle
Log input DNA

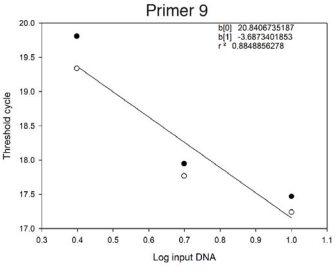
Primer 9
b[0] 20.8406735187
b[1] -3.6873401853
r² 0.8848856278
Threshold cycle
Log input DNA

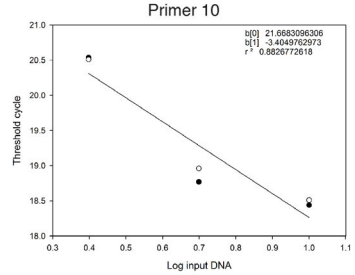
Primer 10
b[0] 21.6583096306
b[1] -3.4049762973
r² 0.8826772618
Threshold cycle
Log input DNA

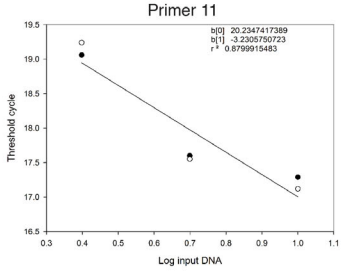
Primer 11
b[0] 20.2347417389
b[1] -3.2305750723
r² 0.8799915483
Threshold cycle
Log input DNA

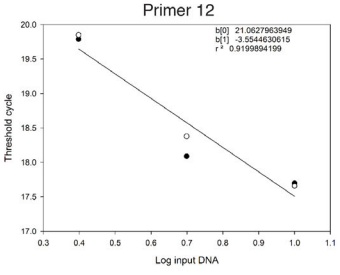
Primer 12
b[0] 21.0627963949
b[1] -3.5544630615
r² 0.9199894199
Threshold cycle
Log input DNA

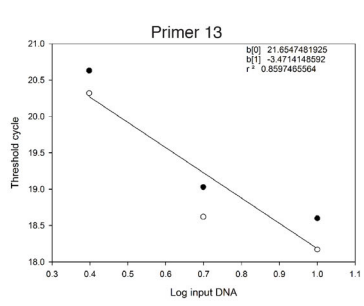
Primer 13
b[0] 21.6547481925
b[1] -3.4714148592
r² 0.8597465564
Threshold cycle
Log input DNA

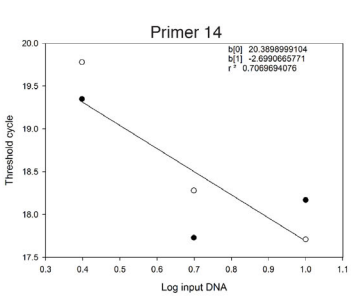
Primer 14
b[0] 20.3898999104
b[1] -2.6990665771
r² 0.7069694076
Threshold cycle
Log input DNA

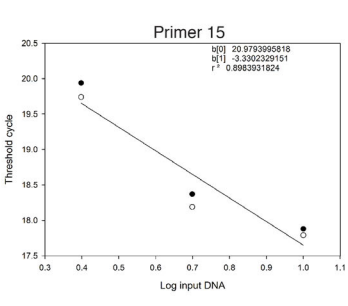
Primer 15
b[0] 20.9793995818
b[1] -3.3302329151
r² 0.8983931824
Threshold cycle
Log input DNA

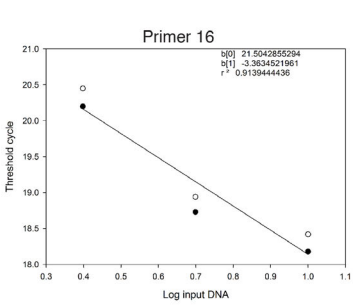
Primer 16
b[0] 21.5042855294
b[1] -3.3634521961
r² 0.9139444436
Threshold cycle
Log input DNA

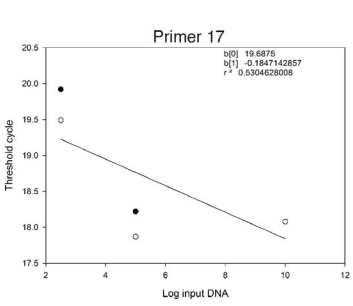
Primer 17
b[0] 19.6875
b[1] -0.1847142857
r² 0.5304628008
Threshold cycle
Log input DNA

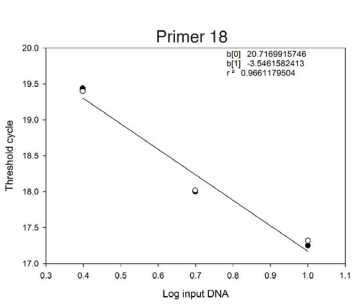
Primer 18
b[0] 20.7169915746
b[1] -3.5461582413
r² 0.9661179504
Threshold cycle
Log input DNA

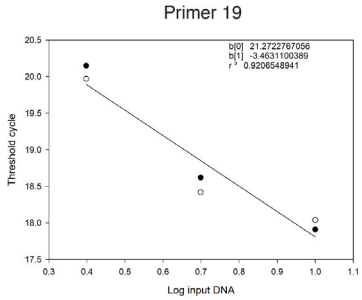

Supplementary Figure 4: AMANZI 3C primers tested by qPCR

Primers designed for UMLILO 3C were tested in combination with the anchor primer on a BAC library by qPCR. A serial dilution of the template BAC library was made and qPCR was performed to ensure that all primers used in the 3C assay were similarly efficient.

Appendix 2: Standard laboratory protocols

A2.1 Direct-zol RNA Miniprep

300 μl TRIzol (Ambion) was added directly into the plate after the culture medium was discarded (for adherent cells) or used to resuspend cell pellets collected by centrifugation (for suspension cells). 300 μl of 98% ethanol was added to the lysed sample and thoroughly mixed. The mixture was then transferred to a Zymo-Spin Column and centrifuged at 10 000 g for 30 seconds. The column was placed in a new collection tube and 400 μl of RNA Wash Buffer was added and passed through the column by centrifugation at 10 000 g for 30 seconds. In the meanwhile, a mixture containing 5 μl DNaseI and 75 μl DNA Digestion Buffer was prepared. This was then added to the column and incubated at room temperature for 30 minutes. 400 μl of Direct-zol RNA PreWash was then added to the column and centrifuged at 10 000 g for 30 seconds. The flow through was discarded and the previous step was repeated. 700 μl of RNA Wash Buffer was then added and centrifuged at 10 000 g for 2 minutes. The column was then carefully transferred into a RNAse-free tube, where the RNA was eluted in 50 μl of DNAse/RNase-Free Water by centrifugation for 1 minute at 10 000 g. The collected RNA was quantified using a Nanodrop ND-1000 spectrophotometer and used immediately or stored at -80˚C.

A2.2 SuperScript IV First-Strand Synthesis System

Primer annealing:
A 13 μl reaction containing the following was set up: 1 μl Oligo $d(T)_{20}$ (50 μM) or 1 μl random hexamers (50 μM), 1 μl dNTP mix (10 mM), 500 - 1 000 ng RNA and water to make up the final volume. The reaction was gently mixed and incubated at 65˚C for 5 minutes and chilled at 4˚C for 5 minutes.

Reverse transcription:

To the primer annealing reaction, the following were then added: 4 μl 5X SSIV Buffer, 1 μl mM DTT (100 mM), 1 μl RNaseOUT and 1 μl Superscript IV reverse transcriptase (200 U/μl). The reaction was gently mixed and incubated as follows: (1) For Oligo $d(T)_{20}$ libraries the reaction was incubated at 55˚C for 10 minutes then 80˚C for 10 minutes (2) For random hexameter libraries, the reaction was first incubated at 23˚C for 10 minutes then 55˚C for 10 minutes and finally 80˚C for 10 minutes.

RNA digestion:
The RNA was the digested by adding 1 μl of RNaseH to the reaction and incubating at 37˚C for 20 minutes. The cDNA was then immediately used of stored at -20˚C.

A2.3 Preparing cells for the Neon Transfection System

Cells were harvested by centrifugation at 300 g for 3 minutes. The supernatant was discarded and the cells were washed in 10 ml calcium and magnesium-free PBS by resuspending the cell pellet and recollecting the cells by centrifugation at 300 g for 3 minutes. The PBS was completely removed and the cell pellet was resuspended into a single cell suspension by repeat pipetting in 12 μl of Buffer R. This was then mixed with the appropriate volume of siRNA or LNA and loaded into a 10 μl gold-plated electroporation tip. This was then inserted into the Neon tube containing 2 ml of Buffer E. The correct parameters were set on the system and the electroporation was then carried out.

A2.4 RNAiMAX transfection

24 hours prior to transfection, $6x10^6$ cells (HeLa) were seeded in a T75 flask with 10 ml of complete culture medium. The following day, the siRNA was prepared by diluting the appropriate volume in DMEM to make a final volume of 750 μl. The RNAiMAX solution was prepared by diluting 59 μl in DMEM to make a final volume of 750 μl. The two mixtures were then combined, mixed

and incubated at room temperature for 5 minutes. This was then added to the HeLa cell culture and mixed by tilting the flask back and forth. The cells were then analysed 48 hours later.

A2.5 GeneJet Gel Extraction Kit

The DNA band of interest was excised from the agarose gel using a clean scalpel. The gel slice was weighed and a 1:1 (mass:volume) amount of Binding Buffer was added to the gel slice. The gel slice was then melted by incubating the mixture at 55˚C for 10 minutes, with periodic agitation. The melted gel mixture was then transferred to a GeneJect purification column and centrifuged at 10 000 g for 1 minute. The flow though was discarded and 700 μl of Wash Buffer was added. The column was centrifuged again at 10 000 g for 1 minute. The flow through was discarded and any residual buffer was removed by repeating the previous centrifugation step. The captured DNA was eluted using 50 μl of pre-warmed Elution Buffer and incubating at the column for 1 minute at room temperature. The DNA was recovered by centrifugation at 10 000 g for 1 minute.

A2.6 GeneJet PCR Extraction Kit

This was carried out as described in section A2.5, with the exception of using a 1:1 ratio of PCR volume to Binding Buffer.

A2.7 Bacterial transformation

Preparing chemically competent Stbl3 *E. coli*:

8 ml of Luria Bertani (LB) broth (Oxoid) was inoculated with a scraping of a Stbl3 *E. coli* glycerol stock. The culture was grown overnight at 37˚C in a shaking incubator. The next day, 2 ml of the culture was used as a starter culture to inoculate 48 ml of fresh LB broth. This was incubated at 37˚C in a shaking incubator and periodically monitored for the exponential phase of

growth using the Nanodrop ND-1000 spectrophotometer (OD_{600} = 0.4). When in this phase of growth, the progression of the culture was immediate suspended by immersing the flask in an ice water bath for 15 minutes, with vigorous agitation. The bacterial cells were then collected by centrifugation at 500 g for 15 mins at 4 ˚C. The supernatant was poured off and the bacterial cell pellet was gently resuspended in 1 ml of Transformation Buffer (Appendix A3.9) and topped up with a further 4 ml of Transformation Buffer. The cell suspension was then incubated on ice for 30 minutes. The cells were then collected again by centrifugation at 136 g for 10 minutes at 4˚C. The supernatant was discarded and the pellet was gently resuspended in 1 ml of Transformation Buffer. This was then distributed into 50 µl aliquots and stored at -80˚C.

Transformation:

Aliquots of the chemically competent Stbl3 *E. coli* were thawed on ice. 2-10 µl of plasmid DNA was then added to the bacterial suspension and incubated on ice for 30 minutes. The cells were then heat shocked at 42˚C for 90 seconds and were allowed to recover on ice for 5 minutes. 1 ml of LB broth was then added to the cells and incubated at 37˚C for 1 hour. The cells were then collected by centrifugation at 800 g for 3 min. 800 µl of the supernatant was removed and the pellet was resuspended in the remaining liquid. The transformed bacteria were then plated on antibiotic LB agar plates (Oxoid) and grown overnight.

A2.8 QIAprep Spin Miniprep Kit

10 ml of LB broth (containing the appropriate selection antibiotic) was inoculated with the bacterial clone of interest and allowed to grow for 14 hours at 30/37˚C in a shaking incubator. The bacterial cells were then harvested by centrifugation at 2750 g for 10 minutes at 4˚C. The bacterial pellet was then resuspended in 250 µl Buffer P1. The cells were lysed by adding 250 µl Buffer P2 and inverting the mixture 24 times and incubating at room temperature for

5 minutes. The lysis process was then stopped using 350 μl Buffer N3 and mixing by inversion. The cell debris was separated from the plasmid DNA by centrifugation at 13 000 g for 10 minutes. The supernatant was then transferred to a QIAprep spin column and passed through by centrifugation at 13 000 g for 1 minute. The column was washed with 500 μl Buffer PB and centrifuged at 13 000 g for 1 minute. 750 μl Buffer PE was then added to the column and centrifuged at 13 000 g for 1 minute. Residual wash buffer was removed by centrifugation at 13 000 g for an additional minute. The plasmid DNA was then eluted by adding 60 μl of Buffer EB, incubated at room temperature for 1 minute and then centrifuged at 13 000 g for 1 minute. Recovered DNA was stored at -20˚C.

A2.9 NucleoBond Xtra Maxi Kit

An overnight culture of 300 ml LB broth, with the appropriate selection antibiotic, was inoculated with the bacterial clone of interest. This was cultured overnight at 30/37˚C for 14 hours in a shaking incubator. The bacterial cells were harvested by centrifugation at 5 000 g for 10 minutes at 4˚C. The bacterial pellet was resuspended in 12 ml of Resuspension Buffer RES. Cells were lysed by adding 12 ml of Buffer LYS and inverting the mixture 5 times and incubating at room temperature for 5 minutes. The lysis was then neutralised by adding 12 ml of Buffer NEU and gently inverting the lysate. A NucleoBond Xtra Column was then equilibrated by applying 25 ml of Buffer EQU around the rim of the column filter. The column was allowed to drain by gravity. The lysate was then applied to the column by pouring it through the filter and allowing it to pass by gravity. The column filter was then washed with 15 ml of Buffer EQU, after which the filter was then discarded from the column. The column was washed with 25 ml of Buffer WASH. The captured plasmid DNA was then eluted with 15 ml Buffer ELU and precipitated by adding 10.5 ml room temperature isopropanol, mixing vigorously and centrifuging at 2 750 g for 2 hours at 4˚C. The DNA pellet was washed with 14 ml of 70 % ethanol and recollected by centrifugation at 2 750 g for 15 minutes

at room temperature. The DNA pellet was then allowed to dry at room temperature for and then resuspended in 100 μl of TE buffer (Appendix A3.2).

Appendix 3: Recipes

A3.1 3C Lysis Buffer

10 mM Tris-HCl (pH 7.5)

10 mM NaCl

5 mM $MgCl_2$

0.1 mM EGTA

1X complete protease inhibitor (Roche)

A3.2 10X TE Buffer

100 ml 1 M Tris-HCl (pH 7.5 for RNA and pH 8.0 for DNA)

20 ml 0.5M EDTA (pH 8.0)

Water to make up 1l.

Autoclave and filter sterilise.

Store at room temperature.

A3.3 FA Lysis Buffer

50 mM HEPES-KOH (pH 7.5)

140 mM NaCl

1 mM EDTA (pH 8.0)

1% Triton X-100

0.1% Sodium Deoxycholate

0.1% SDS

1X complete protease inhibitor (Roche)

A3.4 RIPA Buffer

50 mM Tris-HCl (pH 8.0)

150 mM NaCl

2 mM EDTA (pH 8.0)

1% NP-40
0.5% Sodium Deoxycholate
0.1% SDS
1X complete protease inhibitor (Roche)

A3.5 Wash Buffer

0.1% SDS
1% Triton X-100
2 mM EDTA (pH 8.0)
150 mM NaCl
20 mM Tris-HCl (pH 8.0)

A3.6 Final Wash Buffer

0.1% SDS
1% Triton X-100
2 mM EDTA (pH 8.0)
500 mM NaCl
20 mM Tris-HCl (pH 8.0)

A3.7 Elution Buffer

1% SDS
100mM $NaHCO_3$

A3.8 50X TAE

242 g Tris-base (Sigma-Aldrich)
57.1 ml of 100% acetic acid (Merck)
100 ml of 0.5 M sodium EDTA (pH 8.0)
Water to make up 1l final volume.

A3.9 Transformation Buffer

15 ml Glycerol (Sigma-Aldrich)
1.47 g $CaCl_2.2H_2O$ (Sigma-Aldrich)
302.4 mg PIPES.HCl (Sigma-Aldrich)
NaOH (Sigma-Aldrich)
Water to make up a final volume of 100 ml.

The glycerol, $CaCl_2.2H_2O$ and PIPES.HCl were mixed together with 80 ml of water. The pH of the solution was then adjusted with NaOH until exactly 7.0. The final volume of 100 ml was then made up with water. The buffer was then autoclaved and stored at -20˚C.

References

ABE, N., DROR, I., YANG, L., SLATTERY, M., ZHOU, T., BUSSEMAKER, H. J., ROHS, R. & MANN, R. S. 2015. Deconvolving the recognition of DNA shape from sequence. *Cell,* 161**,** 307-18.

ADAMS, M. D., CELNIKER, S. E., HOLT, R. A., EVANS, C. A., GOCAYNE, J. D., AMANATIDES, P. G., SCHERER, S. E., LI, P. W., HOSKINS, R. A., GALLE, R. F., GEORGE, R. A., LEWIS, S. E., RICHARDS, S., ASHBURNER, M., HENDERSON, S. N., SUTTON, G. G., WORTMAN, J. R., YANDELL, M. D., ZHANG, Q., CHEN, L. X., BRANDON, R. C., ROGERS, Y. H., BLAZEJ, R. G., CHAMPE, M., PFEIFFER, B. D., WAN, K. H., DOYLE, C., BAXTER, E. G., HELT, G., NELSON, C. R., GABOR, G. L., ABRIL, J. F., AGBAYANI, A., AN, H. J., ANDREWS-PFANNKOCH, C., BALDWIN, D., BALLEW, R. M., BASU, A., BAXENDALE, J., BAYRAKTAROGLU, L., BEASLEY, E. M., BEESON, K. Y., BENOS, P. V., BERMAN, B. P., BHANDARI, D., BOLSHAKOV, S., BORKOVA, D., BOTCHAN, M. R., BOUCK, J., BROKSTEIN, P., BROTTIER, P., BURTIS, K. C., BUSAM, D. A., BUTLER, H., CADIEU, E., CENTER, A., CHANDRA, I., CHERRY, J. M., CAWLEY, S., DAHLKE, C., DAVENPORT, L. B., DAVIES, P., DE PABLOS, B., DELCHER, A., DENG, Z., MAYS, A. D., DEW, I., DIETZ, S. M., DODSON, K., DOUP, L. E., DOWNES, M., DUGAN-ROCHA, S., DUNKOV, B. C., DUNN, P., DURBIN, K. J., EVANGELISTA, C. C., FERRAZ, C., FERRIERA, S., FLEISCHMANN, W., FOSLER, C., GABRIELIAN, A. E., GARG, N. S., GELBART, W. M., GLASSER, K., GLODEK, A., GONG, F., GORRELL, J. H., GU, Z., GUAN, P., HARRIS, M., HARRIS, N. L., HARVEY, D., HEIMAN, T. J., HERNANDEZ, J. R., HOUCK, J., HOSTIN, D., HOUSTON, K. A., HOWLAND, T. J., WEI, M. H., IBEGWAM, C., et al. 2000. The genome sequence of Drosophila melanogaster. *Science,* 287**,** 2185-95.

ADELMAN, K., KENNEDY, M. A., NECHAEV, S., GILCHRIST, D. A., MUSE, G. W., CHINENOV, Y. & ROGATSKY, I. 2009. Immediate mediators of the inflammatory response are poised for gene activation through RNA polymerase II stalling. *Proc Natl Acad Sci U S A,* 106**,** 18207-12.

AMIT, I., GARBER, M., CHEVRIER, N., LEITE, A. P., DONNER, Y., EISENHAURE, T., GUTTMAN, M., GRENIER, J. K., LI, W., ZUK, O.,

SCHUBERT, L. A., BIRDITT, B., SHAY, T., GOREN, A., ZHANG, X., SMITH, Z., DEERING, R., MCDONALD, R. C., CABILI, M., BERNSTEIN, B. E., RINN, J. L., MEISSNER, A., ROOT, D. E., HACOHEN, N. & REGEV, A. 2009. Unbiased reconstruction of a mammalian transcriptional network mediating pathogen responses. *Science,* 326**,** 257-63.

AMULIC, B., CAZALET, C., HAYES, G. L., METZLER, K. D. & ZYCHLINSKY, A. 2012. Neutrophil function: from mechanisms to disease. *Annu Rev Immunol,* 30**,** 459-89.

ANDERSEN, P. & DOHERTY, T. M. 2005. The success and failure of BCG - implications for a novel tuberculosis vaccine. *Nat Rev Microbiol,* 3**,** 656-62.

ANDERSSON, R., GEBHARD, C., MIGUEL-ESCALADA, I., HOOF, I., BORNHOLDT, J., BOYD, M., CHEN, Y., ZHAO, X., SCHMIDL, C., SUZUKI, T., NTINI, E., ARNER, E., VALEN, E., LI, K., SCHWARZFISCHER, L., GLATZ, D., RAITHEL, J., LILJE, B., RAPIN, N., BAGGER, F. O., JORGENSEN, M., ANDERSEN, P. R., BERTIN, N., RACKHAM, O., BURROUGHS, A. M., BAILLIE, J. K., ISHIZU, Y., SHIMIZU, Y., FURUHATA, E., MAEDA, S., NEGISHI, Y., MUNGALL, C. J., MEEHAN, T. F., LASSMANN, T., ITOH, M., KAWAJI, H., KONDO, N., KAWAI, J., LENNARTSSON, A., DAUB, C. O., HEUTINK, P., HUME, D. A., JENSEN, T. H., SUZUKI, H., HAYASHIZAKI, Y., MULLER, F., FORREST, A. R. R., CARNINCI, P., REHLI, M. & SANDELIN, A. 2014. An atlas of active enhancers across human cell types and tissues. *Nature,* 507**,** 455-461.

ARABIDOPSIS GENOME, I. 2000. Analysis of the genome sequence of the flowering plant Arabidopsis thaliana. *Nature,* 408**,** 796-815.

ARAS, S. & ZAIDI, M. R. 2017. TAMeless traitors: macrophages in cancer progression and metastasis. *Br J Cancer,* 117**,** 1583-1591.

ARNOLD, C. D., GERLACH, D., STELZER, C., BORYN, L. M., RATH, M. & STARK, A. 2013. Genome-wide quantitative enhancer activity maps identified by STARR-seq. *Science,* 339**,** 1074-7.

ARTS, R. J., NOVAKOVIC, B., TER HORST, R., CARVALHO, A., BEKKERING, S., LACHMANDAS, E., RODRIGUES, F., SILVESTRE, R., CHENG, S. C., WANG, S. Y., HABIBI, E., GONCALVES, L. G., MESQUITA, I., CUNHA, C., VAN LAARHOVEN, A., VAN DE VEERDONK, F. L., WILLIAMS,

D. L., VAN DER MEER, J. W., LOGIE, C., O'NEILL, L. A., DINARELLO, C. A., RIKSEN, N. P., VAN CREVEL, R., CLISH, C., NOTEBAART, R. A., JOOSTEN, L. A., STUNNENBERG, H. G., XAVIER, R. J. & NETEA, M. G. 2016. Glutaminolysis and Fumarate Accumulation Integrate Immunometabolic and Epigenetic Programs in Trained Immunity. *Cell Metab,* 24**,** 807-819.

ARTS, R. J. W., JOOSTEN, L. A. B. & NETEA, M. G. 2018a. The Potential Role of Trained Immunity in Autoimmune and Autoinflammatory Disorders. *Front Immunol,* 9**,** 298.

ARTS, R. J. W., MOORLAG, S., NOVAKOVIC, B., LI, Y., WANG, S. Y., OOSTING, M., KUMAR, V., XAVIER, R. J., WIJMENGA, C., JOOSTEN, L. A. B., REUSKEN, C., BENN, C. S., AABY, P., KOOPMANS, M. P., STUNNENBERG, H. G., VAN CREVEL, R. & NETEA, M. G. 2018b. BCG Vaccination Protects against Experimental Viral Infection in Humans through the Induction of Cytokines Associated with Trained Immunity. *Cell Host Microbe,* 23**,** 89-100 e5.

AWOMOYI, A. A., CHARURAT, M., MARCHANT, A., MILLER, E. N., BLACKWELL, J. M., MCADAM, K. P. & NEWPORT, M. J. 2005. Polymorphism in IL1B: IL1B-511 association with tuberculosis and decreased lipopolysaccharide-induced IL-1beta in IFN-gamma primed ex-vivo whole blood assay. *J Endotoxin Res,* 11**,** 281-6.

BACK, M. & HANSSON, G. K. 2015. Anti-inflammatory therapies for atherosclerosis. *Nat Rev Cardiol,* 12**,** 199-211.

BANNISTER, A. J. & KOUZARIDES, T. 2011. Regulation of chromatin by histone modifications. *Cell Res,* 21**,** 381-95.

BARBA, A. A., BOCHICCHIO, S., DALMORO, A. & LAMBERTI, G. 2019. Lipid Delivery Systems for Nucleic-Acid-Based-Drugs: From Production to Clinical Applications. *Pharmaceutics,* 11.

BELAY, T., EKO, F. O., ANANABA, G. A., BOWERS, S., MOORE, T., LYN, D. & IGIETSEME, J. U. 2002. Chemokine and chemokine receptor dynamics during genital chlamydial infection. *Infect Immun,* 70**,** 844-50.

BERTONE, P., STOLC, V., ROYCE, T. E., ROZOWSKY, J. S., URBAN, A. E., ZHU, X., RINN, J. L., TONGPRASIT, W., SAMANTA, M., WEISSMAN, S.,

GERSTEIN, M. & SNYDER, M. 2004. Global identification of human transcribed sequences with genome tiling arrays. *Science,* 306**,** 2242-6.

BHATT, D. M., PANDYA-JONES, A., TONG, A. J., BAROZZI, I., LISSNER, M. M., NATOLI, G., BLACK, D. L. & SMALE, S. T. 2012. Transcript dynamics of proinflammatory genes revealed by sequence analysis of subcellular RNA fractions. *Cell,* 150**,** 279-90.

BISTONI, F., VECCHIARELLI, A., CENCI, E., PUCCETTI, P., MARCONI, P. & CASSONE, A. 1986. Evidence for macrophage-mediated protection against lethal Candida albicans infection. *Infect Immun,* 51**,** 668-74.

BISTONI, F., VERDUCCI, G., PERITO, S., VECCHIARELLI, A., PUCCETTI, P., MARCONI, P. & CASSONE, A. 1988. Immunomodulation by a low-virulence, agerminative variant of Candida albicans. Further evidence for macrophage activation as one of the effector mechanisms of nonspecific anti-infectious protection. *J Med Vet Mycol,* 26**,** 285-99.

BLATTNER, F. R., PLUNKETT, G., 3RD, BLOCH, C. A., PERNA, N. T., BURLAND, V., RILEY, M., COLLADO-VIDES, J., GLASNER, J. D., RODE, C. K., MAYHEW, G. F., GREGOR, J., DAVIS, N. W., KIRKPATRICK, H. A., GOEDEN, M. A., ROSE, D. J., MAU, B. & SHAO, Y. 1997. The complete genome sequence of Escherichia coli K-12. *Science,* 277**,** 1453-62.

BOETTIGER, A. N., BINTU, B., MOFFITT, J. R., WANG, S., BELIVEAU, B. J., FUDENBERG, G., IMAKAEV, M., MIRNY, L. A., WU, C. T. & ZHUANG, X. 2016. Super-resolution imaging reveals distinct chromatin folding for different epigenetic states. *Nature,* 529**,** 418-22.

BOIJA, A., KLEIN, I. A., SABARI, B. R., DALL'AGNESE, A., COFFEY, E. L., ZAMUDIO, A. V., LI, C. H., SHRINIVAS, K., MANTEIGA, J. C., HANNETT, N. M., ABRAHAM, B. J., AFEYAN, L. K., GUO, Y. E., RIMEL, J. K., FANT, C. B., SCHUIJERS, J., LEE, T. I., TAATJES, D. J. & YOUNG, R. A. 2018. Transcription Factors Activate Genes through the Phase-Separation Capacity of Their Activation Domains. *Cell,* 175**,** 1842-1855 e16.

BOYLE, A. P., DAVIS, S., SHULHA, H. P., MELTZER, P., MARGULIES, E. H., WENG, Z., FUREY, T. S. & CRAWFORD, G. E. 2008. High-resolution mapping and characterization of open chromatin across the genome. *Cell,* 132**,** 311-22.

BUENROSTRO, J. D., GIRESI, P. G., ZABA, L. C., CHANG, H. Y. & GREENLEAF, W. J. 2013. Transposition of native chromatin for fast and sensitive epigenomic profiling of open chromatin, DNA-binding proteins and nucleosome position. *Nat Methods,* 10**,** 1213-8.

BUENROSTRO, J. D., WU, B., LITZENBURGER, U. M., RUFF, D., GONZALES, M. L., SNYDER, M. P., CHANG, H. Y. & GREENLEAF, W. J. 2015. Single-cell chromatin accessibility reveals principles of regulatory variation. *Nature,* 523**,** 486-90.

BUFLER, P., GAMBONI-ROBERTSON, F., AZAM, T., KIM, S. H. & DINARELLO, C. A. 2004. Interleukin-1 homologues IL-1F7b and IL-18 contain functional mRNA instability elements within the coding region responsive to lipopolysaccharide. *Biochem J,* 381**,** 503-10.

CALO, E. & WYSOCKA, J. 2013. Modification of enhancer chromatin: what, how, and why? *Mol Cell,* 49**,** 825-37.

CANO-RODRIGUEZ, D., GJALTEMA, R. A., JILDERDA, L. J., JELLEMA, P., DOKTER-FOKKENS, J., RUITERS, M. H. & ROTS, M. G. 2016. Writing of H3K4Me3 overcomes epigenetic silencing in a sustained but context-dependent manner. *Nat Commun,* 7**,** 12284.

CANVER, M. C., SMITH, E. C., SHER, F., PINELLO, L., SANJANA, N. E., SHALEM, O., CHEN, D. D., SCHUPP, P. G., VINJAMUR, D. S., GARCIA, S. P., LUC, S., KURITA, R., NAKAMURA, Y., FUJIWARA, Y., MAEDA, T., YUAN, G. C., ZHANG, F., ORKIN, S. H. & BAUER, D. E. 2015. BCL11A enhancer dissection by Cas9-mediated in situ saturating mutagenesis. *Nature,* 527**,** 192-7.

CAVALLI, G. & DINARELLO, C. A. 2018. Suppression of inflammation and acquired immunity by IL-37. *Immunol Rev,* 281**,** 179-190.

CAVALLI, G., JUSTICE, J. N., BOYLE, K. E., D'ALESSANDRO, A., EISENMESSER, E. Z., HERRERA, J. J., HANSEN, K. C., NEMKOV, T., STIENSTRA, R., GARLANDA, C., MANTOVANI, A., SEALS, D. R., DAGNA, L., JOOSTEN, L. A., BALLAK, D. B. & DINARELLO, C. A. 2017. Interleukin 37 reverses the metabolic cost of inflammation, increases oxidative respiration, and improves exercise tolerance. *Proc Natl Acad Sci U S A,* 114**,** 2313-2318.

CAVALLI, G. & MISTELI, T. 2013. Functional implications of genome topology. *Nat Struct Mol Biol,* 20**,** 290-9.

CHEN, H., LEVO, M., BARINOV, L., FUJIOKA, M., JAYNES, J. B. & GREGOR, T. 2018. Dynamic interplay between enhancer-promoter topology and gene activity. *Nat Genet,* 50**,** 1296-1303.

CHEN, Y. G., SATPATHY, A. T. & CHANG, H. Y. 2017. Gene regulation in the immune system by long noncoding RNAs. *Nat Immunol,* 18**,** 962-972.

CHENG, S. C., QUINTIN, J., CRAMER, R. A., SHEPARDSON, K. M., SAEED, S., KUMAR, V., GIAMARELLOS-BOURBOULIS, E. J., MARTENS, J. H., RAO, N. A., AGHAJANIREFAH, A., MANJERI, G. R., LI, Y., IFRIM, D. C., ARTS, R. J., VAN DER VEER, B. M., DEEN, P. M., LOGIE, C., O'NEILL, L. A., WILLEMS, P., VAN DE VEERDONK, F. L., VAN DER MEER, J. W., NG, A., JOOSTEN, L. A., WIJMENGA, C., STUNNENBERG, H. G., XAVIER, R. J. & NETEA, M. G. 2014. mTOR- and HIF-1alpha-mediated aerobic glycolysis as metabolic basis for trained immunity. *Science,* 345**,** 1250684.

CHO, W. K., SPILLE, J. H., HECHT, M., LEE, C., LI, C., GRUBE, V. & CISSE, II 2018. Mediator and RNA polymerase II clusters associate in transcription-dependent condensates. *Science,* 361**,** 412-415.

CHONG, S., DUGAST-DARZACQ, C., LIU, Z., DONG, P., DAILEY, G. M., CATTOGLIO, C., HECKERT, A., BANALA, S., LAVIS, L., DARZACQ, X. & TJIAN, R. 2018. Imaging dynamic and selective low-complexity domain interactions that control gene transcription. *Science,* 361.

CONSORTIUM, C. E. S. 1998. Genome sequence of the nematode C. elegans: a platform for investigating biology. *Science,* 282**,** 2012-8.

CORCES, M. R., GRANJA, J. M., SHAMS, S., LOUIE, B. H., SEOANE, J. A., ZHOU, W., SILVA, T. C., GROENEVELD, C., WONG, C. K., CHO, S. W., SATPATHY, A. T., MUMBACH, M. R., HOADLEY, K. A., ROBERTSON, A. G., SHEFFIELD, N. C., FELAU, I., CASTRO, M. A. A., BERMAN, B. P., STAUDT, L. M., ZENKLUSEN, J. C., LAIRD, P. W., CURTIS, C., CANCER GENOME ATLAS ANALYSIS, N., GREENLEAF, W. J. & CHANG, H. Y. 2018. The chromatin accessibility landscape of primary human cancers. *Science,* 362.

CREMER, T. & CREMER, C. 2001. Chromosome territories, nuclear architecture and gene regulation in mammalian cells. *Nat Rev Genet,* 2**,** 292-301.

CRUMP, N. T., HAZZALIN, C. A., BOWERS, E. M., ALANI, R. M., COLE, P. A. & MAHADEVAN, L. C. 2011. Dynamic acetylation of all lysine-4 trimethylated histone H3 is evolutionarily conserved and mediated by p300/CBP. *Proceedings of the National Academy of Sciences,* 108**,** 7814.

DELSING, C. E., GRESNIGT, M. S., LEENTJENS, J., PREIJERS, F., FRAGER, F. A., KOX, M., MONNERET, G., VENET, F., BLEEKER-ROVERS, C. P., VAN DE VEERDONK, F. L., PICKKERS, P., PACHOT, A., KULLBERG, B. J. & NETEA, M. G. 2014. Interferon-gamma as adjunctive immunotherapy for invasive fungal infections: a case series. *BMC Infect Dis,* 14**,** 166.

DENG, W., LEE, J., WANG, H., MILLER, J., REIK, A., GREGORY, P. D., DEAN, A. & BLOBEL, G. A. 2012. Controlling long-range genomic interactions at a native locus by targeted tethering of a looping factor. *Cell,* 149**,** 1233-44.

DIAO, Y., LI, B., MENG, Z., JUNG, I., LEE, A. Y., DIXON, J., MALISKOVA, L., GUAN, K. L., SHEN, Y. & REN, B. 2016. A new class of temporarily phenotypic enhancers identified by CRISPR/Cas9-mediated genetic screening. *Genome Res,* 26**,** 397-405.

DINARELLO, C. A. 2011. A clinical perspective of IL-1beta as the gatekeeper of inflammation. *Eur J Immunol,* 41**,** 1203-17.

DINARELLO, C. A. 2013. Overview of the interleukin-1 family of ligands and receptors. *Semin Immunol,* 25**,** 389-93.

DINARELLO, C. A., SIMON, A. & VAN DER MEER, J. W. 2012. Treating inflammation by blocking interleukin-1 in a broad spectrum of diseases. *Nat Rev Drug Discov,* 11**,** 633-52.

DIXON, J. R., JUNG, I., SELVARAJ, S., SHEN, Y., ANTOSIEWICZ-BOURGET, J. E., LEE, A. Y., YE, Z., KIM, A., RAJAGOPAL, N., XIE, W., DIAO, Y., LIANG, J., ZHAO, H., LOBANENKOV, V. V., ECKER, J. R., THOMSON, J. A. & REN, B. 2015. Chromatin architecture reorganization during stem cell differentiation. *Nature,* 518**,** 331-6.

DIXON, J. R., SELVARAJ, S., YUE, F., KIM, A., LI, Y., SHEN, Y., HU, M., LIU, J. S. & REN, B. 2012. Topological domains in mammalian genomes identified by analysis of chromatin interactions. *Nature,* 485**,** 376-80.

EBERHARTER, A. & BECKER, P. B. 2004. ATP-dependent nucleosome remodelling: factors and functions. *J Cell Sci,* 117**,** 3707-11.

ELOWITZ, M. B. & LEIBLER, S. 2000. A synthetic oscillatory network of transcriptional regulators. *Nature,* 403**,** 335-8.

ESCOUBET-LOZACH, L., BENNER, C., KAIKKONEN, M. U., LOZACH, J., HEINZ, S., SPANN, N. J., CROTTI, A., STENDER, J., GHISLETTI, S., REICHART, D., CHENG, C. S., LUNA, R., LUDKA, C., SASIK, R., GARCIA-BASSETS, I., HOFFMANN, A., SUBRAMANIAM, S., HARDIMAN, G., ROSENFELD, M. G. & GLASS, C. K. 2011. Mechanisms establishing TLR4-responsive activation states of inflammatory response genes. *PLoS Genet,* 7**,** e1002401.

FAN, J., CAI, Y., HUANG, X., WANG, Y., MU, L. & ZHOU, L. 2017. Variations in IL-1R1 Gene Influence Risk for Hepatitis B Virus Infection of Children in a Han Chinese population. *International Journal of Infectious Diseases,* 55**,** 45-50.

FANUCCHI, S., FOK, E. T., DALLA, E., SHIBAYAMA, Y., BORNER, K., CHANG, E. Y., STOYCHEV, S., IMAKAEV, M., GRIMM, D., WANG, K. C., LI, G., SUNG, W. K. & MHLANGA, M. M. 2019. Immune genes are primed for robust transcription by proximal long noncoding RNAs located in nuclear compartments. *Nat Genet,* 51**,** 138-150.

FANUCCHI, S., SHIBAYAMA, Y., BURD, S., WEINBERG, M. S. & MHLANGA, M. M. 2013. Chromosomal contact permits transcription between coregulated genes. *Cell,* 155**,** 606-20.

FELSENFELD, G. & GROUDINE, M. 2003. Controlling the double helix. *Nature,* 421**,** 448-53.

FENOUIL, R., CAUCHY, P., KOCH, F., DESCOSTES, N., CABEZA, J. Z., INNOCENTI, C., FERRIER, P., SPICUGLIA, S., GUT, M., GUT, I. & ANDRAU, J. C. 2012. CpG islands and GC content dictate nucleosome depletion in a transcription-independent manner at mammalian promoters. *Genome Res,* 22**,** 2399-408.

FINN, E. H. & MISTELI, T. 2019. A genome disconnect. *Nat Genet,* 51**,** 1205-1206.

FINN, E. H., PEGORARO, G., BRANDAO, H. B., VALTON, A. L., OOMEN, M. E., DEKKER, J., MIRNY, L. & MISTELI, T. 2019. Extensive Heterogeneity and Intrinsic Variation in Spatial Genome Organization. *Cell,* 176**,** 1502-1515 e10.

FLAVAHAN, W. A., DRIER, Y., LIAU, B. B., GILLESPIE, S. M., VENTEICHER, A. S., STEMMER-RACHAMIMOV, A. O., SUVA, M. L. & BERNSTEIN, B. E. 2016. Insulator dysfunction and oncogene activation in IDH mutant gliomas. *Nature,* 529**,** 110-4.

FLEISCHMANN, R. D., ADAMS, M. D., WHITE, O., CLAYTON, R. A., KIRKNESS, E. F., KERLAVAGE, A. R., BULT, C. J., TOMB, J. F., DOUGHERTY, B. A., MERRICK, J. M. & ET AL. 1995. Whole-genome random sequencing and assembly of Haemophilus influenzae Rd. *Science,* 269**,** 496-512.

FLYAMER, I. M., GASSLER, J., IMAKAEV, M., BRANDAO, H. B., ULIANOV, S. V., ABDENNUR, N., RAZIN, S. V., MIRNY, L. A. & TACHIBANA-KONWALSKI, K. 2017. Single-nucleus Hi-C reveals unique chromatin reorganization at oocyte-to-zygote transition. *Nature,* 544**,** 110-114.

FOK, E. T., DAVIGNON, L., FANUCCHI, S. & MHLANGA, M. M. 2018. The lncRNA Connection Between Cellular Metabolism and Epigenetics in Trained Immunity. *Front Immunol,* 9**,** 3184.

FOK, E. T., SCHOLEFIELD, J., FANUCCHI, S. & MHLANGA, M. M. 2017. The emerging molecular biology toolbox for the study of long noncoding RNA biology. *Epigenomics,* 9**,** 1317-1327.

FOWLER, T., SEN, R. & ROY, A. L. 2011. Regulation of primary response genes. *Mol Cell,* 44**,** 348-60.

FUDENBERG, G. & IMAKAEV, M. 2017. FISH-ing for captured contacts: towards reconciling FISH and 3C. *Nat Methods,* 14**,** 673-678.

FULLWOOD, M. J., LIU, M. H., PAN, Y. F., LIU, J., XU, H., MOHAMED, Y. B., ORLOV, Y. L., VELKOV, S., HO, A., MEI, P. H., CHEW, E. G., HUANG, P. Y., WELBOREN, W. J., HAN, Y., OOI, H. S., ARIYARATNE, P. N., VEGA, V. B., LUO, Y., TAN, P. Y., CHOY, P. Y., WANSA, K. D., ZHAO, B., LIM, K. S., LEOW, S. C., YOW, J. S., JOSEPH, R., LI, H., DESAI, K. V., THOMSEN, J. S., LEE,

Y. K., KARUTURI, R. K., HERVE, T., BOURQUE, G., STUNNENBERG, H. G., RUAN, X., CACHEUX-RATABOUL, V., SUNG, W. K., LIU, E. T., WEI, C. L., CHEUNG, E. & RUAN, Y. 2009. An oestrogen-receptor-alpha-bound human chromatin interactome. *Nature,* 462**,** 58-64.

GANJI, M., SHALTIEL, I. A., BISHT, S., KIM, E., KALICHAVA, A., HAERING, C. H. & DEKKER, C. 2018. Real-time imaging of DNA loop extrusion by condensin. *Science,* 360**,** 102-105.

GARLY, M. L., MARTINS, C. L., BALE, C., BALDE, M. A., HEDEGAARD, K. L., GUSTAFSON, P., LISSE, I. M., WHITTLE, H. C. & AABY, P. 2003. BCG scar and positive tuberculin reaction associated with reduced child mortality in West Africa. A non-specific beneficial effect of BCG? *Vaccine,* 21**,** 2782-90.

GE, Y., ZHOU, H., SHI, J., YE, B., PENG, Q., LU, X. & WANG, G. 2015. The efficacy of tacrolimus in patients with refractory dermatomyositis/polymyositis: a systematic review. *Clin Rheumatol,* 34**,** 2097-103.

GENOMES PROJECT, C., AUTON, A., BROOKS, L. D., DURBIN, R. M., GARRISON, E. P., KANG, H. M., KORBEL, J. O., MARCHINI, J. L., MCCARTHY, S., MCVEAN, G. A. & ABECASIS, G. R. 2015. A global reference for human genetic variation. *Nature,* 526**,** 68-74.

GHAVI-HELM, Y., JANKOWSKI, A., MEIERS, S., VIALES, R. R., KORBEL, J. O. & FURLONG, E. E. M. 2019. Highly rearranged chromosomes reveal uncoupling between genome topology and gene expression. *Nat Genet,* 51**,** 1272-1282.

GIBCUS, J. H. & DEKKER, J. 2013. The hierarchy of the 3D genome. *Mol Cell,* 49**,** 773-82.

GIORGETTI, L., GALUPA, R., NORA, E. P., PIOLOT, T., LAM, F., DEKKER, J., TIANA, G. & HEARD, E. 2014. Predictive polymer modeling reveals coupled fluctuations in chromosome conformation and transcription. *Cell,* 157**,** 950-63.

GOMEZ, J. A., WAPINSKI, O. L., YANG, Y. W., BUREAU, J. F., GOPINATH, S., MONACK, D. M., CHANG, H. Y., BRAHIC, M. & KIRKEGAARD, K. 2013. The NeST long ncRNA controls microbial susceptibility and epigenetic activation of the interferon-gamma locus. *Cell,* 152**,** 743-54.

GONG, Y., LAZARIS, C., SAKELLAROPOULOS, T., LOZANO, A., KAMBADUR, P., NTZIACHRISTOS, P., AIFANTIS, I. & TSIRIGOS, A. 2018. Stratification of TAD boundaries reveals preferential insulation of super-enhancers by strong boundaries. *Nat Commun,* 9**,** 542.

GOODRIDGE, H. S., SIMMONS, R. M. & UNDERHILL, D. M. 2007. Dectin-1 stimulation by Candida albicans yeast or zymosan triggers NFAT activation in macrophages and dendritic cells. *J Immunol,* 178**,** 3107-15.

GOURBAL, B., PINAUD, S., BECKERS, G. J. M., VAN DER MEER, J. W. M., CONRATH, U. & NETEA, M. G. 2018. Innate immune memory: An evolutionary perspective. *Immunol Rev,* 283**,** 21-40.

GRIVENNIKOV, S. I., GRETEN, F. R. & KARIN, M. 2010. Immunity, inflammation, and cancer. *Cell,* 140**,** 883-99.

GUPTA, S. K., LYSKO, P. G., PILLARISETTI, K., OHLSTEIN, E. & STADEL, J. M. 1998. Chemokine receptors in human endothelial cells. Functional expression of CXCR4 and its transcriptional regulation by inflammatory cytokines. *J Biol Chem,* 273**,** 4282-7.

HADADI, E., ZHANG, B., BAIDZAJEVAS, K., YUSOF, N., PUAN, K. J., ONG, S. M., YEAP, W. H., ROTZSCHKE, O., KISS-TOTH, E., WILSON, H. & WONG, S. C. 2016. Differential IL-1beta secretion by monocyte subsets is regulated by Hsp27 through modulating mRNA stability. *Sci Rep,* 6**,** 39035.

HAGEGE, H., KLOUS, P., BRAEM, C., SPLINTER, E., DEKKER, J., CATHALA, G., DE LAAT, W. & FORNE, T. 2007. Quantitative analysis of chromosome conformation capture assays (3C-qPCR). *Nat Protoc,* 2**,** 1722-33.

HAHN, M. W. & WRAY, G. A. 2002. The g-value paradox. *Evol Dev,* 4**,** 73-5.

HANNAH, J., CASIAN, A. & D'CRUZ, D. 2016. Tacrolimus use in lupus nephritis: A systematic review and meta-analysis. *Autoimmun Rev,* 15**,** 93-101.

HANSEN, A. S., CATTOGLIO, C., DARZACQ, X. & TJIAN, R. 2018. Recent evidence that TADs and chromatin loops are dynamic structures. *Nucleus,* 9**,** 20-32.

HAO, S. & BALTIMORE, D. 2009. The stability of mRNA influences the temporal order of the induction of genes encoding inflammatory molecules. *Nat Immunol,* 10**,** 281-8.

HARDIE, D. G., ROSS, F. A. & HAWLEY, S. A. 2012. AMPK: a nutrient and energy sensor that maintains energy homeostasis. *Nat Rev Mol Cell Biol,* 13**,** 251-62.

HARGREAVES, D. C., HORNG, T. & MEDZHITOV, R. 2009. Control of inducible gene expression by signal-dependent transcriptional elongation. *Cell,* 138**,** 129-45.

HARTMANN, J., MUNCH, R. C., FREILING, R. T., SCHNEIDER, I. C., DREIER, B., SAMUKANGE, W., KOCH, J., SEEGER, M. A., PLUCKTHUN, A. & BUCHHOLZ, C. J. 2018. A Library-Based Screening Strategy for the Identification of DARPins as Ligands for Receptor-Targeted AAV and Lentiviral Vectors. *Mol Ther Methods Clin Dev,* 10**,** 128-143.

HOORN, E. J., WALSH, S. B., MCCORMICK, J. A., FURSTENBERG, A., YANG, C. L., ROESCHEL, T., PALIEGE, A., HOWIE, A. J., CONLEY, J., BACHMANN, S., UNWIN, R. J. & ELLISON, D. H. 2011. The calcineurin inhibitor tacrolimus activates the renal sodium chloride cotransporter to cause hypertension. *Nat Med,* 17**,** 1304-9.

HOTCHKISS, R. S., COOPERSMITH, C. M., MCDUNN, J. E. & FERGUSON, T. A. 2009. The sepsis seesaw: tilting toward immunosuppression. *Nat Med,* 15**,** 496-7.

HU, G., TANG, Q., SHARMA, S., YU, F., ESCOBAR, T. M., MULJO, S. A., ZHU, J. & ZHAO, K. 2013. Expression and regulation of intergenic long noncoding RNAs during T cell development and differentiation. *Nat Immunol,* 14**,** 1190-8.

HUANG, X. L., WU, G. C., WANG, Y. J., YANG, X. K., YANG, G. J., TAO, J. H., DUAN, Y., YAN, J. W., LI, X. P., YE, D. Q. & WANG, J. 2016. Association of interleukin-1 family cytokines single nucleotide polymorphisms with susceptibility to systemic sclerosis: an independent case-control study and a meta-analysis. *Immunol Res,* 64**,** 1041-52.

ILOTT, N. E., HEWARD, J. A., ROUX, B., TSITSIOU, E., FENWICK, P. S., LENZI, L., GOODHEAD, I., HERTZ-FOWLER, C., HEGER, A., HALL, N.,

DONNELLY, L. E., SIMS, D. & LINDSAY, M. A. 2014. Long non-coding RNAs and enhancer RNAs regulate the lipopolysaccharide-induced inflammatory response in human monocytes. *Nat Commun,* 5**,** 3979.

IMAKAEV, M., FUDENBERG, G., MCCORD, R. P., NAUMOVA, N., GOLOBORODKO, A., LAJOIE, B. R., DEKKER, J. & MIRNY, L. A. 2012. Iterative correction of Hi-C data reveals hallmarks of chromosome organization. *Nat Methods,* 9**,** 999-1003.

JAVIERRE, B. M., BURREN, O. S., WILDER, S. P., KREUZHUBER, R., HILL, S. M., SEWITZ, S., CAIRNS, J., WINGETT, S. W., VARNAI, C., THIECKE, M. J., BURDEN, F., FARROW, S., CUTLER, A. J., REHNSTROM, K., DOWNES, K., GRASSI, L., KOSTADIMA, M., FREIRE-PRITCHETT, P., WANG, F., CONSORTIUM, B., STUNNENBERG, H. G., TODD, J. A., ZERBINO, D. R., STEGLE, O., OUWEHAND, W. H., FRONTINI, M., WALLACE, C., SPIVAKOV, M. & FRASER, P. 2016. Lineage-Specific Genome Architecture Links Enhancers and Non-coding Disease Variants to Target Gene Promoters. *Cell,* 167**,** 1369-1384 e19.

JIANG, H., WESTERTERP, M., WANG, C., ZHU, Y. & AI, D. 2014. Macrophage mTORC1 disruption reduces inflammation and insulin resistance in obese mice. *Diabetologia,* 57**,** 2393-404.

JIMENEZ-SOUSA, M. A., MEDRANO, L. M., LIU, P., ALMANSA, R., FERNANDEZ-RODRIGUEZ, A., GOMEZ-SANCHEZ, E., RICO, L., HEREDIA-RODRIGUEZ, M., GOMEZ-PESQUERA, E., TAMAYO, E. & RESINO, S. 2017. IL-1B rs16944 polymorphism is related to septic shock and death. *Eur J Clin Invest,* 47**,** 53-62.

JIN, F., LI, Y., DIXON, J. R., SELVARAJ, S., YE, Z., LEE, A. Y., YEN, C. A., SCHMITT, A. D., ESPINOZA, C. A. & REN, B. 2013. A high-resolution map of the three-dimensional chromatin interactome in human cells. *Nature,* 503**,** 290-4.

JOHANSON, T. M., CHAN, W. F., KEENAN, C. R. & ALLAN, R. S. 2019. Genome organization in immune cells: unique challenges. *Nat Rev Immunol,* 19**,** 448-456.

JULIANO, R. L. 2016. The delivery of therapeutic oligonucleotides. *Nucleic Acids Res,* 44**,** 6518-48.

JUNG, Y. J., ISAACS, J. S., LEE, S., TREPEL, J. & NECKERS, L. 2003. IL-1beta-mediated up-regulation of HIF-1alpha via an NFkappaB/COX-2 pathway identifies HIF-1 as a critical link between inflammation and oncogenesis. *FASEB J,* 17**,** 2115-7.

JUVEN-GERSHON, T., HSU, J. Y., THEISEN, J. W. & KADONAGA, J. T. 2008. The RNA polymerase II core promoter - the gateway to transcription. *Curr Opin Cell Biol,* 20**,** 253-9.

KACZMAREK, J. C., KOWALSKI, P. S. & ANDERSON, D. G. 2017. Advances in the delivery of RNA therapeutics: from concept to clinical reality. *Genome Med,* 9**,** 60.

KAPRANOV, P., CHENG, J., DIKE, S., NIX, D. A., DUTTAGUPTA, R., WILLINGHAM, A. T., STADLER, P. F., HERTEL, J., HACKERMULLER, J., HOFACKER, I. L., BELL, I., CHEUNG, E., DRENKOW, J., DUMAIS, E., PATEL, S., HELT, G., GANESH, M., GHOSH, S., PICCOLBONI, A., SEMENTCHENKO, V., TAMMANA, H. & GINGERAS, T. R. 2007. RNA maps reveal new RNA classes and a possible function for pervasive transcription. *Science,* 316**,** 1484-8.

KAUFMANN, E., SANZ, J., DUNN, J. L., KHAN, N., MENDONCA, L. E., PACIS, A., TZELEPIS, F., PERNET, E., DUMAINE, A., GRENIER, J. C., MAILHOT-LEONARD, F., AHMED, E., BELLE, J., BESLA, R., MAZER, B., KING, I. L., NIJNIK, A., ROBBINS, C. S., BARREIRO, L. B. & DIVANGAHI, M. 2018. BCG Educates Hematopoietic Stem Cells to Generate Protective Innate Immunity against Tuberculosis. *Cell,* 172**,** 176-190 e19.

KERA, Y., KATOH, Y., OHTA, M., MATSUMOTO, M., TAKANO-YAMAMOTO, T. & IGARASHI, K. 2013. Methionine adenosyltransferase II-dependent histone H3K9 methylation at the COX-2 gene locus. *J Biol Chem,* 288**,** 13592-601.

KLEINNIJENHUIS, J., QUINTIN, J., PREIJERS, F., JOOSTEN, L. A., IFRIM, D. C., SAEED, S., JACOBS, C., VAN LOENHOUT, J., DE JONG, D., STUNNENBERG, H. G., XAVIER, R. J., VAN DER MEER, J. W., VAN CREVEL, R. & NETEA, M. G. 2012. Bacille Calmette-Guerin induces NOD2-dependent nonspecific protection from reinfection via epigenetic reprogramming of monocytes. *Proc Natl Acad Sci U S A,* 109**,** 17537-42.

KLEMM, S. L., SHIPONY, Z. & GREENLEAF, W. J. 2019. Chromatin accessibility and the regulatory epigenome. *Nat Rev Genet,* 20**,** 207-220.

KOBAYASHI, Y. 2008. The role of chemokines in neutrophil biology. *Front Biosci,* 13**,** 2400-7.

KORNMAN, K. S. 2006. Interleukin 1 genetics, inflammatory mechanisms, and nutrigenetic opportunities to modulate diseases of aging. *Am J Clin Nutr,* 83**,** 475S-483S.

KUNG, J. T., COLOGNORI, D. & LEE, J. T. 2013. Long noncoding RNAs: past, present, and future. *Genetics,* 193**,** 651-69.

KURTZ, J. 2005. Specific memory within innate immune systems. *Trends Immunol,* 26**,** 186-92.

KURTZ, J. & FRANZ, K. 2003. Innate defence: evidence for memory in invertebrate immunity. *Nature,* 425**,** 37-8.

LAI, F., OROM, U. A., CESARONI, M., BERINGER, M., TAATJES, D. J., BLOBEL, G. A. & SHIEKHATTAR, R. 2013. Activating RNAs associate with Mediator to enhance chromatin architecture and transcription. *Nature,* 494**,** 497-501.

LAM, M. T., CHO, H., LESCH, H. P., GOSSELIN, D., HEINZ, S., TANAKA-OISHI, Y., BENNER, C., KAIKKONEN, M. U., KIM, A. S., KOSAKA, M., LEE, C. Y., WATT, A., GROSSMAN, T. R., ROSENFELD, M. G., EVANS, R. M. & GLASS, C. K. 2013. Rev-Erbs repress macrophage gene expression by inhibiting enhancer-directed transcription. *Nature,* 498**,** 511-5.

LANDER, E. S., LINTON, L. M., BIRREN, B., NUSBAUM, C., ZODY, M. C., BALDWIN, J., DEVON, K., DEWAR, K., DOYLE, M., FITZHUGH, W., FUNKE, R., GAGE, D., HARRIS, K., HEAFORD, A., HOWLAND, J., KANN, L., LEHOCZKY, J., LEVINE, R., MCEWAN, P., MCKERNAN, K., MELDRIM, J., MESIROV, J. P., MIRANDA, C., MORRIS, W., NAYLOR, J., RAYMOND, C., ROSETTI, M., SANTOS, R., SHERIDAN, A., SOUGNEZ, C., STANGE-THOMANN, Y., STOJANOVIC, N., SUBRAMANIAN, A., WYMAN, D., ROGERS, J., SULSTON, J., AINSCOUGH, R., BECK, S., BENTLEY, D., BURTON, J., CLEE, C., CARTER, N., COULSON, A., DEADMAN, R., DELOUKAS, P., DUNHAM, A., DUNHAM, I., DURBIN, R., FRENCH, L., GRAFHAM, D., GREGORY, S., HUBBARD, T., HUMPHRAY, S., HUNT, A.,

JONES, M., LLOYD, C., MCMURRAY, A., MATTHEWS, L., MERCER, S., MILNE, S., MULLIKIN, J. C., MUNGALL, A., PLUMB, R., ROSS, M., SHOWNKEEN, R., SIMS, S., WATERSTON, R. H., WILSON, R. K., HILLIER, L. W., MCPHERSON, J. D., MARRA, M. A., MARDIS, E. R., FULTON, L. A., CHINWALLA, A. T., PEPIN, K. H., GISH, W. R., CHISSOE, S. L., WENDL, M. C., DELEHAUNTY, K. D., MINER, T. L., DELEHAUNTY, A., KRAMER, J. B., COOK, L. L., FULTON, R. S., JOHNSON, D. L., MINX, P. J., CLIFTON, S. W., HAWKINS, T., BRANSCOMB, E., PREDKI, P., RICHARDSON, P., WENNING, S., SLEZAK, T., DOGGETT, N., CHENG, J. F., OLSEN, A., LUCAS, S., ELKIN, C., UBERBACHER, E., FRAZIER, M., et al. 2001. Initial sequencing and analysis of the human genome. *Nature,* 409**,** 860-921.

LARSEN, F. S., VAINER, B., EEFSEN, M., BJERRING, P. N. & ADEL HANSEN, B. 2007. Low-dose tacrolimus ameliorates liver inflammation and fibrosis in steroid refractory autoimmune hepatitis. *World J Gastroenterol,* 13**,** 3232-6.

LAUBERTH, S. M., NAKAYAMA, T., WU, X., FERRIS, A. L., TANG, Z., HUGHES, S. H. & ROEDER, R. G. 2013. H3K4me3 interactions with TAF3 regulate preinitiation complex assembly and selective gene activation. *Cell,* 152**,** 1021-36.

LEE, S. & MARGOLIN, K. 2011. Cytokines in cancer immunotherapy. *Cancers (Basel),* 3**,** 3856-93.

LENNOX, K. A. & BEHLKE, M. A. 2016. Cellular localization of long non-coding RNAs affects silencing by RNAi more than by antisense oligonucleotides. *Nucleic Acids Res,* 44**,** 863-77.

LEVINE, M., CATTOGLIO, C. & TJIAN, R. 2014. Looping back to leap forward: transcription enters a new era. *Cell,* 157**,** 13-25.

LI, D., LI, J., WANG, L. & ZHANG, Q. 2015a. Association between IL-1β, IL-8, and IL-10 polymorphisms and risk of acute pancreatitis. *Genet Mol Res,* 14**,** 6635-41.

LI, S., AMO-APARICIO, J., NEFF, C. P., TENGESDAL, I. W., AZAM, T., PALMER, B. E., LOPEZ-VALES, R., BUFLER, P. & DINARELLO, C. A. 2019. Role for nuclear interleukin-37 in the suppression of innate immunity. *Proc Natl Acad Sci U S A*.

LI, S., NEFF, C. P., BARBER, K., HONG, J., LUO, Y., AZAM, T., PALMER, B. E., FUJITA, M., GARLANDA, C., MANTOVANI, A., KIM, S. & DINARELLO, C. A. 2015b. Extracellular forms of IL-37 inhibit innate inflammation in vitro and in vivo but require the IL-1 family decoy receptor IL-1R8. *Proc Natl Acad Sci U S A,* 112**,** 2497-502.

LI, W., NOTANI, D., MA, Q., TANASA, B., NUNEZ, E., CHEN, A. Y., MERKURJEV, D., ZHANG, J., OHGI, K., SONG, X., OH, S., KIM, H. S., GLASS, C. K. & ROSENFELD, M. G. 2013. Functional roles of enhancer RNAs for oestrogen-dependent transcriptional activation. *Nature,* 498**,** 516-20.

LI, Y., OOSTING, M., DEELEN, P., RICANO-PONCE, I., SMEEKENS, S., JAEGER, M., MATZARAKI, V., SWERTZ, M. A., XAVIER, R. J., FRANKE, L., WIJMENGA, C., JOOSTEN, L. A., KUMAR, V. & NETEA, M. G. 2016. Inter-individual variability and genetic influences on cytokine responses to bacteria and fungi. *Nat Med,* 22**,** 952-60.

LIEBERMAN-AIDEN, E., VAN BERKUM, N. L., WILLIAMS, L., IMAKAEV, M., RAGOCZY, T., TELLING, A., AMIT, I., LAJOIE, B. R., SABO, P. J., DORSCHNER, M. O., SANDSTROM, R., BERNSTEIN, B., BENDER, M. A., GROUDINE, M., GNIRKE, A., STAMATOYANNOPOULOS, J., MIRNY, L. A., LANDER, E. S. & DEKKER, J. 2009. Comprehensive mapping of long-range interactions reveals folding principles of the human genome. *Science,* 326**,** 289-93.

LIM, B., HEIST, T., LEVINE, M. & FUKAYA, T. 2018. Visualization of Transvection in Living Drosophila Embryos. *Mol Cell,* 70**,** 287-296 e6.

LIU, M., LUO, F., DING, C., ALBEITUNI, S., HU, X., MA, Y., CAI, Y., MCNALLY, L., SANDERS, M. A., JAIN, D., KLOECKER, G., BOUSAMRA, M., 2ND, ZHANG, H. G., HIGASHI, R. M., LANE, A. N., FAN, T. W. & YAN, J. 2015. Dectin-1 Activation by a Natural Product beta-Glucan Converts Immunosuppressive Macrophages into an M1-like Phenotype. *J Immunol,* 195**,** 5055-65.

LIU, X. S., WU, H., JI, X., STELZER, Y., WU, X., CZAUDERNA, S., SHU, J., DADON, D., YOUNG, R. A. & JAENISCH, R. 2016. Editing DNA Methylation in the Mammalian Genome. *Cell,* 167**,** 233-247 e17.

LONG, Y., WANG, X., YOUMANS, D. T. & CECH, T. R. 2017. How do lncRNAs regulate transcription? *Science advances,* 3**,** eaao2110.

LUPIANEZ, D. G., KRAFT, K., HEINRICH, V., KRAWITZ, P., BRANCATI, F., KLOPOCKI, E., HORN, D., KAYSERILI, H., OPITZ, J. M., LAXOVA, R., SANTOS-SIMARRO, F., GILBERT-DUSSARDIER, B., WITTLER, L., BORSCHIWER, M., HAAS, S. A., OSTERWALDER, M., FRANKE, M., TIMMERMANN, B., HECHT, J., SPIELMANN, M., VISEL, A. & MUNDLOS, S. 2015. Disruptions of topological chromatin domains cause pathogenic rewiring of gene-enhancer interactions. *Cell,* 161**,** 1012-1025.

LUPIANEZ, D. G., SPIELMANN, M. & MUNDLOS, S. 2016. Breaking TADs: How Alterations of Chromatin Domains Result in Disease. *Trends Genet,* 32**,** 225-237.

MANTOVANI, A., DINARELLO, C. A., MOLGORA, M. & GARLANDA, C. 2019. Interleukin-1 and Related Cytokines in the Regulation of Inflammation and Immunity. *Immunity,* 50**,** 778-795.

MATSUDA, S., ADACHI, J., IHARA, M., TANUMA, N., SHIMA, H., KAKIZUKA, A., IKURA, M., IKURA, T. & MATSUDA, T. 2016. Nuclear pyruvate kinase M2 complex serves as a transcriptional coactivator of arylhydrocarbon receptor. *Nucleic Acids Res,* 44**,** 636-47.

MATTICK, J. S. 2004. RNA regulation: a new genetics? *Nat Rev Genet,* 5**,** 316-23.

MAURANO, M. T., HUMBERT, R., RYNES, E., THURMAN, R. E., HAUGEN, E., WANG, H., REYNOLDS, A. P., SANDSTROM, R., QU, H., BRODY, J., SHAFER, A., NERI, F., LEE, K., KUTYAVIN, T., STEHLING-SUN, S., JOHNSON, A. K., CANFIELD, T. K., GISTE, E., DIEGEL, M., BATES, D., HANSEN, R. S., NEPH, S., SABO, P. J., HEIMFELD, S., RAUBITSCHEK, A., ZIEGLER, S., COTSAPAS, C., SOTOODEHNIA, N., GLASS, I., SUNYAEV, S. R., KAUL, R. & STAMATOYANNOPOULOS, J. A. 2012. Systematic localization of common disease-associated variation in regulatory DNA. *Science,* 337**,** 1190-5.

MEDZHITOV, R. 2008. Origin and physiological roles of inflammation. *Nature,* 454**,** 428-35.

MELO, C. A., DROST, J., WIJCHERS, P. J., VAN DE WERKEN, H., DE WIT, E., OUDE VRIELINK, J. A., ELKON, R., MELO, S. A., LEVEILLE, N., KALLURI, R., DE LAAT, W. & AGAMI, R. 2013. eRNAs are required for p53-dependent enhancer activity and gene transcription. *Mol Cell,* 49**,** 524-35.

MERCER, T. R., GERHARDT, D. J., DINGER, M. E., CRAWFORD, J., TRAPNELL, C., JEDDELOH, J. A., MATTICK, J. S. & RINN, J. L. 2011. Targeted RNA sequencing reveals the deep complexity of the human transcriptome. *Nat Biotechnol,* 30**,** 99-104.

MERCER, T. R. & MATTICK, J. S. 2013. Structure and function of long noncoding RNAs in epigenetic regulation. *Nat Struct Mol Biol,* 20**,** 300-7.

MIN, I. M., WATERFALL, J. J., CORE, L. J., MUNROE, R. J., SCHIMENTI, J. & LIS, J. T. 2011. Regulating RNA polymerase pausing and transcription elongation in embryonic stem cells. *Genes Dev,* 25**,** 742-54.

MITROULIS, I., RUPPOVA, K., WANG, B., CHEN, L. S., GRZYBEK, M., GRINENKO, T., EUGSTER, A., TROULLINAKI, M., PALLADINI, A., KOURTZELIS, I., CHATZIGEORGIOU, A., SCHLITZER, A., BEYER, M., JOOSTEN, L. A. B., ISERMANN, B., LESCHE, M., PETZOLD, A., SIMONS, K., HENRY, I., DAHL, A., SCHULTZE, J. L., WIELOCKX, B., ZAMBONI, N., MIRTSCHINK, P., COSKUN, U., HAJISHENGALLIS, G., NETEA, M. G. & CHAVAKIS, T. 2018. Modulation of Myelopoiesis Progenitors Is an Integral Component of Trained Immunity. *Cell,* 172**,** 147-161 e12.

MONAHAN, K., HORTA, A. & LOMVARDAS, S. 2019. LHX2- and LDB1-mediated trans interactions regulate olfactory receptor choice. *Nature,* 565**,** 448-453.

MOORLAG, S., RORING, R. J., JOOSTEN, L. A. B. & NETEA, M. G. 2018. The role of the interleukin-1 family in trained immunity. *Immunol Rev,* 281**,** 28-39.

MORETTI, S., BOZZA, S., OIKONOMOU, V., RENGA, G., CASAGRANDE, A., IANNITTI, R. G., PUCCETTI, M., GARLANDA, C., KIM, S., LI, S., VAN DE VEERDONK, F. L., DINARELLO, C. A. & ROMANI, L. 2014. IL-37 inhibits inflammasome activation and disease severity in murine aspergillosis. *PLoS Pathog,* 10**,** e1004462.

MORGAN, S. L., MARIANO, N. C., BERMUDEZ, A., ARRUDA, N. L., WU, F., LUO, Y., SHANKAR, G., JIA, L., CHEN, H., HU, J. F., HOFFMAN, A. R., HUANG, C. C., PITTERI, S. J. & WANG, K. C. 2017. Manipulation of nuclear architecture through CRISPR-mediated chromosomal looping. *Nat Commun,* 8**,** 15993.

MUIK, A., REUL, J., FRIEDEL, T., MUTH, A., HARTMANN, K. P., SCHNEIDER, I. C., MUNCH, R. C. & BUCHHOLZ, C. J. 2017. Covalent coupling of high-affinity ligands to the surface of viral vector particles by protein trans-splicing mediates cell type-specific gene transfer. *Biomaterials,* 144**,** 84-94.

NASO, M. F., TOMKOWICZ, B., PERRY, W. L., 3RD & STROHL, W. R. 2017. Adeno-Associated Virus (AAV) as a Vector for Gene Therapy. *BioDrugs,* 31**,** 317-334.

NATOLI, G. 2016. From the Beauty of Genomic Landscapes to the Strength of Transcriptional Mechanisms. *Cell,* 165**,** 18-19.

NATOLI, G., GHISLETTI, S. & BAROZZI, I. 2011. The genomic landscapes of inflammation. *Genes Dev,* 25**,** 101-6.

NETEA, M. G., BALKWILL, F., CHONCHOL, M., COMINELLI, F., DONATH, M. Y., GIAMARELLOS-BOURBOULIS, E. J., GOLENBOCK, D., GRESNIGT, M. S., HENEKA, M. T., HOFFMAN, H. M., HOTCHKISS, R., JOOSTEN, L. A. B., KASTNER, D. L., KORTE, M., LATZ, E., LIBBY, P., MANDRUP-POULSEN, T., MANTOVANI, A., MILLS, K. H. G., NOWAK, K. L., O'NEILL, L. A., PICKKERS, P., VAN DER POLL, T., RIDKER, P. M., SCHALKWIJK, J., SCHWARTZ, D. A., SIEGMUND, B., STEER, C. J., TILG, H., VAN DER MEER, J. W. M., VAN DE VEERDONK, F. L. & DINARELLO, C. A. 2017. A guiding map for inflammation. *Nat Immunol,* 18**,** 826-831.

NETEA, M. G., NOLD-PETRY, C. A., NOLD, M. F., JOOSTEN, L. A., OPITZ, B., VAN DER MEER, J. H., VAN DE VEERDONK, F. L., FERWERDA, G., HEINHUIS, B., DEVESA, I., FUNK, C. J., MASON, R. J., KULLBERG, B. J., RUBARTELLI, A., VAN DER MEER, J. W. & DINARELLO, C. A. 2009. Differential requirement for the activation of the inflammasome for processing and release of IL-1beta in monocytes and macrophages. *Blood,* 113**,** 2324-35.

NI, G., WANG, T., WALTON, S., ZHU, B., CHEN, S., WU, X., WANG, Y., WEI, M. Q. & LIU, X. 2015. Manipulating IL-10 signalling blockade for better immunotherapy. *Cell Immunol,* 293**,** 126-9.

NISHIZAKI, S. S. & BOYLE, A. P. 2017. Mining the Unknown: Assigning Function to Noncoding Single Nucleotide Polymorphisms. *Trends Genet,* 33**,** 34-45.

NOLD, M. F., NOLD-PETRY, C. A., LO, C., LI, S., RUDLOFF, I., ZEPP, J. A., AZAM, T., BUFLER, P., GARLANDA, C. & MANTOVANI, A. 2013. 187: interleukin 37 employs the IL-1 family inhibitory receptor SIGIRR and the alpha chain of the IL-18 receptor to suppress innate immunity. *Cytokine,* 63**,** 287.

NOLD, M. F., NOLD-PETRY, C. A., ZEPP, J. A., PALMER, B. E., BUFLER, P. & DINARELLO, C. A. 2010. IL-37 is a fundamental inhibitor of innate immunity. *Nat Immunol,* 11**,** 1014-22.

NOLD-PETRY, C. A., LO, C. Y., RUDLOFF, I., ELGASS, K. D., LI, S., GANTIER, M. P., LOTZ-HAVLA, A. S., GERSTING, S. W., CHO, S. X., LAO, J. C., ELLISDON, A. M., ROTTER, B., AZAM, T., MANGAN, N. E., ROSSELLO, F. J., WHISSTOCK, J. C., BUFLER, P., GARLANDA, C., MANTOVANI, A., DINARELLO, C. A. & NOLD, M. F. 2015. IL-37 requires the receptors IL-18Ralpha and IL-1R8 (SIGIRR) to carry out its multifaceted anti-inflammatory program upon innate signal transduction. *Nat Immunol,* 16**,** 354-65.

NOORDERMEER, D., DE WIT, E., KLOUS, P., VAN DE WERKEN, H., SIMONIS, M., LOPEZ-JONES, M., EUSSEN, B., DE KLEIN, A., SINGER, R. H. & DE LAAT, W. 2011. Variegated gene expression caused by cell-specific long-range DNA interactions. *Nat Cell Biol,* 13**,** 944-51.

NORA, E. P., LAJOIE, B. R., SCHULZ, E. G., GIORGETTI, L., OKAMOTO, I., SERVANT, N., PIOLOT, T., VAN BERKUM, N. L., MEISIG, J., SEDAT, J., GRIBNAU, J., BARILLOT, E., BLUTHGEN, N., DEKKER, J. & HEARD, E. 2012. Spatial partitioning of the regulatory landscape of the X-inactivation centre. *Nature,* 485**,** 381-5.

O'LEARY, J. G., GOODARZI, M., DRAYTON, D. L. & VON ANDRIAN, U. H. 2006. T cell- and B cell-independent adaptive immunity mediated by natural killer cells. *Nat Immunol,* 7**,** 507-16.

O'NEILL, L. A., KISHTON, R. J. & RATHMELL, J. 2016. A guide to immunometabolism for immunologists. *Nat Rev Immunol,* 16**,** 553-65.

OFFENBACHER, S., JIAO, Y., KIM, S. J., MARCHESAN, J., MOSS, K. L., JING, L., DIVARIS, K., BENCHARIT, S., AGLER, C. S., MORELLI, T., ZHANG, S., SUN, L., SEAMAN, W. T., COWLEY, D., BARROS, S. P., BECK, J. D., MUNZ, M., SCHAEFER, A. S. & NORTH, K. E. 2018. GWAS for Interleukin-1beta levels in gingival crevicular fluid identifies IL37 variants in periodontal inflammation. *Nat Commun,* 9**,** 3686.

PAPANTONIS, A., KOHRO, T., BABOO, S., LARKIN, J. D., DENG, B., SHORT, P., TSUTSUMI, S., TAYLOR, S., KANKI, Y., KOBAYASHI, M., LI, G., POH, H. M., RUAN, X., ABURATANI, H., RUAN, Y., KODAMA, T., WADA, Y. & COOK, P. R. 2012. TNFalpha signals through specialized factories where responsive coding and miRNA genes are transcribed. *EMBO J,* 31**,** 4404-14.

PARRA, V. & ROTHERMEL, B. A. 2017. Calcineurin signaling in the heart: The importance of time and place. *J Mol Cell Cardiol,* 103**,** 121-136.

PAULSEN, M. T., VELOSO, A., PRASAD, J., BEDI, K., LJUNGMAN, E. A., TSAN, Y. C., CHANG, C. W., TARRIER, B., WASHBURN, J. G., LYONS, R., ROBINSON, D. R., KUMAR-SINHA, C., WILSON, T. E. & LJUNGMAN, M. 2013. Coordinated regulation of synthesis and stability of RNA during the acute TNF-induced proinflammatory response. *Proc Natl Acad Sci U S A,* 110**,** 2240-5.

POLISENO, L., SALMENA, L., ZHANG, J., CARVER, B., HAVEMAN, W. J. & PANDOLFI, P. P. 2010. A coding-independent function of gene and pseudogene mRNAs regulates tumour biology. *Nature,* 465**,** 1033-8.

PRADEEPA, M. M. 2017. Causal role of histone acetylations in enhancer function. *Transcription,* 8**,** 40-47.

PRASANTH, K. V. & SPECTOR, D. L. 2007. Eukaryotic regulatory RNAs: an answer to the 'genome complexity' conundrum. *Genes Dev,* 21**,** 11-42.

QUINN, J. J. & CHANG, H. Y. 2016. Unique features of long non-coding RNA biogenesis and function. *Nat Rev Genet,* 17**,** 47-62.

QUINTIN, J., SAEED, S., MARTENS, J. H. A., GIAMARELLOS-BOURBOULIS, E. J., IFRIM, D. C., LOGIE, C., JACOBS, L., JANSEN, T., KULLBERG, B. J., WIJMENGA, C., JOOSTEN, L. A. B., XAVIER, R. J., VAN DER MEER, J. W. M., STUNNENBERG, H. G. & NETEA, M. G. 2012. Candida albicans infection affords protection against reinfection via functional reprogramming of monocytes. *Cell Host Microbe,* 12**,** 223-32.

RABANI, M., LEVIN, J. Z., FAN, L., ADICONIS, X., RAYCHOWDHURY, R., GARBER, M., GNIRKE, A., NUSBAUM, C., HACOHEN, N., FRIEDMAN, N., AMIT, I. & REGEV, A. 2011. Metabolic labeling of RNA uncovers principles of RNA production and degradation dynamics in mammalian cells. *Nat Biotechnol,* 29**,** 436-42.

RAMIREZ, R. N., EL-ALI, N. C., MAGER, M. A., WYMAN, D., CONESA, A. & MORTAZAVI, A. 2017. Dynamic Gene Regulatory Networks of Human Myeloid Differentiation. *Cell Syst,* 4**,** 416-429 e3.

RAMIREZ-CARROZZI, V. R., BRAAS, D., BHATT, D. M., CHENG, C. S., HONG, C., DOTY, K. R., BLACK, J. C., HOFFMANN, A., CAREY, M. & SMALE, S. T. 2009. A unifying model for the selective regulation of inducible transcription by CpG islands and nucleosome remodeling. *Cell,* 138**,** 114-28.

RAMIREZ-PRADO, J. S., ABULFARAJ, A. A., RAYAPURAM, N., BENHAMED, M. & HIRT, H. 2018. Plant Immunity: From Signaling to Epigenetic Control of Defense. *Trends Plant Sci,* 23**,** 833-844.

RAN, F. A., HSU, P. D., WRIGHT, J., AGARWALA, V., SCOTT, D. A. & ZHANG, F. 2013. Genome engineering using the CRISPR-Cas9 system. *Nat Protoc,* 8**,** 2281-2308.

RAO, S. S., HUNTLEY, M. H., DURAND, N. C., STAMENOVA, E. K., BOCHKOV, I. D., ROBINSON, J. T., SANBORN, A. L., MACHOL, I., OMER, A. D., LANDER, E. S. & AIDEN, E. L. 2014. A 3D map of the human genome at kilobase resolution reveals principles of chromatin looping. *Cell,* 159**,** 1665-80.

RAPICAVOLI, N. A., QU, K., ZHANG, J., MIKHAIL, M., LABERGE, R. M. & CHANG, H. Y. 2013. A mammalian pseudogene lncRNA at the interface of inflammation and anti-inflammatory therapeutics. *Elife,* 2**,** e00762.

RATAJCZAK, W., NIEDZWIEDZKA-RYSTWEJ, P., TOKARZ-DEPTULA, B. & DEPTULA, W. 2018. Immunological memory cells. *Cent Eur J Immunol,* 43**,** 194-203.

RICCI, M. A., MANZO, C., GARCIA-PARAJO, M. F., LAKADAMYALI, M. & COSMA, M. P. 2015. Chromatin fibers are formed by heterogeneous groups of nucleosomes in vivo. *Cell,* 160**,** 1145-58.

RINN, J. L., KERTESZ, M., WANG, J. K., SQUAZZO, S. L., XU, X., BRUGMANN, S. A., GOODNOUGH, L. H., HELMS, J. A., FARNHAM, P. J., SEGAL, E. & CHANG, H. Y. 2007. Functional demarcation of active and silent chromatin domains in human HOX loci by noncoding RNAs. *Cell,* 129**,** 1311-23.

RIVERS-AUTY, J., DANIELS, M. J. D., COLLIVER, I., ROBERTSON, D. L. & BROUGH, D. 2018. Redefining the ancestral origins of the interleukin-1 superfamily. *Nat Commun,* 9**,** 1156.

RIZZETTO, L., IFRIM, D. C., MORETTI, S., TOCCI, N., CHENG, S. C., QUINTIN, J., RENGA, G., OIKONOMOU, V., DE FILIPPO, C., WEIL, T., BLOK, B. A., LENUCCI, M. S., SANTOS, M. A., ROMANI, L., NETEA, M. G. & CAVALIERI, D. 2016. Fungal Chitin Induces Trained Immunity in Human Monocytes during Cross-talk of the Host with Saccharomyces cerevisiae. *J Biol Chem,* 291**,** 7961-72.

ROBSON, M. I., RINGEL, A. R. & MUNDLOS, S. 2019. Regulatory Landscaping: How Enhancer-Promoter Communication Is Sculpted in 3D. *Mol Cell,* 74**,** 1110-1122.

RODRIGUEZ, I. 2013. Singular expression of olfactory receptor genes. *Cell,* 155**,** 274-7.

ROGATSKY, I. & ADELMAN, K. 2014. Preparing the first responders: building the inflammatory transcriptome from the ground up. *Mol Cell,* 54**,** 245-54.

ROWLEY, M. J. & CORCES, V. G. 2018. Organizational principles of 3D genome architecture. *Nat Rev Genet,* 19**,** 789-800.

RUSEK, P., WALA, M., DRUSZCZYNSKA, M. & FOL, M. 2018. Infectious Agents as Stimuli of Trained Innate Immunity. *Int J Mol Sci,* 19.

SABARI, B. R., DALL'AGNESE, A., BOIJA, A., KLEIN, I. A., COFFEY, E. L., SHRINIVAS, K., ABRAHAM, B. J., HANNETT, N. M., ZAMUDIO, A. V.,

MANTEIGA, J. C., LI, C. H., GUO, Y. E., DAY, D. S., SCHUIJERS, J., VASILE, E., MALIK, S., HNISZ, D., LEE, T. I., CISSE, II, ROEDER, R. G., SHARP, P. A., CHAKRABORTY, A. K. & YOUNG, R. A. 2018. Coactivator condensation at super-enhancers links phase separation and gene control. *Science,* 361.

SAEED, S., QUINTIN, J., KERSTENS, H. H., RAO, N. A., AGHAJANIREFAH, A., MATARESE, F., CHENG, S. C., RATTER, J., BERENTSEN, K., VAN DER ENT, M. A., SHARIFI, N., JANSSEN-MEGENS, E. M., TER HUURNE, M., MANDOLI, A., VAN SCHAIK, T., NG, A., BURDEN, F., DOWNES, K., FRONTINI, M., KUMAR, V., GIAMARELLOS-BOURBOULIS, E. J., OUWEHAND, W. H., VAN DER MEER, J. W., JOOSTEN, L. A., WIJMENGA, C., MARTENS, J. H., XAVIER, R. J., LOGIE, C., NETEA, M. G. & STUNNENBERG, H. G. 2014. Epigenetic programming of monocyte-to-macrophage differentiation and trained innate immunity. *Science,* 345**,** 1251086.

SANBORN, A. L., RAO, S. S., HUANG, S. C., DURAND, N. C., HUNTLEY, M. H., JEWETT, A. I., BOCHKOV, I. D., CHINNAPPAN, D., CUTKOSKY, A., LI, J., GEETING, K. P., GNIRKE, A., MELNIKOV, A., MCKENNA, D., STAMENOVA, E. K., LANDER, E. S. & AIDEN, E. L. 2015. Chromatin extrusion explains key features of loop and domain formation in wild-type and engineered genomes. *Proc Natl Acad Sci U S A,* 112**,** E6456-65.

SATO, T., TERAI, M., TAMURA, Y., ALEXEEV, V., MASTRANGELO, M. J. & SELVAN, S. R. 2011. Interleukin 10 in the tumor microenvironment: a target for anticancer immunotherapy. *Immunol Res,* 51**,** 170-82.

SAXENA, A., KHOSRAVIANI, S., NOEL, S., MOHAN, D., DONNER, T. & HAMAD, A. R. 2015. Interleukin-10 paradox: A potent immunoregulatory cytokine that has been difficult to harness for immunotherapy. *Cytokine,* 74**,** 27-34.

SCHRUM, J. E., CRABTREE, J. N., DOBBS, K. R., KIRITSY, M. C., REED, G. W., GAZZINELLI, R. T., NETEA, M. G., KAZURA, J. W., DENT, A. E., FITZGERALD, K. A. & GOLENBOCK, D. T. 2018. Cutting Edge: Plasmodium falciparum Induces Trained Innate Immunity. *J Immunol,* 200**,** 1243-1248.

SEIDEL, J. A., OTSUKA, A. & KABASHIMA, K. 2018. Anti-PD-1 and Anti-CTLA-4 Therapies in Cancer: Mechanisms of Action, Efficacy, and Limitations. *Front Oncol,* 8**,** 86.

SHARAF, N., NICKLIN, M. J. & DI GIOVINE, F. S. 2014. Long-range DNA interactions at the IL-1/IL-36/IL-37 gene cluster (2q13) are induced by activation of monocytes. *Cytokine,* 68**,** 16-22.

SHARMA, S., KULK, N., NOLD, M. F., GRAF, R., KIM, S. H., REINHARDT, D., DINARELLO, C. A. & BUFLER, P. 2008. The IL-1 family member 7b translocates to the nucleus and down-regulates proinflammatory cytokines. *J Immunol,* 180**,** 5477-82.

SHIN, Y., CHANG, Y. C., LEE, D. S. W., BERRY, J., SANDERS, D. W., RONCERAY, P., WINGREEN, N. S., HAATAJA, M. & BRANGWYNNE, C. P. 2018. Liquid Nuclear Condensates Mechanically Sense and Restructure the Genome. *Cell,* 175**,** 1481-1491 e13.

SHIRAKI, T., KONDO, S., KATAYAMA, S., WAKI, K., KASUKAWA, T., KAWAJI, H., KODZIUS, R., WATAHIKI, A., NAKAMURA, M., ARAKAWA, T., FUKUDA, S., SASAKI, D., PODHAJSKA, A., HARBERS, M., KAWAI, J., CARNINCI, P. & HAYASHIZAKI, Y. 2003. Cap analysis gene expression for high-throughput analysis of transcriptional starting point and identification of promoter usage. *Proc Natl Acad Sci U S A,* 100**,** 15776-81.

SIKMA, M. A., VAN MAARSEVEEN, E. M., VAN DE GRAAF, E. A., KIRKELS, J. H., VERHAAR, M. C., DONKER, D. W., KESECIOGLU, J. & MEULENBELT, J. 2015. Pharmacokinetics and Toxicity of Tacrolimus Early After Heart and Lung Transplantation. *Am J Transplant,* 15**,** 2301-13.

SIMS, R. J., 3RD & REINBERG, D. 2009. Processing the H3K36me3 signature. *Nat Genet,* 41**,** 270-1.

SOARES, L. M., HE, P. C., CHUN, Y., SUH, H., KIM, T. & BURATOWSKI, S. 2017. Determinants of Histone H3K4 Methylation Patterns. *Mol Cell,* 68**,** 773-785 e6.

STROM, A. R., EMELYANOV, A. V., MIR, M., FYODOROV, D. V., DARZACQ, X. & KARPEN, G. H. 2017. Phase separation drives heterochromatin domain formation. *Nature,* 547**,** 241-245.

SU, X., WELLEN, K. E. & RABINOWITZ, J. D. 2016. Metabolic control of methylation and acetylation. *Curr Opin Chem Biol,* 30**,** 52-60.

SUN, J. C., MADERA, S., BEZMAN, N. A., BEILKE, J. N., KAPLAN, M. H. & LANIER, L. L. 2012. Proinflammatory cytokine signaling required for the generation of natural killer cell memory. *J Exp Med,* 209**,** 947-54.

SZABO, Q., JOST, D., CHANG, J. M., CATTONI, D. I., PAPADOPOULOS, G. L., BONEV, B., SEXTON, T., GURGO, J., JACQUIER, C., NOLLMANN, M., BANTIGNIES, F. & CAVALLI, G. 2018. TADs are 3D structural units of higher-order chromosome organization in Drosophila. *Sci Adv,* 4**,** eaar8082.

THOMAS, M. C. & CHIANG, C. M. 2006. The general transcription machinery and general cofactors. *Crit Rev Biochem Mol Biol,* 41**,** 105-78.

TIAN, J., MA, J., MA, K., GUO, H., BAIDOO, S. E., ZHANG, Y., YAN, J., LU, L., XU, H. & WANG, S. 2013. beta-Glucan enhances antitumor immune responses by regulating differentiation and function of monocytic myeloid-derived suppressor cells. *Eur J Immunol,* 43**,** 1220-30.

TIGGES, M., MARQUEZ-LAGO, T. T., STELLING, J. & FUSSENEGGER, M. 2009. A tunable synthetic mammalian oscillator. *Nature,* 457**,** 309-12.

TODA, Y., TSUKADA, J., MISAGO, M., KOMINATO, Y., AURON, P. E. & TANAKA, Y. 2002. Autocrine induction of the human pro-IL-1beta gene promoter by IL-1beta in monocytes. *J Immunol,* 168**,** 1984-91.

TOLHUIS, B., PALSTRA, R.-J., SPLINTER, E., GROSVELD, F. & DE LAAT, W. 2002. Looping and interaction between hypersensitive sites in the active β-globin locus. *Molecular cell,* 10**,** 1453-1465.

TSAI, M. C., MANOR, O., WAN, Y., MOSAMMAPARAST, N., WANG, J. K., LAN, F., SHI, Y., SEGAL, E. & CHANG, H. Y. 2010. Long noncoding RNA as modular scaffold of histone modification complexes. *Science,* 329**,** 689-93.

VAN ARENSBERGEN, J., PAGIE, L., FITZPATRICK, V. D., DE HAAS, M., BALTISSEN, M. P., COMOGLIO, F., VAN DER WEIDE, R. H., TEUNISSEN, H., VOSA, U., FRANKE, L., DE WIT, E., VERMEULEN, M., BUSSEMAKER, H. J. & VAN STEENSEL, B. 2019. High-throughput identification of human SNPs affecting regulatory element activity. *Nat Genet,* 51**,** 1160-1169.

VAN STRAALEN, N. M. & ROELOFS, D. 2011. *An introduction to ecological genomics*, OUP Oxford.

VECCHIARELLI, A., CENCI, E., PULITI, M., BLASI, E., PUCCETTI, P., CASSONE, A. & BISTONI, F. 1989. Protective immunity induced by low-virulence Candida albicans: cytokine production in the development of the anti-infectious state. *Cell Immunol,* 124**,** 334-44.

VENTER, J. C., ADAMS, M. D., MYERS, E. W., LI, P. W., MURAL, R. J., SUTTON, G. G., SMITH, H. O., YANDELL, M., EVANS, C. A., HOLT, R. A., GOCAYNE, J. D., AMANATIDES, P., BALLEW, R. M., HUSON, D. H., WORTMAN, J. R., ZHANG, Q., KODIRA, C. D., ZHENG, X. H., CHEN, L., SKUPSKI, M., SUBRAMANIAN, G., THOMAS, P. D., ZHANG, J., GABOR MIKLOS, G. L., NELSON, C., BRODER, S., CLARK, A. G., NADEAU, J., MCKUSICK, V. A., ZINDER, N., LEVINE, A. J., ROBERTS, R. J., SIMON, M., SLAYMAN, C., HUNKAPILLER, M., BOLANOS, R., DELCHER, A., DEW, I., FASULO, D., FLANIGAN, M., FLOREA, L., HALPERN, A., HANNENHALLI, S., KRAVITZ, S., LEVY, S., MOBARRY, C., REINERT, K., REMINGTON, K., ABU-THREIDEH, J., BEASLEY, E., BIDDICK, K., BONAZZI, V., BRANDON, R., CARGILL, M., CHANDRAMOULISWARAN, I., CHARLAB, R., CHATURVEDI, K., DENG, Z., DI FRANCESCO, V., DUNN, P., EILBECK, K., EVANGELISTA, C., GABRIELIAN, A. E., GAN, W., GE, W., GONG, F., GU, Z., GUAN, P., HEIMAN, T. J., HIGGINS, M. E., JI, R. R., KE, Z., KETCHUM, K. A., LAI, Z., LEI, Y., LI, Z., LI, J., LIANG, Y., LIN, X., LU, F., MERKULOV, G. V., MILSHINA, N., MOORE, H. M., NAIK, A. K., NARAYAN, V. A., NEELAM, B., NUSSKERN, D., RUSCH, D. B., SALZBERG, S., SHAO, W., SHUE, B., SUN, J., WANG, Z., WANG, A., WANG, X., WANG, J., WEI, M., WIDES, R., XIAO, C., YAN, C., et al. 2001. The sequence of the human genome. *Science,* 291**,** 1304-51.

VERMEULEN, M., MULDER, K. W., DENISSOV, S., PIJNAPPEL, W. W., VAN SCHAIK, F. M., VARIER, R. A., BALTISSEN, M. P., STUNNENBERG, H. G., MANN, M. & TIMMERS, H. T. 2007. Selective anchoring of TFIID to nucleosomes by trimethylation of histone H3 lysine 4. *Cell,* 131**,** 58-69.

WANG, K. C. & CHANG, H. Y. 2011. Molecular mechanisms of long noncoding RNAs. *Mol Cell,* 43**,** 904-14.

WANG, K. C., YANG, Y. W., LIU, B., SANYAL, A., CORCES-ZIMMERMAN, R., CHEN, Y., LAJOIE, B. R., PROTACIO, A., FLYNN, R. A., GUPTA, R. A.,

WYSOCKA, J., LEI, M., DEKKER, J., HELMS, J. A. & CHANG, H. Y. 2011. A long noncoding RNA maintains active chromatin to coordinate homeotic gene expression. *Nature,* 472**,** 120-4.

WANG, X., ZHU, K., LI, S., LIAO, Y., DU, R., ZHANG, X., SHU, H. B., GUO, A. Y., LI, L. & WU, M. 2012. MLL1, a H3K4 methyltransferase, regulates the TNFalpha-stimulated activation of genes downstream of NF-kappaB. *J Cell Sci,* 125**,** 4058-66.

WANG, Z. & ZHENG, Y. 2018. lncRNAs Regulate Innate Immune Responses and Their Roles in Macrophage Polarization. *Mediators Inflamm,* 2018**,** 8050956.

WATERHOUSE, A. T., LESLIE, D. C., BOLGEN, D. E., LIGHTBOWN, S., DIMITRAKAKIS, N., CARTWRIGHT, M. J., SEILER, B. T., LIGHTBOWN, K., SMITH, K., LOMBARDO, P., HICKS-BERTHET, J. B., JUREK, S., DONOVAN, K., SUPER, M. S., NEDDER, A. & INGBER, D. E. 2018. Modified Clinical Monitoring Assessment Criteria for Multi-Organ Failure during Bacteremia and Sepsis Progression in a Pig Model. *Advan Crit Care Med*.

WEBER, J. S., YANG, J. C., ATKINS, M. B. & DISIS, M. L. 2015. Toxicities of Immunotherapy for the Practitioner. *J Clin Oncol,* 33**,** 2092-9.

WEN, A. Q., WANG, J., FENG, K., ZHU, P. F., WANG, Z. G. & JIANG, J. X. 2006. Effects of haplotypes in the interleukin 1beta promoter on lipopolysaccharide-induced interleukin 1beta expression. *Shock,* 26**,** 25-30.

WIJCHERS, P. J., KRIJGER, P. H. L., GEEVEN, G., ZHU, Y., DENKER, A., VERSTEGEN, M., VALDES-QUEZADA, C., VERMEULEN, C., JANSSEN, M., TEUNISSEN, H., ANINK-GROENEN, L. C. M., VERSCHURE, P. J. & DE LAAT, W. 2016. Cause and Consequence of Tethering a SubTAD to Different Nuclear Compartments. *Mol Cell,* 61**,** 461-473.

WILLYARD, C. 2018. New human gene tally reignites debate. *Nature,* 558**,** 354-355.

WOJTOWICZ, A., GRESNIGT, M. S., LECOMPTE, T., BIBERT, S., MANUEL, O., JOOSTEN, L. A., RUEGER, S., BERGER, C., BOGGIAN, K., CUSINI, A., GARZONI, C., HIRSCH, H. H., WEISSER, M., MUELLER, N. J., MEYLAN, P. R., STEIGER, J., KUTALIK, Z., PASCUAL, M., VAN DELDEN, C., VAN DE VEERDONK, F. L., BOCHUD, P. Y., SWISS TRANSPLANT COHORT, S. &

SWISS TRANSPLANT COHORT STUDY, S. 2015. IL1B and DEFB1 Polymorphisms Increase Susceptibility to Invasive Mold Infection After Solid-Organ Transplantation. *J Infect Dis,* 211**,** 1646-57.

WU, X., OFFENBACHER, S., L′OPEZ, N., CHEN, D., WANG, H. Y., ROGUS, J., ZHOU, J., BECK, J., JIANG, S. & BAO, X. 2015. Association of interleukin-1 gene variations with moderate to severe chronic periodontitis in multiple ethnicities. *Journal of periodontal research,* 50**,** 52-61.

XU, W.-D., ZHAO, Y. & LIU, Y. 2015. Insights into IL-37, the role in autoimmune diseases. *Autoimmunity reviews,* 14**,** 1170-1175.

YANG, L., LIN, C., JIN, C., YANG, J. C., TANASA, B., LI, W., MERKURJEV, D., OHGI, K. A., MENG, D., ZHANG, J., EVANS, C. P. & ROSENFELD, M. G. 2013. lncRNA-dependent mechanisms of androgen-receptor-regulated gene activation programs. *Nature,* 500**,** 598-602.

YANG, Y. W., FLYNN, R. A., CHEN, Y., QU, K., WAN, B., WANG, K. C., LEI, M. & CHANG, H. Y. 2014. Essential role of lncRNA binding for WDR5 maintenance of active chromatin and embryonic stem cell pluripotency. *Elife,* 3**,** e02046.

YU, Y., ZHONG, J., PENG, L., WANG, B., LI, S., HUANG, H., DENG, Y., ZHANG, H., YANG, R., WANG, C. & YUAN, J. 2017. Tacrolimus downregulates inflammation by regulating pro/antiinflammatory responses in LPSinduced keratitis. *Mol Med Rep,* 16**,** 5855-5862.

ZENG, Y. & CULLEN, B. R. 2002. RNA interference in human cells is restricted to the cytoplasm. *RNA,* 8**,** 855-60.

ZHANG, L., RU, H. W., CHEN, F. Z., JIN, C. Y., SUN, R. F., FAN, X. Y., GUO, M., MAI, J. T., XU, W. X., LIN, Q. X. & LIU, J. 2016. Variable Virulence and Efficacy of BCG Vaccine Strains in Mice and Correlation With Genome Polymorphisms. *Mol Ther,* 24**,** 398-405.

ZHOU, T., YANG, L., LU, Y., DROR, I., DANTAS MACHADO, A. C., GHANE, T., DI FELICE, R. & ROHS, R. 2013. DNAshape: a method for the high-throughput prediction of DNA structural features on a genomic scale. *Nucleic Acids Res,* 41**,** W56-62.